REAL SPACE APPROACH TO THE CALCULATION OF THE ELECTRONIC STRUCTURE OF TRANSITION METALS

KUNITOMO HIRAI

September 1981

Contents

	Abstract	1
I.	Introduction	3
II.	Real Space Approach to the Calculation of the Electronic Structure of Transition Metals	8
§1.	The Real Space Expansion of the Green Function	8
§2.	The Role of the d Symmetry of Atomic Orbitals	13
§3.	The Effective Locator and its Application	17
§4.	Application to Disordered Alloys	30
§5.	Discussion and Summary	37
III.	Magnetism in Transition Metals	41
§6.	Review of Some Previous Attempts	41
§7.	Model Hamiltonian	44
§8.	Real Space Approach Applied to Magnetic States	50
§9.	Unenhanced Susceptibility	62
§10.	Phase Diagrams	68
§11.	Concluding Remarks	73
	Acknowledgements	74
	Appendix	75
	References	82
	Figure Captions	84
	Tables and Figures	

Abstract

The role of the d symmetry of atomic orbitals in determining the electronic structure of transition metals is discussed by use of a real space expansion of the Green function. Terms which are sensitive to the crystal structures are separated from those corresponding to the path integrals on a Bethe type lattice. On the basis of this discussion a simple method is developed for calculating the electronic structure of transition metals. By use of the method the correspondence between the band theory and atomic interaction models can be established. It is found that the density of states for bcc and fcc transition metals are satisfactorily reproduced with the information from the interactions among near neighboring atoms, and that the difference between bcc and fcc arises mostly from three or four atoms interactions, while distant neighbors contribute mostly to the structure insensitive self-energy.

The method is next applied to magnetic states, i.e. ferromagnetic, antiferromagnetic, helical spin density wave and paramagnetic states. It is found that the unenhanced susceptibilities for bcc and fcc are also satisfactorily reproduced. By use of the method, the magnitude of local moments, energy, etc. are calculated within the Hartree-Fock approximation. The relative stability of those states is investigated for a given valence, and phase diagrams of bcc and fcc transition metals are constructed. It is found that

the most stable state changes continuously from an antiferromagnetic one to a ferromagnetic one via a helical spin density wave one when the valence changes from five to ten. The correspondence between the obtained phase diagrams and experimentally observed ones for 3d metals is discussed.

I. Introduction

The electronic structure of transition metals, which is an indispensable knowledge in interpreting their cohesive and magnetic properties, is usually obtained through band structure calculations based on the Bloch theorem. On the other hand, one sometimes uses in the discussion of transition metals some atomic interaction models which express the structure- and atomic-state-sensitive energy as a sum of single atom terms and interactions among a small cluster of atoms. An example of such models is the interacting virtual state approach which has been successfully used in the discussion of magnetic properties.[1,2] Though the atomic interaction models are superficially far from the band theory, qualitative arguments based on the models are consistent with those based on the band theory. We suppose that the d symmetry of atomic orbitals may play some roles in connecting the atomic interaction models to the band theory, since the d electrons in transition metals are not so free as the sp electrons in transition metals. The purpose of this investigation is to present a justification for these atomic interaction models on the basis of the band theory, which enables us to obtain a deeper insight into the role of the d symmetry of atomic orbitals and local atomic arrangements in determining the local electronic structure. Moreover, the justification leads us to a new approach to the calculation of the electronic structure

which is simple enough to apply it to aperiodic systems as well as periodic ones.

We start from the methods which have been proposed for calculating the local electronic structure at a given atomic site in view of the local environment produced by near neighboring atoms. These methods, i.e. the moment method[3,4] and the recursion method[5-7] are based on a real space (locator) expansion of the Green function, and do not involve the Bloch theorem in any way. The methods can therefore be applied to the electronic structure of aperiodic systems such as the surface, an impurity in the bulk solids, disordered alloys and noncrystalline solids. Even for a perfect crystal, the methods have some advantages in carrying out numerical calculation, especially for a crystal of complex structure. However, the moment method or the recursion method is not transparent enough to yield an insight into the nature of atomic interactions, since a calculation over a fairly large number of atoms is involved. We therefore simplify these real space approach and develop a new approach which enables us to calculate the electronic structure with less number of atoms.

The basic idea of the present approach is to reorganize the real space expansion of the Green function to renormalize the atomic locators and the electron transfer matrix elements by summing up a special type of terms which are insensitive to atomic arrangements. We then taken into account remaining

near neighbor interaction terms with renormalized locators and interatomic transfers. Through this approach we can determine the terms which are responsible for producing, for example, the difference of the density of states of the d band between bcc metals and fcc ones. It will be shown also that the d symmetry of atomic orbitals plays a very important role in determining relative weights of structure-sensitive terms and insensitive ones.

In the first half of this thesis, we devote ourselves to the derivation of the present approach, and discuss some applications of the present approach. We briefly outline the real space expansion of the Green function in §1. In §2 we discuss the role of the d symmetry of atomic orbitals. In §3 we develop a new scheme of calculating the electronic structure. The density of states in bcc and fcc transition metals is taken as an illustrating example. In §4 we extend the present approach to the case of disordered alloys. We discuss in §5 the correspondence between the present approach and the interacting virtual state approach, and summarize our conclusion.

In the latter half of this thesis, we discuss the magnetism in transition metals on the basis of the electronic structure calculated by the present approach. As was mentioned above, the present approach yields a justification for the interacting virtual state approach, in which the concept of local moments and that of itinerant electrons are unified. The present

approach appreciates the concept of local moments in the itinerant electrons system more fully than the interacting virtual state approach does. The local moment attaching to a given atomic site is no more rigid as that in insulators, and is influenced by the circumstances of the whole crystal, i.e. the configuration of local moments with variable magnitude and direction. We can easily apply the present approach to magnetic cases either ordered or disordered, which enables us to compare various kinds of magnetic states within the same framework and on the basis of a realistic band structure.

We calculate the electronic structure of ferromagnetic, antiferromagnetic, helical spin density wave (SDW) and paramagnetic states by determining the magnitude of local moments in a self-consistent way, and investigate the relative stability of those states. As a result of this investigation, we construct the phase diagrams of bcc and fcc transition metals for a given number of the d electrons and given strengths of the intra-atomic interactions. It will be shown that the obtained phase diagrams can explain the wide variety of the observed magnetism in 3d transition metals not only for the ground state porperties but also for the properties at finite temperature.

We review in §6 some previous attempts in which the magnetism in transition metals is discussed. We present the model Hamiltonian in §7. In §8 the details of the method

for calculating the electronic structures of ferromagnetic, antiferromagnetic, helical SDW and paramagnetic states are discussed. In §9 we compare the unenhanced susceptibility obtained through the usual band structure calculation and that through the present approach in order to check the accuracy of the present approach. We discuss the calculated phase diagrams in §10. Finally we summarize our conclusion in §11.

II. Real Space Approach to the Calculation of the Electronic Structure of Transition Metals

§ 1. The Real Space Expansion of the Green Function

We start with a general tight binding model in which five d orbitals of each atom only are taken into account. Our treatment can be extended to the case where nearly free electron states corresponding to s and p atomic states are included, though such an extension will not be discussed in this paper. The model Hamiltonian can be expressed as

$$H = \sum_{i,m,j,n\ (i\neq j)} t_{ij}^{mn}\, a_{im}^{*}\, a_{jn} + \sum_{i,m} E_{im}\, a_{im}^{*}\, a_{im}, \tag{1.1}$$

where i and j denote the sites of atoms, and m, n, $\cdots$ specify the type of atomic d orbitals (m=1,2, $\cdots$5). The matrix elements of the Green function are defined by

$$G_{ij}^{mn}(\omega) = \langle i,m\,|(\omega - H)^{-1}|\,j,n\rangle . \tag{1.2}$$

The local density of states of the orbital ℓ at the origin is given by

$$\rho_0^{\ell}(\omega) = -(1/\pi)\ \mathrm{Im}[G_{00}^{\ell\ell}(\omega+i\varepsilon)]_{\varepsilon\to 0+}. \tag{1.3}$$

We denote the locator of the state $|i.m\rangle$ by

$$g_i^m(\omega) = (\omega - E_{im})^{-1}. \tag{1.4}$$

The wellknown locator expansion of $G_{00}^{\ell\ell}(\omega)$ is given by

$$G_{00}^{\ell\ell}(\omega) = g_0^\ell + \sum_{i,m} g_0^\ell\, t_{0i}^{\ell m}\, g_i^m\, t_{i0}^{m\ell}\, g_0^\ell + \sum_{i,m}\sum_{j,n} g_0^\ell\, t_{0i}^{\ell m}\, g_i^m\, t_{ij}^{mn}\, g_j^n\, t_{j0}^{n\ell}\, g_0^\ell + \cdots , \tag{1.5}$$

where the ν-th order term is the sum of all closed paths starting at the origin and returning to it by ν steps. We can rewrite eq.(1.5) by use of the irreducible sum for the ν-th order term in which the paths are not allowed to return to the origin at intermediate steps (see Fig. 1a). We then obtain

$$G_{00}^{\ell\ell}(\omega) = [(g_0^\ell)^{-1} - \sum_{i,m} t_{0i}^{\ell m}\, g_i^m\, t_{i0}^{m\ell} - \sum_{i,m}\sum_{j,n} t_{0i}^{\ell m}\, g_i^m\, t_{ij}^{mn}\, g_j^n\, t_{j0}^{n\ell} - \cdots]^{-1} , \tag{1.6}$$

where the sums are taken over the irreducible paths. Regarding eqs.(1.5) and (1.6) as the expansion in powers of $1/\omega$, we can rewrite them as

$$G_{00}^{\ell\ell}(\omega) = (1/\omega) + \sum_{\nu} M_{\nu}^{\ell}/\omega^{\nu+1} , \qquad (1.7)$$

and

$$G_{00}^{\ell\ell}(\omega) = [\omega - \sum_{\nu} \bar{M}_{\nu}^{\ell}/\omega^{\nu-1}]^{-1} , \qquad (1.8)$$

where M_{ν}^{ℓ} and $\bar{M}_{\nu}^{\ell}$ are expressed in terms of t_{ij}^{mn} and E_{im}, and M_{ν}^{ℓ} corresponds to the ν-th moments of the density of states;

$$M_{\nu}^{\ell} = \int_{-\infty}^{\infty} \omega^{\nu} \rho_{0}^{\ell}(\omega)\, d\omega . \qquad (1.9)$$

An approximate $G_{00}^{\ell\ell}(\omega)$ which is obtained by truncating the series in eqs.(1.5) - (1.8) at a finite ν-th order term is not always a Herglotz function[8,9] for which a positive value of the density of states is guaranteed. Therefore we rewrite $G_{00}^{\ell\ell}(\omega)$ as a continued fraction such that

$$G_{00}^{\ell\ell}(\omega) = \left[\omega - a_1 - \cfrac{b_1}{\omega - a_2 - \cfrac{b_2}{\omega - a_3 \cdots}}\right]^{-1} . \qquad (1.10)$$

If all b_{ν}'s are positive, $G_{00}^{\ell\ell}(\omega)$ is a Herglotz function even when the fraction is terminated by assuming $b_{N+1}=0$ for arbitrary N. The continued fraction coefficients (a_{ν}, b_{ν})

are complicated functions of M_ν^ℓ and hence t_{ij}^{mn} and E_{im}. Both being based on the continued fraction expansion, the moment method and the recursion method differ in the way of determining the coefficients (a_ν, b_ν). In the moment method one first calculates the moments of the density of states, and then determines the coefficients by use of sophisticated numerical methods. On the other hand, one determines directly the coefficients by tridiagonalizing the Hamiltonian matrix in the recursion method. The tridiagonal matrix is one whose non-zero elements appear only on the main diagonal and two sub-diagonals, upper right and lower left. The corresponding $G_{00}^{\ell\ell}(\omega)$ of the tridiagonal matrix is easily verified to be equal to the continued fraction (1.10). Our approach is also based on the continued fraction; the coefficients are calculated in a somewhat different way from those used in the previous method.

For the discussion given in §3, we summarize the usually used technique for terminating the continued fraction in the moment method or the recursion method. After computing (a_ν, b_ν) to $\nu=N$ (which corresponds to computing the ν'-th moment to $\nu'=2N$), we assume asymptotic values (a_∞, b_∞) for $\nu > N$. Then the fraction after N is given by

$$T(\omega)= \cfrac{1}{\omega - a_\infty - \cfrac{b_\infty}{\omega - a_\infty - \cdots}} = \cfrac{1}{\omega - a_\infty - b_\infty T(\omega)} \,, \tag{1.11}$$

which can be solved as

$$T(\omega) = [1/(2b_\infty)] \cdot [(\omega - a_\infty) - \sqrt{(\omega - a_\infty)^2 - 4b_\infty}]. \qquad (1.12)$$

§ 2. The Role of the d Symmetry of Atomic Orbitals

In order to simplify the following discussion, we assume that all E_{im}'s and g_i^m's are equal to each other irrespective of i and m. By shifting the zero of energy we assume then

$$g_i^m(\omega) = 1/\omega. \tag{2.1}$$

The contribution of a path of ν steps to the series in eq.(1.5) and eq.(1.6) is given except for a factor $1/\omega^{\nu-1}$ or $1/\omega^{\nu+1}$ by

$$m_\nu^\ell(i,j,\cdots,\nu-1) = \sum_{m,n,\cdots,m'} t_{0i}^{\ell m} t_{ij}^{mn} \cdots t_{\nu-1 0}^{m'\ell}. \tag{2.2}$$

The ν-th moment M_ν^ℓ in eq.(1.7) is reduced to the sum of m_ν^ℓ of all the ν-th order paths including those passing the origin at intermediate steps, and correspondingly $\overline{M}_\nu^\ell$ in eq.(1.8) is reduced to the sum of irreducible paths.

The transfer matrix elements t_{ij}^{mn} can be expressed as a linear combination of the Slater-Koster integrals ddσ, ddπ and ddδ. Before going into the discussion based on the realistic values of these integrals, we present a qualitative discussion of the role of the d symmetry of atomic orbitals by use of the asymptotic behavior of the integrals for a large separation R of interacting atoms. Pettifor[10] has shown that ddπ and ddδ are asymptotically equal to zero for large R, while ddσ is proportional to an oscillating function

with a factor 1/R. If we assume $dd_\pi = dd_\delta = 0$ for each step, we can show easily that

$$\sum_\ell m_\nu^\ell \propto P_2(\cos\theta_1)\, P_2(\cos\theta_2) \cdots P_2(\cos\theta_\nu), \qquad (2.3)$$

where the sum is taken over the five atomic orbitals at the origin, θ_j is the inflection angle of a given path at the j-th atom, θ_ν corresponds to tha angle between the initial step and the final one (see Fig. 1), and P_2 is the Legendre polynomial P_ℓ of $\ell=2$. If we consider the nearest-neighbor transfer on a fcc lattice, possible values of $P_2(\cos\theta_j)$ are given by

$$1 \text{ or } -(1/8) \text{ or } -(1/2).$$

Similarly the corresponding values for the nearest and next-nearest neighbor transfers on a bcc lattice are

$$1 \text{ or } 0 \text{ or } -(1/3) \text{ or } -(1/2).$$

Thus the angular factor reduces the contribution of those paths which involve the inflections $\theta_j \neq 0$ or π. For example the angular factors of $\sum_\ell m_\nu^\ell$ of typical fourth order paths of the fcc lattice, A_1, B_2 and C_5 defined in Fig. 2 are 1, 1/4 and 1/256, respectively. In the case of the s band where the transfer matrix elements have no angular dependence, all paths mentioned above will make the

contributions of the same magnitude.

In order to carry out a more realistic calculation, we take into account again the nearest neighbor transfers only in the case of a fcc lattice and the nearest and next nearest neighbor ones in the case of a bcc lattice. We adopt the values of $dd\sigma$, $dd\pi$ and $dd\delta$ for these transfers estimated by Pettifor[11,12] which are listed in Table I. The numerical estimates of $\sum_{\ell} m_{\nu}^{\ell}$ of the fourth order paths shown in Figs. 2 and 3 are listed in Tables II and III together with the ratios estimated by use of the asymptotic relation (2.3). We can see from Tables II and III that the reduction due to the angular dependence of d orbitals inferred from the asymptotic behavior of the integrals is supported semi quantitatively by the calculation using realistic values of the integrals.

Inspecting the forth order terms, we classify the paths into three categories, A, B and C (see Figs. 2 and 3). To the category A, reducible paths belong; their contribution to the sum M_4^{ℓ}, M_{4A}^{ℓ} satisfies $M_{4A}^{\ell} = (M_2^{\ell})^2$. The category B comprises those paths in which we go from the origin to atom 1, then to atom 2 and come back to the origin, tracing the same path. Those paths which visit three different atom fall in category C. We list the numerical values of M_2^{ℓ}, M_3^{ℓ}, M_4^{ℓ}, M_{4A}^{ℓ}, M_{4B}^{ℓ} and M_{4C}^{ℓ} for fcc and bcc lattices in Tables IV and V. We show also the relative magnitudes of these sums, $M_3^{\ell}/(M_2^{\ell})^{3/2}$, $M_4^{\ell}/(M_2^{\ell})^2$, etc. there together with

the corresponding quantities for the s band.

The irreducible sums, $\bar{M}_\nu^\ell$ appearing in eq.(1.8) are given by

$$\bar{M}_2^\ell = M_2^\ell \ , \ \bar{M}_3^\ell = M_3^\ell \quad \text{and} \quad \bar{M}_4^\ell = M_{4B}^\ell + M_{4C}^\ell . \tag{2. 4}$$

From Tables IV and V we can see that $M_3^\ell/(M_2^\ell)^{3/2}$ and $M_{4C}^\ell/(M_2^\ell)^2$ of the d band is much smaller than those of the s band, while $M_{4B}^\ell/(M_2^\ell)^2$ of the d band is comparable with that of the s band. This situation can be understood, since the paths contributing to M_3^ℓ and M_{4C}^ℓ corresond to (twisted) polygons having $\theta_j \neq 0$ or π. Extending the discussion to higher order terms, we may conclude that among the irreducible path those which go on a broken line and trace it back to the origin make a relatively large contribution compared with those corresponding to (twisted) polygons. Utilizing this reasoning, we develop a new treatment of the real space expansion in the next section, where we renormalize the locator by summing up the contribution of the paths of type B.

§ 3. The Effective Locator and its Application

We have noticed in the preceding section that the paths of the type B on which one goes to a lattice site without making a loop and traces back the same way make a dominant contribution to the self-energy. We divide the whole irreducible paths into two parts, $\Sigma_B^{\ell}(\omega)$ consisting of the type B paths and $\Sigma_C^{\ell}(\omega)$ corresponding to the remainder; we write the Green function $G_{00}^{\ell\ell}(\omega)$ as

$$G_{00}^{\ell\ell}(\omega)= [\omega -\Sigma_B^{\ell}(\omega) - \Sigma_C^{\ell}(\omega)]^{-1}, \tag{3. 1}$$

where $\Sigma_B^{\ell}(\omega)$ is expanded into powers of $1/\omega$ such that

$$\Sigma_B^{\ell}(\omega)= M_2^{\ell}/\omega + M_{4B}^{\ell}/\omega^3 + M_{6B}^{\ell}/\omega^5 + \cdots , \tag{3. 2}$$

and $\Sigma_C^{\ell}(\omega)$ is expressed as

$$\Sigma_C^{\ell}(\omega)= M_3^{\ell}/\omega^2 + M_{4C}^{\ell}/\omega^3 + \cdots . \tag{3. 3}$$

The purpose of the following discussion is to derive an expression of $G_{00}^{\ell\ell}(\omega)$ in terms of the effective locator $\lambda^{\ell}(\omega)$ which includes the B type self-energy $\Sigma_B^{\ell}(\omega)$. We express $G_{00}^{\ell\ell}(\omega)$ as

$$G_{00}^{\ell\ell}(\omega)= \left[\omega - \cfrac{M_2^{\ell}}{\lambda^{\ell}(\omega) - a^{\ell} - \cfrac{b^{\ell}}{\lambda^{\ell}(\omega)}}\right]^{-1} . \tag{3. 4}$$

The effective locator $\tilde{\Lambda}^{\ell}(\omega)$ should satisfy the condition that $\tilde{\Lambda}^{\ell}(\omega) \sim \omega$ for $|\omega| \to \infty$ and

$$\Sigma_B^{\ell}(\omega) = M_2^{\ell}/\tilde{\Lambda}^{\ell}(\omega). \tag{3. 5}$$

Then if we choose

$$a^{\ell} = M_3^{\ell}/M_2^{\ell} \quad \text{and} \quad b^{\ell} = M_{4C}^{\ell}/M_2^{\ell} - (a^{\ell})^2, \tag{3. 6}$$

we can easily see that the self-energy part of the Green function is correctly reproduced up to $1/\omega^3$. The expression (3. 4) yields a non-negative density of states provided that

$$|\tilde{\Lambda}^{\ell}(\omega)| + b^{\ell} > 0. \tag{3. 7}$$

This condition is satisfied in the calculations which we present later.

§ 3. 1 The derivation of the effective locator

The effective locator $\tilde{\Lambda}^{\ell}(\omega)$ is defined by eq.(3.5). We note that $\Sigma_B^{\ell}(\omega)$ is equivalent to the self-energy in the case of the Bethe lattice if we neglect some double counting of higher order paths and the five-fold degeneracy of the d orbitals. If we deal with the s band on the Bethe lattice, we obtain

$$\Sigma_B^s(\omega) = \cfrac{zt^2}{\omega - \cfrac{(z-1)t^2}{\omega - \cfrac{(z-1)t^2}{\omega - \cdots}}}, \qquad (3.8)$$

where z denotes the coordination number. Thus $\tilde{\Lambda}^s(\omega)$ is given by

$$\tilde{\Lambda}^s(\omega) = \omega - (z-1)t^2 / \tilde{\Lambda}^s(\omega)$$

$$= (1/2)\,(\omega + \sqrt{\omega^2 - 4(z-1)t^2}). \qquad (3.9)$$

In the case of the d band we cannot derive a simple expression such as eq.(3.9) for $\tilde{\Lambda}^\ell(\omega)$. However, it behaves to good approximation very much like the self-energy on the Bethe lattice. Thus in the expression (3.4) the crystal structure manifests itself only through a^ℓ and b^ℓ, while $\tilde{\Lambda}^\ell(\omega)$ remains almost independent of the crystal structure. In the following we derive an approximate expression for $\tilde{\Lambda}^\ell(\omega)$ on the basis of eq.(3.5).

The guiding principle of deriving $\tilde{\Lambda}^\ell(\omega)$ is again to reproduce the $1/\omega$ expansion of $\Sigma_B^\ell(\omega)$ correctly up to $1/\omega^3$. We believe that our procedure yields a good approximation even for terms of higher order than $1/\omega^3$, since our method is exact for the case of the s band on the Bethe lattice. We introduce the average effective locators $\Lambda^\alpha(\omega)$ for the

orbitals belonging to an irreducible representation of the point group denoted by α. Specifying the types of the irreducible representations to which the d orbitals at intermediate steps belong, we first express $\Sigma_B^{\ell}(\omega)$ as

$$\Sigma_B^{\ell}(\omega) = \sum_{\alpha} M_2^{\ell}(\alpha)/\omega + \sum_{\alpha,\beta} M_{4B}^{\ell}(\alpha,\beta) \; / \; \omega^3 + \cdots, \qquad (3.10)$$

where $M_2^{\ell}(\alpha)$, $M_{4B}^{\ell}(\alpha,\beta)$ $\cdots$ are defined by

$$M_2^{\ell}(\alpha) = \sum_{i} \sum_{m \epsilon \alpha} t_{0i}^{\ell m} \, t_{i0}^{m\ell}$$

$$M_{4B}^{\ell}(\alpha,\beta) = \sum_{i,j} \sum_{m \epsilon \alpha} \sum_{n \epsilon \beta} \sum_{p \epsilon \alpha} t_{0i}^{\ell m} \, t_{ij}^{mn} \, t_{ji}^{np} \, t_{i0}^{p\ell} \; . \qquad (3.11)$$

Note that the superscript ℓ specifies one of the d orbitals and the Greek letters the irreducible representations. In the expression (3.11) we excluded from $\Sigma_B^{\ell}(\omega)$ such terms corresponding to those paths on which the atomic orbitals used on the return belongs to a different representation from that used initially (note that $p \epsilon \alpha$ in $M_{4B}^{\ell}(\alpha,\beta)$ in eq. (3.11)). These terms are included in $\Sigma_C^{\ell}(\omega)$; they turn out in any case to be negligibly small. We now express $\Sigma_B^{\ell}(\omega)$ in a continued fraction given by

$$\Sigma_B^{\ell}(\omega) = \sum_{\alpha} \cfrac{M_2^{\ell}(\alpha)}{\omega - \sum_{\beta} \cfrac{\mu_1^{\ell}(\alpha,\beta)}{\omega - \sum_{\gamma} \cfrac{\mu_2^{\ell}(\alpha,\beta,\gamma)}{\omega - \cdots}}} . \qquad (3.12)$$

The choice of the parameters $\mu_1^{\ell}(\alpha,\beta)$, $\mu_2^{\ell}(\alpha,\beta,\gamma),\cdots$ is not unique, since the expression of $\Sigma_B^{\ell}(\omega)$ depends only on the sum over α, $\beta,\cdots$ at intermediate steps. Nevertheless we may assume

$$\mu_1^{\ell}(\alpha,\beta) = M_{4B}^{\ell}(\alpha,\beta)/M_2^{\ell}(\alpha), \qquad (3.13)$$

which yields the $1/\omega^3$ term correctly. Since we are summing up the Bethe lattice type paths, we expect that the parameters $\mu_{\nu}^{\ell}(\alpha_1, \alpha_2,\cdots, \alpha_{\nu}, \alpha_{\nu+1})$ converges into a value independent of ℓ and $\alpha_1, \cdots, \alpha_{\nu-1}$, though it may depend on α_{ν} and $\alpha_{\nu+1}$. We therefore introduce an approximation, assuming

$$\mu_{\nu}^{\ell}(\alpha_1, \alpha_2, \cdots, \beta, \gamma) = \tilde{\mu}^{\beta\gamma} \qquad (3.14)$$

which is independent of ℓ and α_1, α_2 $\cdots$ for $\nu \geq 2$ (see Fig. 4). Then we can define the average locator $\Lambda^{\alpha}(\omega)$ by

$$\Lambda^{\alpha}(\omega) = \omega - \sum_{\beta} \overset{\sim}{\mu}{}^{\alpha\beta} / \Lambda^{\beta}(\omega)$$

$$= \omega - \sum_{\beta} \cfrac{\overset{\sim}{\mu}{}^{\alpha\beta}}{\omega - \sum_{\gamma} \cfrac{\overset{\sim}{\mu}{}^{\beta\gamma}}{\omega - \cdots}} \quad . \tag{3.15}$$

We obtain then

$$\Sigma_B^{\ell}(\omega) = \sum_{\alpha} M_2^{\ell}(\alpha) / [\omega - \sum_{\beta} \mu_1^{\ell}(\alpha, \beta) / \Lambda^{\beta}(\omega)] . \tag{3.16}$$

We determine $\overset{\sim}{\mu}{}^{\alpha\beta}$ by the condition that

$$\sum_{\ell} \Sigma_B^{\ell}(\omega) = \sum_{\alpha, \ell} M_2^{\ell}(\alpha) / \Lambda^{\alpha}(\omega) \quad . \tag{3.17}$$

In other words the average locators $\Lambda^{\alpha}(\omega)$ weighted with $M_2^{\ell}(\alpha)$ can reproduce the total self-energy summed over ℓ. With eqs.(3.13), (3.15) and (3.17) we can determine $\Lambda^{\alpha}(\omega)$ with the knowledge of $M_2^{\ell}(\alpha)$ and $M_{4B}^{\ell}(\alpha,\beta)$. Then we can calculate the effective locator $\overset{\sim}{\Lambda}{}^{\ell}(\omega)$ in the expression (3.4).

By expanding eq.(3.4) in powers of $1/\overset{\sim}{\Lambda}{}^{\ell}(\omega)$ we can see that eq.(3.4) is equivalent to the approximate expression (see Fig. 5)

$$\Sigma_C^{\ell}(\omega) = M_3^{\ell}/(\tilde{\Lambda}^{\ell}(\omega))^2 + M_{4C}^{\ell}/(\tilde{\Lambda}^{\ell}(\omega))^3 + \cdots . \qquad (3.18)$$

Thus by replacing $1/\omega^2$ and $1/\omega^3$ in the original expression (3.3) by $1/(\tilde{\Lambda}^{\ell}(\omega))^2$ and $1/(\tilde{\Lambda}^{\ell}(\omega))^3$, we claim that higher order terms are taken into account by renormalizing the locators at intermediate steps. One may question that a more straightforward renormalization would give

$$\Sigma_C^{\ell}(\omega) = \sum_{\alpha,\beta} M_3^{\ell}(\alpha,\beta)/\Lambda^{\alpha}\Lambda^{\beta}$$

$$+ \sum_{\alpha,\beta,\gamma} M_{4C}^{\ell}(\alpha,\beta,\gamma)/\Lambda^{\alpha}\Lambda^{\beta}\Lambda^{\gamma} , \qquad (3.19)$$

where the average locators replace $\tilde{\Lambda}^{\ell}(\omega)$. Equation (3.19) combined with eq.(3.1) yields almost the same results as eq. (3.4). However eq.(3.4) is free from the pathological negative density of states, while the direct use of eq.(3.19) suffers from it sometimes, though only in a restricted energy region.

§ 3. 2 Improved average locator

We show the result of our calculation based on eq.(3.4) for bcc and fcc in Fig.6, and the numerical values of a^{ℓ}, b^{ℓ}, etc. are listed in Table VI. We show also in Fig.6 the result of the band structure calculation in which the

same parameters are used. We calculate eigenvalues at 3311 points for bcc and at 3345 points for fcc in the irreducible 1/48 Brillouin zone. Considering the fact that our calculation is very simple, we may conclude from Fig.6 that the expression (3.4) can reproduce well the band structure calculation especially the difference between bcc and fcc crystal. Our calculation, however, does not describe well the difference of the band limits between bcc and fcc. Then we improve our calculation without changing the expression (3.4).

The average locator given by eq.(3.15) alone yields a density of states of the semi-elliptic type which does not show structures characteristic of a given crystal. Therefore we redefine the average locators by

$$\Lambda^{\alpha}(\omega)= \omega - \sum_{\beta} \tilde{\mu}^{\alpha\beta}/[\Lambda^{\beta}(\omega) - \tilde{a}^{\alpha\beta}] , \qquad (3.20)$$

in place of eq.(3.15). The term $\tilde{a}^{\alpha\beta}$ enables us to include the triangular path $(i\alpha)$-$(j\beta)$-$(k\beta)$-$(i\alpha)$ with i,j,k indicating neighboring sites (see Fig.4). We calculate $\tilde{a}^{\alpha\beta}$ by the condition that it can reproduce the effect of the triangle correctly. We then express $\Sigma_B^{\ell}(\omega)$ as

$$\Sigma_B^{\ell}(\omega)= \sum_{\alpha} M_2^{\ell}(\alpha)/[\omega - \sum_{\beta} \mu_1^{\ell}(\alpha,\beta)/\{\Lambda^{\beta}(\omega) - \tilde{a}^{\alpha\beta}\}]. \qquad (3.21)$$

In this expression we include in $\Sigma_B^{\ell}(\omega)$ some odd order paths, but we need not alter the expression (3.3) for $\Sigma_C^{\ell}(\omega)$ as far as the term M_3^{ℓ} and M_{4C}^{ℓ} are concerned and then the expression (3.4) for $G_{00}^{\ell\ell}(\omega)$.

The average locators given by eq.(3.20) and the effective locators given by eq.(3.5) combined with eq.(3.21) depend, though slightly, on a given crystal structure because of the term $\tilde{a}^{\alpha\beta}$. For example, the width of the locators and their center change their values according to crystal structure.

We show the result of the improved version of our calculation in Figs. 7 and 8. We conclude from Fig. 7 that a considerable improvement is achieved for the density of states for bcc and fcc. Not only the structures characteristic of a given crystal but also the band limits are well reproduced; the band limits from our calculation are (-0.096, 0.100) for bcc and (-0.123, 0.083) for fcc, while those from the band structure calculation are (-0.119, 0.097) for bcc and (-0.131, 0.085) for fcc (in Rydbergs).

In conclusion we may say on the basis of Figs. 6,7 and 8 that our calculation can reproduce well the band structure calculation even without the modification (3.20). The Bethe lattice type self-energy or the improved version of it including the triangle diagrams do not depend on the crystal structure very much and leads us to a monotonous density of states of the locators. The self-energy part M_3^{ℓ} and M_{4C}^{ℓ}, on the other hand, are mainly responsible for producing the difference

between bcc and fcc; in particular the contribution of M_{4C}^{ℓ} is predominant.

§ 3-3. Simplified expressions of $\Sigma_B^{\ell}(\omega)$ and $\Lambda^{\alpha}(\omega)$

As above mentioned, we calculate the effective locators in a lengthy manner on account of the five-fold degeneracy of the d orbitals. However, the essential properties of the effective locators are not far from those of the s band one given by eq.(3.9) or the s band one with the modification of triangle paths. We discuss here some simplified expressions of $\Sigma_B^{\ell}(\omega)$ and $\Lambda^{\alpha}(\omega)$.

The expression (3.21) of $\Sigma_B^{\ell}(\omega)$ which can reproduce the $1/\omega$ expansion of $\Sigma_B^{\ell}(\omega)$ up to $1/\omega^3$ is reduced to

$$\Sigma_B^{\ell}(\omega)= \sum_{\alpha} M_2^{\ell}(\alpha)/ \Lambda^{\alpha}(\omega) , \qquad (3.22)$$

when we assume $\mu_1^{\ell}(\alpha,\beta)= \tilde{\mu}^{\alpha\beta}$. Furthermore this expression can be approximated as

$$\Sigma_B^{\ell}(\omega)=M_2^{\ell} / (\sum_{\alpha} M_2^{\ell}(\alpha)\Lambda^{\alpha}(\omega)/M_2^{\ell}), \qquad (3.23)$$

where the harmonic mean of the average locators $\Lambda^{\alpha}(\omega)$ is replaced by the arithmetic mean. In both expressions (3.22) and (3.23), $\sum_{\ell} \Sigma_B^{\ell}(\omega)$ is correctly reproduced up to $1/\omega^3$ on account of the condition (3.17), though $\Sigma_B^{\ell}(\omega)$ itself is an

approximation even in the order of $1/\omega^3$. The deviation of $\Sigma_B^{\ell}(\omega)$ from these approximations, which turns out to be small, is taken care of in $\Sigma_C^{\ell}(\omega)$ in the present calculation. By adopting the expression (3.23), the effective locator is reduced to

$$\overset{\sim}{\Lambda}^{\ell}(\omega) = \sum_{\alpha} M_2^{\ell}(\alpha)\ \Lambda^{\alpha}(\omega)/M_2^{\ell} \quad . \tag{3.24}$$

We show in Fig. 9 the results of the calculation in which eq.(3.23) is used in place of eq.(3.21). The results of the original calculation in which eq.(3.21) is used are also shown in Fig.9. We can see from Fig.9 that these two results are almost identical to each other. We may add that the calculation in which eq.(3.22) is used also yields almost same results.

In the next place, we simplify the expression (3.20) of $\Lambda^{\alpha}(\omega)$. We calculate $\Lambda^{\alpha}(\omega)$'s by solving numerically simultaneous equations (3.20), which impairs the computational merits of the present approach when the number of $\Lambda^{\alpha}(\omega)$'s is increased. Equation (3.20) is rewriten as

$$\Lambda^{\alpha}(\omega) = \omega - \sum_{\beta} \overset{\sim}{\mu}{}^{\alpha\beta} / \left[\omega - \tilde{a}{}^{\alpha\beta} - \sum_{\gamma} \overset{\sim}{\mu}{}^{\beta\gamma}/(\omega \cdots)\right]$$

$$= \omega - \cfrac{\overset{\sim}{\mu}{}^{\alpha} \cdots}{\omega - \tilde{a}{}^{\alpha} - \cfrac{\tilde{b}{}^{\alpha} \cdots}{\omega - \cdots}} \quad , \tag{3.25}$$

where $\tilde{\mu}^{\alpha} = \sum_{\beta} \tilde{\mu}^{\alpha\beta}$, $\tilde{a}^{\alpha} = \sum_{\beta} \tilde{\mu}^{\alpha\beta}\, \tilde{a}^{\alpha\beta} / \tilde{\mu}^{\alpha}$, $\cdots$. We expect that the first few coefficients of the continued fraction $\tilde{\mu}^{\alpha}$, $\tilde{a}^{\alpha}$ and $\tilde{b}^{\alpha}$ may decide the essential properties of $\Lambda^{\alpha}(\omega)$, then we express $\Lambda^{\alpha}(\omega)$ as

$$\Lambda^{\alpha}(\omega) = \omega - \tilde{\mu}^{\alpha} / T^{\alpha}(\omega) \quad , \tag{3.26}$$

where

$$T^{\alpha}(\omega) = \omega - \tilde{a}^{\alpha} - \tilde{b}^{\alpha} / T^{\alpha}(\omega)$$

$$= (1/2)\left[(\omega - \tilde{a}^{\alpha}) + \sqrt{(\omega - \tilde{a}^{\alpha})^2 - 4\tilde{b}^{\alpha}} \right]. \tag{3.27}$$

We show also in Fig.9 the results of the calculation in which the simplified expression (3.26) of $\Lambda^{\alpha}(\omega)$ is used combined with the expression (3.23). Though slight changes are observed for fcc, the essential feature is not changed.

It may be emphasized that these simplifications are still consistent with the idea which we followed in deriving the original expressions of $\Sigma_{B}^{\ell}(\omega)$ and $\Lambda^{\alpha}(\omega)$, and that they do not cause any serious error. When we apply the present approach to the cases of disordered alloys and magnetic metals which will be discussed later, we use chiefly the expression (3.26) for $\tilde{\Lambda}^{\ell}(\omega)$ in order to diminish the compu-

tational efforts and the expression (3.23) for $\Sigma_B^{\ell}(\omega)$ and hence the expression (3.24) for $\chi^{\ell}(\omega)$ in order to avoid a pathological negative density of states.

§ 4. Application to Disordered Alloys

In this section we discuss the case of disordered alloys, which is a typical example of random systems. The atomic level of the i-th site takes two values according to the type of atom on the site;

$$E_{im} = \begin{cases} E_A & \text{for } i = \text{A atom} \\ E_B & \text{for } i = \text{B atom} \end{cases}, \qquad (4.1)$$

here we assume all E_{im}'s of the i-th site are equal to each other irrespective of m. The locator is then given by

$$g_i^m(\omega) = \begin{cases} 1/L_A(\omega) \equiv 1/(\omega - E_A) & \text{for } i = \text{A atom} \\ 1/L_B(\omega) \equiv 1/(\omega - E_B) & \text{for } i = \text{B atom.} \end{cases} \qquad (4.2)$$

The transfer matrix elements t_{ij}^{mn} are assumed to be independent of the type of atoms on the i-th site or the j-th site, though we can easily extend to the case where the transfer matrix elements between A and B atoms, $t_{ij}^{mn}(AB)$, are equal to the geometrical mean of $t_{ij}^{mn}(AA)$ and $t_{ij}^{mn}(BB)$.[13]

To discuss the local density of states at the origin, we need $\langle G_{00}^{\ell\ell}(\omega)\rangle$ or $\langle G_{00}^{\ell\ell}(\omega)\rangle_\xi$, where $\langle\cdots\rangle$ denotes the average over all possible configurations and $\langle\cdots\rangle_\xi$ denotes that with ξ (ξ=A or B) atom on the origin.

Denoting the concentration of A and B atoms by c_A and c_B respectively, we obtain

$$\langle G_{00}^{\ell\ell}(\omega)\rangle = c_A \langle G_{00}^{\ell\ell}(\omega)\rangle_A + c_B \langle G_{00}^{\ell\ell}(\omega)\rangle_B . \qquad (4.3)$$

The average of locators and that of the products of locators are given by

$$\langle g_i^m(\omega)\rangle = c_A/L_A + c_B/L_B \equiv \langle 1/L\rangle$$

$$\langle g_i^m(\omega)\cdot g_j^n(\omega)\rangle = \begin{cases} (c_A/L_A + c_B/L_B)^2 = \langle 1/L\rangle^2 & i\neq j \\ c_A/L_A^2 + c_B/L_B^2 \equiv \langle 1/L^2\rangle & i=j \end{cases} \quad \text{for}$$

(4.4)

irrespective of i,j,$\cdots$ and n,m, $\cdots$. Then we obtain

$$\langle G_{00}^{\ell\ell}(\omega)\rangle_\xi = 1/L_\xi + 1/L_\xi^2 \sum_{i,m} t_{0i}^{\ell m}\, t_{i0}^{m\ell} \langle 1/L\rangle$$

$$+ 1/L_\xi^2 \sum_{i,m}\sum_{j,n} t_{0i}^{\ell m}\, t_{ij}^{mn}\, t_{j0}^{n\ell} \langle 1/L\rangle^2 + \cdots . \qquad (4.5)$$

Correspondingly we obtain approximately

$$\langle G_{00}^{\ell\ell}(\omega)\rangle_\xi \tilde{=} [L_\xi - \sum_{i,m} t_{0i}^{\ell m}\, t_{i0}^{m\ell}\langle 1/L\rangle - \sum_{i,m}\sum_{j,n} t_{0i}^{\ell m}\, t_{ij}^{mn} t_{j0}^{n\ell}\langle 1/L\rangle^2 \cdots]^{-1},$$

(4.6)

where the inequality is due to the miscalculation for some reducible paths. The lowest order one of such paths is the fourth order one in which we go and return from the origin to an atom 1 then go and return again to the same atom 1; the contribution of the pths which is equal to $1/L_\xi^3 \cdot \langle 1/L^2 \rangle$ except for transfer matrix elements is treated as $1/L_\xi^3 \cdot \langle 1/L \rangle^2$ in eq.(4.6). Therefore the approximate equation (4.6) for $\langle G_{00}^{\ell\ell}(\omega) \rangle_\xi$ which corresponds to taking the configuration average of the irreducible paths only is valid so far as the low order paths are concerned.

We divide the configuration average of the whole irreducible paths into two parts, as is done in § 3;

$$\langle G_{00}^{\ell\ell}(\omega) \rangle_\xi = [L_\xi(\omega) - \langle \Sigma^\ell(\omega) \rangle]^{-1} = [L_\xi(\omega) - \langle \Sigma_B^\ell(\omega) \rangle - \langle \Sigma_C^\ell(\omega) \rangle]^{-1} , \tag{4.7}$$

where

$$\langle \Sigma_B^\ell(\omega) \rangle = M_2^\ell \langle 1/L \rangle + M_{4B}^\ell \langle 1/L^2 \rangle \langle 1/L \rangle + \cdots , \tag{4.8}$$

and

$$\langle \Sigma_C^\ell(\omega) \rangle = M_3^\ell \langle 1/L \rangle^2 + M_{4C}^\ell \langle 1/L \rangle^3 + \cdots . \tag{4.9}$$

We notice from eqs.(4.8) and (4.9) another aspect of the division of the paths than that derived from the discussion about the role of d symmetry of atomic orbitals in §3.

To obtain the expression of $\langle G_{00}^{\ell\ell}(\omega)\rangle_\xi$ corresponding to eq.(3.4), we define the effective locators $\tilde{\Lambda}_A^\ell(\omega)$ and $\tilde{\Lambda}_B^\ell(\omega)$ by

$$\langle \Sigma_B^\ell(\omega)\rangle = M_2^\ell(c_A/\tilde{\Lambda}^\ell{}_A(\varepsilon) + c_B/\tilde{\Lambda}_B^\ell(\omega)). \tag{4.10}$$

We express $\langle \Sigma^\ell(\omega)\rangle$ as

$$\langle \Sigma^\ell(\omega)\rangle = M_2^\ell / [(\frac{c_A}{\tilde{\Lambda}_A^\ell(\omega)} + \frac{c_B}{\tilde{\Lambda}_B^\ell(\omega)})^{-1} - a^\ell - b^\ell(\frac{c_A}{\tilde{\Lambda}_A^\ell(\omega)} + \frac{c_B}{\tilde{\Lambda}_B^\ell(\omega)})], \tag{4.11}$$

which is equivalent to the approximate expression of

$$\langle \Sigma_C^\ell(\omega)\rangle = M_3^\ell(\frac{c_A}{\tilde{\Lambda}_A^\ell(\omega)} + \frac{c_B}{\tilde{\Lambda}_B^\ell(\omega)})^2 + M_{4C}^\ell(\frac{c_A}{\tilde{\Lambda}_A^\ell(\omega)} + \frac{c_B}{\tilde{\Lambda}_B^\ell(\omega)})^3 + \cdots , \tag{4.12}$$

where L_ξ in the original expression (4.9) is replaced by $\tilde{\Lambda}_\xi^\ell$.

The derivation of the effective locators is as follows. We can rewrite eq.(4.8) as

$$\langle \Sigma_B^\ell(\omega)\rangle = \sum_\alpha M_2^\ell(\alpha) \left\langle \frac{1}{L - \sum_\beta \mu_1^\ell(\alpha,\beta) \left\langle \frac{1}{L \cdots} \right\rangle} \right\rangle , \tag{4.13}$$

where the same kind of errors as eq.(4.6) involves are neglected. Defining the average locators $\Lambda_\xi^\alpha(\omega)$ by

$$\Lambda_\xi^\alpha(\omega)= L_\xi(\omega) - \sum_\beta \tilde{\mu}^{\alpha\beta} [c_A/(\Lambda_A^\beta(\omega)- \tilde{a}^{\alpha\beta})+c_B/ (\Lambda_B^\beta(\omega)- \tilde{a}^{\alpha\beta})], \tag{4.14}$$

we obtain

$$\langle \sum_B^\ell(\omega)\rangle = \sum_\alpha M_2^\ell(\alpha) \left\{ \frac{c_A}{L_A(\omega)-\sum_\beta \mu_1^\ell(\alpha,\beta)[c_A/(\Lambda_A^\beta(\omega)-\tilde{a}^{\alpha\beta})+c_B/(\Lambda_B^\beta(\omega)-\tilde{a}^{\alpha\beta})]} + \frac{c_B}{L_B(\omega) - \sum_\beta \mu_1^\ell(\alpha,\beta)[c_A/(\Lambda_A^\beta(\omega)-\tilde{a}^{\alpha\beta})+c_B/(\Lambda_B^\beta(\omega)-\tilde{a}^{\alpha\beta})]} \right\}. \tag{4.15}$$

In numerical calculation we use the simplified expression of $\Lambda_\xi^\alpha(\omega)$ which corresponds to eq.(3.26) in place of eq.(4.14);

$$\Lambda_\xi^\alpha(\omega)=L_\xi(\omega)- \tilde{\mu}^\alpha(c_A/T_A^\alpha(\omega)+c_B/T_B^\alpha(\omega)), \tag{4.16}$$

where

$$T_\xi^\alpha(\omega)= L_\xi(\omega) - \tilde{a}^\alpha - \tilde{b}^\alpha(c_A/T_A^\alpha(\omega) + c_B/T_B^\alpha(\omega)). \tag{4.17}$$

We also use the simplified expression of $\langle \Sigma_B^{\ell}(\omega) \rangle$ which corresponds to eq.(3.23) in place of eq.(4.15), and then we obtain

$$\overset{\sim}{\Lambda}{}_{\xi}^{\ell}(\omega) = \sum_{\alpha} M_2^{\ell}(\alpha)\, \Lambda_{\xi}^{\alpha}(\omega) / M_2^{\ell} \,. \tag{4.18}$$

We show in Figs.10-13 some results of the present calculation in which eqs.(4.16)-(4.18) are used. We also show in Figs.10 and 11 the results of the CPA (coherent potential approximation[13-15]) calculation for the sake of comparison. It is found from Figs.10 and 11 that the general features of the density of states obtained from the present calculation and those from the CPA calculation are similar to each other.

In the CPA calculation we determine the coherent locator $\tilde{L}{}^{\ell}(\omega)$ by the condition

$$\frac{1}{\tilde{F}{}^{\ell}} = \frac{c_A}{L_A - \tilde{L}{}^{\ell} + (\tilde{F}{}^{\ell})^{-1}} + \frac{c_B}{L_B - \tilde{L}{}^{\ell} + (\tilde{F}{}^{\ell})^{-1}} \,, \tag{4.19}$$

where

$$\tilde{F}{}^{\ell} = [\tilde{L}{}^{\ell} - \frac{M_2^{\ell}}{\overset{\sim}{\lambda}{}^{\ell}(\tilde{L}{}^{\ell}) - a^{\ell} - \frac{b^{\ell}}{\overset{\sim}{\lambda}{}^{\ell}(\tilde{L}{}^{\ell})}}]^{-1}, \tag{4.20}$$

and $\overset{\sim}{\lambda}{}^{\ell}(\tilde{L}{}^{\ell})$ is obtained from eqs.(3.24), (3.26) and (3.27) by replacing ω by $\tilde{L}{}^{\ell}(\omega)$. The corresponding condition in the present calculation is eq.(4.17), which decides the

the essential features of the density of states. We can rewrite eq.(4.17) as

$$\frac{1}{\tilde{T}^{\alpha}} = \frac{c_A}{L_A - \tilde{a}^{\alpha} - \tilde{b}^{\alpha}(\tilde{T}^{\alpha})^{-1}} + \frac{c_B}{L_B - \tilde{a}^{\alpha} - \tilde{b}^{\alpha}(\tilde{T}^{\alpha})^{-1}} , \tag{4.21}$$

where $(\tilde{T}^{\alpha})^{-1} = c_A/T_A^{\alpha} + c_B/T_B^{\alpha}$. We can notice from eqs.(4.19) and (4.21) some similarity between the present approach and the CPA calculation; in the case of the s band on the Bethe lattice with z being infinite, eq.(4.21) is in practice reduced to eq.(4.19).[16]

We have mainly discussed the case of disordered alloys in this section. However, we can easily extend the present approach to the cases of alloys with short-range order[16] and those with long -range order, which enables us to discuss the ordering energy of alloys.[17, 18] In addition we can investigate directly the local environment effects.[19,20] We expect that the present approach may serve as useful tool for the problems of transition metal alloys, though we will not discuss such problems in this paper.

§ 5. Discussion and Summary

We discuss here the significance of the effective locators. The essential properties of the effective locators are, as mentioned before, not far from those of the s band one, which enbles us to express the effective locator in an approximate expression as

$$\tilde{\Lambda}^{\ell}(\omega) = \omega - \mu^{\ell} / \tilde{\Lambda}^{\ell}(\omega)$$

$$= (1/2)(\omega + \sqrt{\omega^2 - 4\mu^{\ell}}), \qquad (5.1)$$

where μ^{ℓ} is determined by the condition $M_{4B}^{\ell}=M_2^{\ell}\mu^{\ell}$. With this expression we obtain

$$\omega - \Sigma_B^{\ell}(\omega)= \tilde{\Lambda}^{\ell}(\omega) -(M_2^{\ell} - \mu^{\ell})/ \tilde{\Lambda}^{\ell}(\omega). \qquad (5.2)$$

Then $G_{00}^{\ell\ell}(\omega)$ is expressed as the expansion of $1/\tilde{\Lambda}^{\ell}(\omega)$;

$$G_{00}^{\ell\ell}(\omega)= [\tilde{\Lambda}^{\ell}(\omega) - (M_2^{\ell} -\mu^{\ell})/\tilde{\Lambda}^{\ell}(\omega)$$

$$- M_3^{\ell}/ (\tilde{\Lambda}^{\ell}(\omega))^2 - M_{4C}^{\ell}/(\tilde{\Lambda}^{\ell}(\omega))^3\cdots]^{-1}. \qquad (5.3)$$

The above discussion can be further extended to the case of disordered alloys discussed in § 4. We can express the effective locators in the same way as eq.(5.1) as

$$\tilde{\Lambda}^{\ell}_{\xi}(\omega) = L_{\xi}(\omega) - \mu^{\ell}(c_A/\tilde{\Lambda}^{\ell}_{A}(\omega) + c_B/\tilde{\Lambda}^{\ell}_{B}(\omega)). \qquad (5.4)$$

Similarly to eqs.(5.2) and (5.3), we obtain

$$L_{\xi}(\omega) - \langle\Sigma^{\ell}_{B}(\omega)\rangle = \tilde{\Lambda}^{\ell}_{\xi}(\omega) - (M^{\ell}_{2} - \mu^{\ell})(c_A/\tilde{\Lambda}^{\ell}_{A}(\omega) + c_B/\tilde{\Lambda}^{\ell}_{B}(\omega)), \qquad (5.5)$$

and

$$\langle G^{\ell\ell}_{00}(\omega)\rangle_{\xi} = [\tilde{\Lambda}^{\ell}_{\xi}(\omega) - (M^{\ell}_{2} - \mu^{\ell})\left(\frac{c_A}{\lambda^{\ell}_{A}(\omega)} + \frac{c_B}{\lambda^{\ell}_{B}(\omega)}\right) - M^{\ell}_{3}\left(\frac{c_A}{\lambda^{\ell}_{A}(\omega)} + \frac{c_B}{\lambda^{\ell}_{B}(\omega)}\right)^2 - M^{\ell}_{4C}\left(\frac{c_A}{\lambda^{\ell}_{A}(\omega)} + \frac{c_B}{\lambda^{\ell}_{B}(\omega)}\right)^3 - \cdots]^{-1} \qquad (5.6)$$

We can notice from eqs.(5.3) and (5.6) the correspondence between the present approach and the interacting virtual state approach. The effective locators $\lambda^{\ell}(\omega)$ and $\lambda^{\ell}_{\xi}(\omega)$ correspond to the locators of the virtual state with the resonance level being 0 and E_{ξ} respectively, and $(M^{\ell}_{2} - \mu^{\ell})$, M^{ℓ}_{3} and M^{ℓ}_{4C} correspond to the interactions among the virtual states. While the width of the virtual state in the original sence comes from the admixture with the conduction band[21], that of the effective locators comes from the band effect by the itinerancy of d electrons and depends on the

circumstances of the whole crystal. However, the crudest approximation may lead the width of the effective locators $\Delta(\omega)$ (where $\lambda^{\ell}(\omega) = \omega + i\Delta(\omega)$ or $\lambda^{\ell}_{\xi}(\omega) = L_{\xi}(\omega) + i\Delta(\omega)$) to a constant value, and hence lead the effective locators to the locators of the virtual state. Thus the interacting virtual state approach can be justified to be consistent with the band theory.

In this part we first elucidated the role of d symmetry of atomic orbitals, in determining the energy band and we develop a new method which is considerably simple in comparison with the moment method or the recursion method. It may be emphasized that the method yields a conceptual simplification; that is, the electronic structure of transition metals can be described with the effective locators and the interactions among the near neighboring effective locators. We can examine the effect of these interactions and investigate the origin of the difference between bcc and fcc. As a result, it is shown that the band width is decided by the effective locators, and that the feature characteristic of bcc and fcc structure is decided by the interactions among three or four sites.

We have mainly discussed the cases of nonmagnetic metals and alloys in this part. However, the application to other systems some of which we discussed in Introduction is straightforward after some modification and the argument based on the interactions among near neighboring sites will

be useful for these systems. Especially the application to amorphous metals seems to be very interesting. It may be possible that we parametrize the electronic structure of amorphous metals in terms of the three- and four-site interactions reflecting the local arrangement of atoms and the structure insensitive effective locators.

III. Magnetism in Transition Metals

§ 6. Review of Some Previous Attempts

Several attempts have been made to explain the systematic change of the magnetism in transition metals. There have been two streams in these attempts; one is based on the band theory in which the interactions between the Bloch electrons in the momentum space are discussed, the other is based on the picture of interacting local moments which was first suggested by Friedel, Leman and Olszewski.[22] Though the streams start from opposite points, they join into the same conclusion discussed below, which is easily realized from the above-mentioned discussion of the correspondence between the band theory and the atomic interaction models. Here we briefly review these attempts.

Moriya[1] treated the model which consists of two adjacent local moments in a metal. He pointed out that the sign of the interaction between two local moments is governed by the occupied fraction of the local orbitals. When the orbitals are nearly half-filled the coupling of two local moments is antiferromagnetic, and when the occupied or empty fraction of the orbitals are small the coupling is ferromagnetic. Following the band theory combined with the generalized Hartree-Fock approximation, Penn[23] studied the stability of a ferromagnetic state, an antiferromagnetic

state and some special type of states in the case of the s band on a simple cubic lattice. He found that ferromagnetism is found for those metals with a valence well away from five and that antiferromagnetism is found for a valence of around five. Asano and Yamashita[24] investigated the stability of ferromagnetic and antiferromagnetic states on the basis of a realistic energy band structure, and drew the same conclusion. They also found that the observed magnitude of local moments of each 3d metal can be reproduced with an almost unchanged value of the effective exchange interactions. Thus conclusions of these attempts have been rather similar to each other.

However, most of the discussions have been restricted within ferromagnetism and antiferromagnetism whose spatial variation is described by the wave vector $\vec{Q}=\vec{0}$ and $\vec{Q}=\vec{K}/2$ ($\vec{K}$: reciprocal lattice vector) respectively. Therefore the stability of a ferromagnetic state itself or that of an antiferromagnetic one with respect to a general $\vec{Q}$ state has not been investigated. In this connection, Roth[25] discussed a state with disordered local moments besides a ferromagnetic state and an antiferromagnetic one by use of CPA. Similarly fictitious short-range ordered states where each local moment may point up or down was discussed by Liu[26] for the case of the s band on the Bethe lattice. They both found that the above-mentioned conclusion holds true, and also that the state with disordered local moments or the short-range ordered states can be stable in an intermediate

region between a ferromagnetic region and an antiferromagnetic one. We expect that such disordered state and short-range ordered states may be replaced by the long-range ordered state with $\vec{Q} \neq \vec{0}$ and $\vec{Q} \neq \vec{K}/2$. We can mention helical, conical and sinusoidal SDW states as the example of the state characterized by a general $\vec{Q}$, of which a sinusoidal SDW state is observed experimentally in chromium and its alloys. Thus such states characterized by general $\vec{Q}$ should be included in the discussion of the magnetism in transition metals.

In the next section we present a model Hamiltonian in which a ferromagnetic state, an antiferromagnetic one, a state with a general $\vec{Q}$ and also disordered states are equaly treated within the Hartree-Fock approximation.

§ 7. Model Hamiltonian

Assuming that d electrons are principally responsible for the magnetism in transition metals, we adopt a tight binding model in which only the five atomic d orbitals are taken into account. The Hamiltonian is assumed to be given by

$$H = \sum_i W_i + V \,, \tag{7.1}$$

with

$$W_i = \sum_m \sum_\sigma E_d a^*_{im\sigma} a_{im\sigma} + U \sum_{m,n} a^*_{im\uparrow} a_{im\uparrow} a^*_{in\downarrow} a_{in\downarrow}$$

$$+ \frac{1}{2} (U-J) \sum_{\substack{m,n \\ (m\neq n)}} \sum_\sigma a^*_{im\sigma} a_{im\sigma} a^*_{in\sigma} a_{in\sigma}$$

$$- \frac{1}{2} J \sum_{\substack{m,n \\ (m\neq n)}} \sum_\sigma a^*_{im\sigma} a_{im-\sigma} a^*_{in-\sigma} a_{in\sigma} \,, \tag{7.2}$$

and

$$V = \sum_{i,j} \sum_{m,n} \sum_\sigma t^{mn}_{ij} a^*_{im\sigma} a_{jn\sigma} \,, \tag{7.3}$$

where σ denotes the spin state. The atomic energy level is denoted by E_d, the intra-atomic Coulomb and exchange

integrals are denoted by U and J respectively. Other notations are same as those in eq.(1.1).

We next apply the Hartree-Fock approximation to W_i with due consideration for the spin rotational invariance of W_i. Then we obtain

$$W_i^{HF} = \sum_m \sum_\sigma E_{im\sigma} c^*_{im\sigma} c_{im\sigma}$$

$$- U \sum_{m,n} \langle c^*_{im\uparrow} c_{im\uparrow} \rangle \langle c^*_{in\downarrow} c_{in\downarrow} \rangle$$

$$- \frac{1}{2}(U-J) \sum_{\substack{m,n \\ (m \neq n)}} \sum_\sigma \langle c^*_{im\sigma} c_{im\sigma} \rangle \langle c^*_{in\sigma} c_{in\sigma} \rangle , \qquad (7.4)$$

with

$$E_{im\sigma} = E_d + U \sum_n \langle c^*_{in-\sigma} c_{in-\sigma} \rangle + (U-J) \sum_{n(\neq m)} \langle c^*_{in\sigma} c_{in\sigma} \rangle , \qquad (7.5)$$

where $c^*_{im\sigma}$ and $c_{im\sigma}$ are electron operators referred to the local spin quantization axis parallel to the direction of the local magnetic moment of a given atom. On the other hand $a^*_{im\sigma}$ and $a_{im\sigma}$ in the eqs.(7.2) and (7.3) are referred to a common quantization axis denoted by the laboratory z axis. When the local spin axis on the i-th site is rotated by the polar angle θ_i and the azimuthal angle ψ_i with

respect to the laboratory z axis, the relation between $a_{im\sigma}$ and $c_{im\sigma}$ is given by

$$\begin{pmatrix} c_{im\uparrow} \\ \\ c_{im\downarrow} \end{pmatrix} = \begin{pmatrix} e^{\frac{i}{2}\psi_i}\cos\frac{\theta_i}{2} & e^{-\frac{i}{2}\psi_i}\sin\frac{\theta_i}{2} \\ \\ -e^{\frac{i}{2}\psi_i}\sin\frac{\theta_i}{2} & e^{\frac{i}{2}\psi_i}\cos\frac{\theta_i}{2} \end{pmatrix} \begin{pmatrix} a_{im\uparrow} \\ \\ a_{im\downarrow} \end{pmatrix} \equiv R(\theta_i,\psi_i) \begin{pmatrix} a_{im\uparrow} \\ \\ a_{im\downarrow} \end{pmatrix}. \tag{7.6}$$

By this relation eq.(7.4) is rewritten as

$$W_i^{HF} = \sum_{m\sigma,\sigma'} (E_{im})_{\sigma\sigma'} a^*_{im\sigma} a_{im\sigma'} \tag{7.7}$$

- (the term corresponding to the double counting) ,

where

$$(E_{im}) = \begin{pmatrix} \cos^2\frac{\theta_i}{2} E_{im\uparrow} + \sin^2\frac{\theta_i}{2} E_{im\downarrow} & -\frac{1}{2}\sin\theta_i\, e^{-i\psi_i}(E_{im\uparrow}-E_{im\downarrow}) \\ \\ \frac{1}{2}\sin\theta_i\, e^{i\psi_i}(E_{im\uparrow}-E_{im\downarrow}) & \sin^2\frac{\theta_i}{2}E_{im\uparrow} + \cos^2\frac{\theta_i}{2}E_{im\downarrow} \end{pmatrix} \tag{7.8}$$

We define the Green function in the laboratory frame by

$$(G_{ij}^{mn}(\omega))_{\sigma\sigma'} = <im\sigma|(\omega - H^{HF})^{-1} |jn\sigma'> , \qquad (7.9)$$

with $H^{HF} = \sum_i W_i^{HF} + V$. The matrix elements of H^{HF} are given by

$$<im\sigma| H^{HF}| in\sigma'> = \delta_{mn}(E_{im})_{\sigma\sigma'}$$

$$<im\sigma| H^{HF}| jn\sigma'> = t_{ij}^{mn} \delta_{\sigma\sigma'} . \qquad (7.10)$$

The expectation value $<c_{im\sigma}^{*} c_{im\sigma}>$ is determined self-consistently by the condition

$$<c_{im\sigma}^{*} c_{im\sigma}> = (\frac{-1}{\pi} \mathrm{Im}) \int^{E_F} d\omega (R(\theta_i,\psi_i) G_{ii}^{mm}(\omega) R(\theta_i,\psi_i)^{-1})_{\sigma\sigma} .$$

(7.11)

The number of d electrons on the i-th site and the magnitude of the local moment on the i-th site are given by

$$N_i = \sum_m (< c_{im\uparrow}^{*} c_{im\uparrow}> + <c_{im\downarrow}^{*} c_{im\downarrow}>)$$

$$M_i = \sum_m (< c_{im\uparrow}^{*} c_{im\uparrow}> - <c_{im\downarrow}^{*} c_{im\downarrow}>). \qquad (7.12)$$

In the following discussion we neglect the orbital difference of $\langle c^*_{im\sigma} c_{im\sigma} \rangle$ in eqs.(7.4) and (7.5) for the sake of simplicity, and we substitute $\langle c^*_{i\sigma} c_{i\sigma} \rangle$ for $\langle c^*_{im\sigma} c_{im\sigma} \rangle$, where

$$\langle c^*_{i\sigma} c_{i\sigma} \rangle \equiv \frac{1}{5} \sum_m \langle c^*_{im\sigma} c_{im\sigma} \rangle \quad . \tag{7.13}$$

Then $E_{im\sigma}$ is reduced to $E_{i\sigma}$ which is defined by

$$E_{i\sigma} = E_d + 5U \langle c^*_{i-\sigma} c_{i-\sigma} \rangle + 4(U-J) \langle c^*_{i\sigma} c_{i\sigma} \rangle$$

$$= E_d + \frac{9U-4J}{10} N_i - \sigma \frac{U+4J}{10} M_i \quad , \tag{7.14}$$

irrespective of m.

In the case of ferromagnetic, antiferromagnetic, helical SDW and paramagnetic states, there is no spatial variation of the charge or the magnitude of local moments. Thus we can impose the conditions

$$N_i = N_0 \equiv N_d \quad , \; M_i = M_0 \equiv M, \; \langle c^*_{i\sigma} c_{i\sigma} \rangle = \langle c^*_{0\sigma} c_{0\sigma} \rangle \equiv \langle c^*_\sigma c_\sigma \rangle$$

and $E_{i\sigma} = E_{0\sigma} \equiv E_\sigma$ irrespective of i. (7.15)

The spatial variation of the directions of local moments which distinguishes the above-mentioned states from each other is characterized by the set of (θ_i, ψ_i). In the next section we discuss the method for calculating $G_{00}^{\ell\ell}(\omega)$ of ferromagnetic, antiferromagnetic, helical SDW and paramagnetic states.

§ 8. Real Space Approach Applied to Magnetic States

We define the locator matrix $g_i(\omega)$ by

$$g_i(\omega)=\begin{pmatrix} \cos^2\frac{\theta_i}{2}L_\uparrow^{-1} + \sin^2\frac{\theta_i}{2}L_\downarrow^{-1} & \frac{1}{2}\sin\theta_i e^{-i\psi_i}(L_\uparrow^{-1}-L_\downarrow^{-1}) \\ \frac{1}{2}\sin\theta_i e^{i\psi_i}(L_\uparrow^{-1}-L_\downarrow^{-1}) & \sin^2\frac{\theta_i}{2}L_\uparrow^{-1}+\cos^2\frac{\theta_i}{2}L_\downarrow^{-1} \end{pmatrix}, \tag{8.1}$$

with $L_\sigma(\omega)=\omega - E_\sigma$. The locator expansion of $G_{00}^{\ell\ell}(\omega)$ is given by

$$G_{00}^{\ell\ell}(\omega)= [g_0^{-1} - \sum_{i,m} t_{0i}^{\ell m} g_i t_{i0}^{m\ell} - \sum_{i,m}\sum_{j,n} t_{0i}^{\ell m} g_i t_{ij}^{mn} g_j t_{j0}^{n\ell} - \cdots]^{-1}, \tag{8.2}$$

where the sums are taken over the irreducible paths. As is done in §3, we first divide the whole self-energy matrix into two parts; that is,

$$G_{00}^{\ell\ell}(\omega) = [g_0^{-1} - \Sigma^\ell(\omega)]^{-1}=[g_0^{-1} - \Sigma_B^\ell(\omega) - \Sigma_C^\ell(\omega)]^{-1}. \tag{8.3}$$

where the dominant part $\Sigma_B^\ell(\omega)$ consists of the paths which one goes to a lattice site without making a loop and traces back the same way, and $\Sigma_C^\ell(\omega)$ corresponds to the remainder.

We next define the effective locator matrix $\tilde{\Lambda}^{\ell}(\omega)$ which includes $\Sigma_B^{\ell}(\omega)$. $\Sigma_B^{\ell}(\omega)$ and thus the effective locator can be calculated to the infinite order of electron transfers, though approximately, since $\Sigma_B^{\ell}(\omega)$ has a close resemblance to the self-energy of the Bethe lattice. We finally derive an approximate expression of $G_{00}^{\ell\ell}(\omega)$ in terms of $\tilde{\Lambda}^{\ell}(\omega)$ so that the whole self-energy $\Sigma^{\ell}(\omega)$ may be correctly reproduced up to $1/\omega^3$.

We discuss the further details of the method for each case; that is, ferromagnetic, antiferromagnetic, helical SDW and paramagnetic cases.

§8-1. Ferromagnetic state

A ferromagnetic state is described by the conditions $\theta_i = \theta_0$ and $\psi_i = \psi_0$ irrespective of i, which can be put to $\theta_0 = 0$ and $\psi_0 = 0$ without the loss of generality. Then the self-energy matrix is reduced to

$$\Sigma^{\ell}(\omega) = \begin{pmatrix} \Sigma_{\uparrow}^{\ell}(\omega) & 0 \\ 0 & \Sigma_{\downarrow}^{\ell}(\omega) \end{pmatrix} = \begin{pmatrix} \Sigma_{B\uparrow}^{\ell}(\omega) + \Sigma_{C\uparrow}^{\ell}(\omega) & 0 \\ 0 & \Sigma_{B\downarrow}^{\ell}(\omega) + \Sigma_{C\downarrow}^{\ell}(\omega) \end{pmatrix} , \tag{8.4}$$

where

$$\Sigma_{B\sigma}^{\ell}(\omega) = M_2^{\ell} / L_{\sigma} + M_{4B}^{\ell} / L_{\sigma}^3 + \cdots$$

$$\Sigma_{C\sigma}^{\ell}(\omega) = M_3^{\ell} / L_{\sigma}^2 + M_{4C}^{\ell} / L_{\sigma}^3 + \cdots . \tag{8.5}$$

The procedure to obtain the expression of $\Sigma_\sigma^\ell(\omega)$ is quite identical with that in the nonmagnetic case which was discussed in §3, except that ω is replaced by $L_\sigma(\omega)$. As a result, we obtain

$$\Sigma_\sigma^\ell(\omega) = M_2^\ell / [\, \tilde{\Lambda}_\sigma^\ell(\omega) - a^\ell - b^\ell / \tilde{\Lambda}_\sigma^\ell(\omega)\,], \tag{8.6}$$

where the effective locator is defined by

$$\Sigma_{B\sigma}^\ell(\omega) = M_2^\ell / \tilde{\Lambda}_\sigma^\ell(\omega) \ . \tag{8.7}$$

The Bethe-like part $\Sigma_{B\sigma}^\ell(\omega)$ is expressed in terms of the average locator $\Lambda_\sigma^\alpha(\omega)$ for the orbital belonging to an irreducible representation α. In order to simplify the calculation particularly for the helical SDW case, we adopt a simplified expression of $\Lambda_\sigma^\alpha(\omega)$ discussed in §3, which is given by

$$\Lambda_\sigma^\alpha(\omega) = L_\sigma(\omega) - \tilde{\mu}^\alpha / T_\sigma^\alpha(\omega) \ , \tag{8.8}$$

where

$$\begin{aligned} T_\sigma^\alpha(\omega) &= L_\sigma(\omega) - \tilde{a}^\alpha - \tilde{b}^\alpha / T_\sigma^\alpha(\omega) \\ &= (1/2)[(L_\sigma(\omega) - \tilde{a}^\alpha) + \sqrt{(L_\sigma(\omega) - \tilde{a}^\alpha)^2 - 4\tilde{b}^\alpha}]. \end{aligned} \tag{8.9}$$

We furthermore adopt a simplified expression of $\Sigma^{\ell}_{B\sigma}(\omega)$, then we obtain

$$\tilde{\Lambda}^{\ell}_{\sigma}(\omega) = \sum_{\alpha} M_2^{\ell}(\alpha)\Lambda^{\alpha}_{\sigma}(\omega) \;/\; M_2^{\ell} \quad . \tag{8.10}$$

The definitions of the parameters $\tilde{\mu}^{\alpha}$, $\tilde{a}^{\alpha}$, $\tilde{b}^{\alpha}$ and $M_2^{\ell}(\alpha)$ are referred to §3.

§8-2. Helical SDW and antiferromagnetic states

A helical SDW state is described by the conditions $\theta_i = \vec{Q}\,\vec{R}_i + \delta$ and $\psi_i = \psi_0$ irrespective of i. An antiferromagnetic state and also a ferromagnetic one correspond to the special types of helical SDW states with $\vec{Q} = \vec{K}/2$ and $\vec{Q} = \vec{0}$ respectively. We choose $\delta = 0$ so that θ_0 may equals to 0, and choose $\psi_0 = 0$. We obtain again the expression (8.4) for the self-energy matrix, since both bcc and fcc lattices have the inversion symmetry. We can write $\Sigma^{\ell}_{\sigma}(\omega)$ as

$$\Sigma_\sigma^\ell(\omega)=\sum_{i,m} t_{0i}^{\ell m}\, t_{i0}^{m\ell}\,\frac{1}{2}[(1+A_i)/L_\sigma + (1-A_i)/L_{-\sigma}]$$

$$+ \sum_{i,m}\sum_{j,n} t_{0i}^{\ell m}\, t_{ij}^{mn}\, t_{j0}^{n\ell}\,\frac{1}{4}[(1+A_{ij}+B_{ij})/L_\sigma^{\,2}+(2-2B_{ij})/(L_\sigma L_{-\sigma})$$

$$+ (1-A_{ij}+B_{ij})/L_{-\sigma}^{\,2}]$$

$$+ \sum_{i,mj,n}\sum_{k,p} t_{0i}^{\ell m}\, t_{ij}^{mn}\, t_{jk}^{np}\, t_{k0}^{p\ell}\,\frac{1}{8}[(1+A_{ijk}+B_{ijk}+C_{ijk})/L_\sigma^{\,3}$$

$$+ (3+A_{ijk}-B_{ijk}-3C_{ijk})/(L_\sigma^{\,2}L_{-\sigma})+(3-A_{ijk}-B_{ijk}+3C_{ijk})/(L_\sigma L_{-\sigma}^{\,2})$$

$$+ (1 - A_{ijk}+B_{ijk}-C_{ijk})/L_{-\sigma}^{\,3}] + \cdots$$

$$= (M_{21}^\ell/L_\sigma + M_{22}^\ell/L_{-\sigma}) + (M_{31}^\ell/L_\sigma^{\,2}+M_{32}^\ell/(L_\sigma L_{-\sigma})+M_{33}^\ell/L_{-\sigma}^{\,2})$$

$$+ \cdots \quad , \tag{8.11}$$

where

$$A_i = \cos\theta_i,\ A_{ij} = \cos\theta_i + \cos\theta_j,\ A_{ijk} = \cos\theta_i + \cos\theta_j + \cos\theta_k,$$

$$B_{ij} = \cos(\theta_i - \theta_j),\ B_{ijk} = \cos(\theta_i - \theta_j) + \cos(\theta_j - \theta_k) + \cos(\theta_k - \theta_i),$$

$$C_{ijk} = \cos(\theta_i - \theta_j + \theta_k),\ \cdots\ , \qquad (8.12)$$

and

$$M_{21}^{\ell} = \sum_{i,m} t_{0i}^{\ell m}\, t_{i0}^{m\ell}\, \frac{1}{2}(1+A_i),\ M_{22}^{\ell} = \sum_{i,m} t_{0i}^{\ell m}\, t_{i0}^{m\ell}\, \frac{1}{2}(1 - A_i),$$

$$M_{31}^{\ell} = \sum_{i,m}\sum_{j,n} t_{0i}^{\ell m}\, t_{ij}^{mn}\, t_{j0}^{n\ell}\, \frac{1}{4}(1+A_{ij}+B_{ij}),\ \cdots\ . \qquad (8.13)$$

We define the effective locators $\tilde{\Lambda}_{\uparrow}^{\ell}(\omega)$ and $\tilde{\Lambda}_{\downarrow}^{\ell}(\omega)$ by

$$\Sigma_{B\sigma}^{\ell}(\omega) = M_{21}^{\ell}/\tilde{\Lambda}_{\sigma}(\omega) + M_{22}^{\ell}/\tilde{\Lambda}_{-\sigma}^{\ell}(\omega)\ . \qquad (8.14)$$

Since an electron can be transferred from the σ state of an ion to the $-\sigma$ state of adjacent ions, the expression of $\Sigma_{\sigma}^{\ell}(\omega)$ corresponding to eq.(8.6) should be modified to include both $\tilde{\Lambda}_{\sigma}^{\ell}(\omega)$ and $\tilde{\Lambda}_{-\sigma}^{\ell}(\omega)$. We choose the expression given by

$$\Sigma_\sigma^\ell(\omega)=M_2^\ell/[(\frac{p^\ell}{\tilde{\Lambda}_\sigma^\ell(\omega)}+\frac{1-p^\ell}{\tilde{\Lambda}_{-\sigma}^\ell(\omega)})^{-1}-a^\ell-b_\sigma^\ell(\frac{\tilde{p}_\sigma^\ell}{\tilde{\Lambda}_\sigma^\ell(\omega)}+\frac{1-\tilde{p}_\sigma^\ell}{\tilde{\Lambda}_{-\sigma}^\ell(\omega)})], \tag{8.15}$$

where $p^\ell = M_{21}^\ell/M_2^\ell$ and $1 - p^\ell = M_{22}^\ell/M_2^\ell$ representing the relative ratio between the transfer from the σ state of the central atom to the σ state and $-\sigma$ one of neighboring atoms, respectively; $a^\ell=(M_{31}^\ell+M_{32}^\ell+M_{33}^\ell)/M_2^\ell$ which is independent of θ_i's; $b_\sigma^\ell\,\tilde{p}_\sigma^\ell$ and $b_\sigma^\ell\,(1-\tilde{p}_\sigma^\ell)$ represent the weights of going to the σ state and $-\sigma$ one in the second step which are to be determined so as to be consistent with the expansion (8.3) up to $1/\omega^3$ in principle. For the ferromagnetic state, the antiferromagnetic state in bcc with the nearest neighbor transfer only and the paramagnetic state with randomly oriented local moments which will be discussed below, we can show that the choices $b_\sigma^\ell = \sum_i M_{4iC}^\ell/M_2^\ell - (a^\ell)^2$ and $\tilde{p}_\sigma^\ell$ corresponding to the probability of finding a neighboring atom with parallel moment can reproduce the expansion (8.11) up to the order of $1/L_\sigma^3$, $1/(L_\sigma^2 L_{-\sigma})$, $1/(L_\sigma L_{-\sigma}^2)$ and $1/L_{-\sigma}^3$. For a general $\vec{Q}$, however, we cannot achieve the consistency in the expansion in terms of $1/L_\sigma$ and $1/L_{-\sigma}$. Thus we reexpand both $1/L_{\pm\sigma}$ and $1/\tilde{\Lambda}_{\pm\sigma}^\ell(\omega)$ up to the order of $1/\omega^2$ to achieve the consistency to that order within M_2^ℓ, M_3^ℓ and M_4^ℓ. We obtain then

$$b_\sigma^\ell = [M_{4C}^\ell / M_2^\ell - (a^\ell)^2] + (E_{-\sigma} - E_\sigma)[-M_{31}^\ell + M_{33}^\ell + M_3^\ell(2p^\ell - 1)]/M_2^\ell$$

$$\tilde{p}_\sigma^\ell = p^\ell - \{(E_{-\sigma} - E_\sigma)[M_{31}^\ell(9 - 12p^\ell) + M_{32}^\ell + M_{33}^\ell(-3 + 12p^\ell)$$

$$+ M_3^\ell(20p^\ell(p^\ell - 1) + 3)]$$

$$+ 2[-3M_{41C}^\ell - M_{42C}^\ell + M_{43C}^\ell + 3M_{44C}^\ell + 3M_{4C}^\ell(2p^\ell - 1)]\}/(4M_2^\ell b_\sigma^\ell) \ , \qquad (8.16)$$

which are free of the terms proportional to $(E_\sigma - E_{-\sigma})$ in the cases mentioned above, i.e, the ferromagnetic one, etc. (the details are discussed in Appendix A).

In order to calculate $\lambda_\sigma^\ell(\omega)$, we need to treat the self-energy on the Bethe lattice, introducing the average locators as before. The average locators denoted by $\Lambda_\sigma^\alpha(\omega)$ previously can now have off-diagonal elements between σ and $-\sigma$ in principle for a general $\hat{Q}$, since no symmetry argument can be invoked to suppress them. We assume in the following argument, however that the average locators are diagonal with repect to σ, since the off-diagonal contribution is expected to be the order of $1/z^2$ compared with the diagonal contribution, where z is the coordination

number of a given lattice*. We assume that the average locator is given by

$$\Lambda_\sigma^\alpha(\omega) = L_\sigma(\omega) - \tilde{\mu}_1^\alpha / T_\sigma^\alpha(\omega) - \tilde{\mu}_2^\alpha / T_{-\sigma}^\alpha(\omega) , \qquad (8.17)$$

$$T_\sigma^\alpha(\omega) = L_\sigma(\omega) - \tilde{a}^\alpha - \tilde{b}_1^\alpha / T_\sigma^\alpha(\omega) - \tilde{b}_2^\alpha / T_{-\sigma}^\alpha(\omega) , \qquad (8.18)$$

where $\tilde{a}^\alpha$ is the same as that in the case of the ferromagnetic state (see eq.(8.9) and following discussion) and $\tilde{\mu}_1^\alpha$, $\tilde{\mu}_2^\alpha$, $\tilde{b}_1^\alpha$ and $\tilde{b}_2^\alpha$ are defined by use of $\tilde{\mu}^\alpha$ and $\tilde{b}^\alpha$ defined previously as

$$\tilde{\mu}_1^\alpha = \tilde{\mu}^\alpha \cdot M_{21}^\ell / M_2^\ell , \quad \tilde{\mu}_2^\alpha = \tilde{\mu}^\alpha \cdot M_{22}^\ell / M_2^\ell , \qquad (8.19)$$

---

* As was discussed in §3, the average locator includes the self-energy arising from the interaction with (z-1) atoms. If we add the contribution from one missing neighbors, the self-energy can recover the full symmetry of lattice which eliminates the off-diagonal part. The estimate mentioned in the text is based on this fact.

and

$$\tilde{b}_1^{\alpha} = \tilde{b}^{\alpha}(M_{41B}^{\ell}+M_{44B}^{\ell})/M_{4B}^{\ell} \ , \ \tilde{b}_2^{\alpha} = \tilde{b}^{\alpha}(M_{42B}^{\ell}+M_{43B}^{\ell})/M_{4B}^{\ell}, \tag{8.20}$$

where ℓ stands for $\ell\epsilon\alpha$. With $\Lambda_{\sigma}^{\alpha}(\omega)$ thus defined we calculate $\tilde{\Lambda}_{\sigma}^{\ell}(\omega)$ by use of eq.(8.14), which is reduced to eq.(8.10) by adopting a simplified expression of $\Sigma_{B\sigma}^{\ell}(\omega)$. We show in Figs. 14 and 15 some examples of the density of states of helical SDW states.

The expression (8.15) can lead us to a pathological negative density of states for $\vec{Q}\neq\vec{0}$ in a certain region of energy, if $|E_{\sigma} - E_{-\sigma}|$ exceeds a critical value, i.e. when the magnitude of local magnetic moment becomes large particularly in the antiferromagnetic case of fcc. A conceivable origin of this fault may lie in eq.(8.16). It is possible to use in place of eq.(8.15) an alternative expression which is free from this fault, though its derivation involves an arbitrary assumption (refer to Appendix A). It turns out, however, that the calculated density of states, energy and magnitude of local moment depend little on the choice of the self-energy expression.

§ 8-3. Paramagnetic state with randomly oriented local moments

Though the paramagnetic state with randomly oriented local moments is never of lowest energy in the present calculation, we mention it for the purpose of discussing the ordering energy and hence the transition temperature of an ordered state. In the paramagnetic case the self-energy matrix is reduced to

$$\Sigma^{\ell}(\omega) = \Sigma^{\ell}_{\text{para}}(\omega)\begin{pmatrix} 1 & 0 \\ 0 & 1 \end{pmatrix} , \tag{8.21}$$

and $\Sigma^{\ell}_{\text{para}}(\omega)$ is written as

$$\begin{aligned}\Sigma^{\ell}_{\text{para}}(\omega) = {} & M^{\ell}_{2}\,\frac{1}{2}(1/L_{\uparrow} + 1/L_{\downarrow}) + M^{\ell}_{3}\,\frac{1}{4}(1/L_{\uparrow} + 1/L_{\downarrow})^{2} \\ & + M^{\ell}_{4B}\,\frac{1}{4}(1/L_{\uparrow}^{2} + 1/L_{\downarrow}^{2})(1/L_{\uparrow} + 1/L_{\downarrow}) \\ & + M^{\ell}_{4C}\,\frac{1}{8}(1/L_{\uparrow} + 1/L_{\downarrow})^{3} + \cdots .\end{aligned} \tag{8.22}$$

The expression of $\Sigma^{\ell}_{\text{para}}(\omega)$ is easily derived from eqs.(8.15) and (8.16) as

$$\Sigma^{\ell}_{\text{para}}(\omega) = M^{\ell}_{2}/\left[\left(\frac{1/2}{\tilde{\Lambda}^{\ell}_{\uparrow}(\omega)} + \frac{1/2}{\tilde{\Lambda}^{\ell}_{\downarrow}(\omega)}\right)^{-1} - a^{\ell} - b^{\ell}\left(\frac{1/2}{\tilde{\Lambda}^{\ell}_{\uparrow}(\omega)} + \frac{1/2}{\tilde{\Lambda}^{\ell}_{\downarrow}(\omega)}\right)\right], \tag{8.23}$$

where the effective locator is given by eq.(8.10), and the average locator is obtained from eqs.(8.17) and (8.18) with

$$\tilde{\mu}_1^{\alpha} = \tilde{\mu}_2^{\alpha} = \frac{1}{2}\tilde{\mu}^{\alpha} \quad \text{and} \quad \tilde{b}_1^{\alpha} = \tilde{b}_2^{\alpha} = \frac{1}{2}\tilde{b}^{\alpha} \; . \tag{8.24}$$

Thus one can notice by replacing E_{σ} and $E_{-\sigma}$ by E_A and E_B that the paramagnetic state coincides with the state of a disordered alloy with $c_A=c_B=1/2$ in the present calculation.

§ 9. Unenhanced Susceptibility

Before proceeding to the presentation of the results of calculation, we compare here the calculation of the unenhanced susceptibility in the nonmagnetic state based on the present method with a more orthodox calculation based on the band structure calculation. The purpose of the discussion is to demonstrate the reliability of the present method which has been so far tested in the calculation of the density of states only.

The unenhanced susceptibility[24,27] is usualy calculated by using the Lindhard expression

$$\chi(\vec{Q}) = 2\mu_B^2 \sum_{\vec{k},\mu}^{occ} \sum_{\nu} \frac{\left| \sum_m C^*_{\mu m}(\vec{k}) C_{\nu m}(\vec{k}+\vec{Q}) \right|^2}{E^{\nu}_{\vec{k}+\vec{Q}} - E^{\mu}_{\vec{k}}} , \qquad (9.1)$$

(μ_B: the Bohr magneton)

where the summation $\sum_{\vec{k},\mu}^{occ}$ is taken over the occupied state, $E^{\mu}_{\vec{k}}$ is the energy eigenvalue of the $(\vec{k},\mu)$ Bloch state, and $C_{\mu m}(\vec{k})$ is the hybridization coefficient of the m-th d orbitals of the $(\vec{k},\mu)$ Bloch state. On the other hand, we can relate $\chi(\vec{Q})$ to the Green function by

$$\chi(\vec{Q}) = (-2\mu_B/\pi)\,\mathrm{Im} \int^{E_F} d\omega [\partial G^{\ell\ell}_{00}(\omega, \vec{Q}, h)/\partial h]_{h=0}, \qquad (9.2)$$

where $G(\omega, \vec{Q}, h)$ is the Green function of a helical SDW state with a wave vector $\vec{Q}$ under the condition $E_\sigma = -\sigma\mu_B h$. Thus the method developed so far for the Green function can be applied to the calculation of $\chi(\vec{Q})$.

In Figs. 16(a) and 17(a), we show $\chi(\vec{Q})$ of bcc and fcc transition metals obtained by evaluating the summation in the expression (9.1) for various $\vec{Q}$ corresponding to ferromagnetic, antiferromagnetic and helical SDW states. Here we confine ourselves to the case $\vec{Q} = 2/a(0,0,Q)$ (a: lattice constant). For the evaluation, the eigenvalues and the eigenvectors were calculated at 3311 points for bcc and at 3345 points for fcc in the irreducible 1/48 Brillouin zone. Corresponding $\chi(\vec{Q})$ by our method is shown in Figs. 16(b) and 17(b). We may conclude from Figs.16 and 17 that our calculation can reproduce well the band structure calculation for the unenhanced susceptibility (note that the density of states corresponds to $\chi(\vec{0})$).

As is well known, the SDW state with a wave vector $\vec{Q}_0$ is the most favorable state to occur when $\chi(\vec{Q})$ has the maximum value at $\vec{Q}_0$, though the discussion is restricted to infinitesimal moments. We can find from Fig.16 and 17 that $\chi(\vec{0})$ is maximum near the end of band and that $\chi(\vec{K}/2)$ is maximum around the middle of band, which is naturally expected. We can also find that $\chi(\vec{Q})$ of a general $\vec{Q}$ can be maximum in an intermediate region. We calculate $\chi(Q)$ of several values of Q, and investigate the region in which

$\chi(Q)$ of a general Q is maximum, in other words, $Q_0 \neq 0$ and $Q_0 \neq \pi$, which is shown in Figs.16 and 17. In the case of bcc we also calculate $\chi(Q)$ of Q being close to π (in practice, $Q/\pi = 36/40$, $37/40$, $38/40$ and $39/40$) for the purpose of investigating the nesting mechanism which have been discussed to explain the sinusoidal SDW of chromium as arising from its characteristic Fermi surface.[28,29] We find the region in which $\chi(Q)$ of $Q \sim \pi$ is maximum by the band structure calculation but not by our method (see Fig. 18). The disagreement between the band structure calculation and our method is naturally expected by considering that our method is a real space approach which does not involve any knowledge of Fermi surface. We show in Fig.16 (a) the region $Q_0 \sim \pi$ separately from the region $Q_0 \neq 0$, $\neq \pi$, though the region $Q_0 \sim \pi$ ought to be included in the region $Q_0 \neq 0$, $\neq \pi$, since these two regions are different from each other as to the mechanism how $\chi(Q)$ of a general Q is maximum.

We discuss here another mechanism than the nesting one which is an analogy of the mechanism in the case of insulator helical magnet.[30,31] We introduce the non-local susceptibility[32] which is defined as follows;

$$\chi_{ij} = (\delta m_i / h_j)_{h_j \to 0} , \qquad (9.3)$$

where δm_i represents the induced moment on the i-th site when a magnetic field h_j is applied locally at the j-th

site. Denoting the Green function of a nonmagnetic state by $\bar{G}(\omega)$, we can obtain

$$\chi_{ij} = (2\mu_B{}^2/\pi)\mathrm{Im}\int^{E_F} d\omega \sum_{m,n} \bar{G}_{ij}^{mn}(\omega)\cdot \bar{G}_{ji}^{nm}(\omega). \qquad (9.4)$$

In terms of χ_{ij}, the unenhanced susceptibility is expressed as

$$\chi(\vec{Q}) = \sum_j \chi_{0j} \exp(i\vec{Q}\vec{R}_j), \qquad (9.5)$$

where R_j is the lattice vector of the j-th site. The local term in eq.(9.5), χ_{00}, is responsible for the appearance of the local moment at the origin[22] and is identical to the unenhanced susceptibility of a paramagnetic state with randomly oriented local moments. Another terms than χ_{00}, on the other hand, responsible for the formation of an ordered state.

In the case of bcc, eq.(9.5) is rewritten as

$$\chi(Q) = \chi_{00} + 8\cos Q\, \chi_{0(111)} + (4+2\cos 2Q)\chi_{0(200)} + (4+8\cos 2Q)\, \chi_{0(220)} + 8\cos 2Q\, \chi_{0(222)} + \cdots, \qquad (9.6)$$

by taking $\vec{Q}=2/a(0,0,Q)$. If the higher terms than $\chi_0(222)$ are neglected, the optimum value Q_0 can be solved as

$$Q_0=\begin{cases} 0 & \chi_{0(111)}>0,\ \chi_R> -\chi_{0(111)} \\ \cos^{-1}(-\chi_{0(111)}/\chi_R) \text{ for} & \chi_R<0\ ,\ -\chi_R>|\chi_{0(111)}| \\ \pi & \chi_{0(111)}<0,\ \chi_R>\chi_{0(111)}\ , \end{cases} \tag{9.7}$$

where $\chi_R=\chi_{0(200)}+4\chi_{0(220)}+4\chi_{0(222)}$. In the case of fcc, $\chi_{0(111)}$ is replaced by $\chi_{0(110)}+2\chi_{0(211)}$, and χ_R stands for $\chi_{0(200)}+4\chi_{0(211)}+4\chi_{0(220)}$. In Figs. 19 and 20, we show $\chi_{0\delta}$ calculated by our method, the details of which we discuss in Appendix B, and show the each region obtained by eq.(9.7). It is found that the obtained regions coincide almost with the corresponding regions in Figs.16 and 17. Therefore we can say that $\chi(Q)$ is expected to have the maximum value at a general Q when $|\chi_{0(111)}|$ is sufficiently small and χ_R is negative. In other words, the unenhanced susceptibility is governed by the effective interaction among near neighboring sites, which is consistent with the general conclusion given in §3.

Though the discussion based on the unenhanced susceptibility is principally restricted to infinitesimal moments,

we expect that the discussion holds true even when a state has finite local moments. In the next section we present some numerical results as to the states with finite local moments.

§ 10. Phase Diagrams

By use of the method discussed in §8, we look for self-consistent solutions of ferromagnetic, antiferromagnetic, helical SDW and paramagnetic states for bcc and fcc lattices. We again confine ourselves to the case $\vec{Q}= 2/a(0,0,Q)$, then helical SDW and antiferromagnetic states have uniaxial symmetry except that an antiferromagnetic state of bcc lattice has cubic symmetry. Comparing the energies of those solutions, we investigate the state of the lowest energy, and construct the phase diagrams. The phase diagram consists of two parameters, that is, a number of d electrons, N_d and a reduced intra-atomic interaction, $U_R=(U+4J)/5$.

We show in Figs.21 and 22 the calculated phase diagrams for bcc and fcc respectively. The region in which no solutions can exist but a nonmagnetic one (no local moment) appears when U_R is small. We determine the phase boundary above which a nonmagnetic state is unstable from the inverse of the unenhanced susceptibility. When U_R is sufficiently large, the region AF in which an antiferromagnetic state is stable is found if N_d is around five. Increasing N_d from five, the region H in which a helical SDW state is stable appears, and the region F in which a ferromagnetic state is stable follows it. In the region H the optimum value Q_0 by which we mean Q of the lowest energy state changes continuously from π to 0.

Although it involves some ambiguity to choose the points corresponding to pure 3d metals Cr, Mn, Fe, Co and Ni in the calculated phase diagrams, we have shown the approximate positions by choosing N_d's and U_R's listed in Table VII. The magnitude of local moments for each metal is shown also. When the difference of the band width among 3d elements is taken into account, the chosen values of U_R are nearly unchanged through 3d elements, which is consistent with the discussion by Asano and Yamashita[24], except for Cr. The obtained magnitude of local moments for each metal is in good agreement with the observed one. The chosen point corresponding to bcc Fe (αFe) is located in the region F, which leads us to somewhat large values of N_d and M for Fe. We expect that another set of tight-binding parameters may leads us to more plausible values of N_d and M.[33] As for fcc Fe (γFe), we choose the point in the region H with $\cos Q_0 \sim -0.5$. Our treatment, however, contains some ambiguity, and we cannot say definitely whether the ground state of γFe is an antiferromagnetic one or a helical SDW one. In the case of Cr, we have only an antiferromagnetic solution except for a trivial non-magnetic one. We find that the appearance of the solution is nerely first-order with respect to U_R and N_d, which supports the discussion by Teraoka and Kanamori[2] as for the origin of the sinusoidal modulation. However, as is indicated by our band structure calculation of $\chi(Q)$ shown

in Fig.16(a), the nesting mechanism will be important also. We do not go into the problem of the ground state of Cr in this paper, since the present method cannot be applied to it easily.

In the next place, we discuss the character of local moments for each metal. In the phase diagrams we show the region in which a paramagnetic solution is found, though paramagnetic states never have the lowest energy. We find from Figs.21 and 22 that a paramagnetic solution is not found for Cr, fcc Mn (γMn) and Ni, which implies that the local moments of these metals are expected to be reduced to a considerable extent when temperature is raised. In other words, the local character of Cr, γMn and Ni is weak. We show in Fig.23 and 24 the magnitude of local moments and the energy difference from a paramagnetic state of several magnetic states in the vicinity of bcc Mn, αFe, γFe and Co. The energy difference between a paramagnetic state and the lowest energy state, ΔE_{para} ought to be related to the ordering temperature T_C or T_N, while that between a nonmagnetic state and the lowest energy state, ΔE_{non} is related to the critical temperature for the disappearance of local moments. Therefore we can conjecture how strong the local character is by the knowledge of ΔE_{para} and ΔE_{non}; the larger $\Delta E_{non}/\Delta E_{para}$ is, the stronger the local character is. We may say from Figs.23 and 24 that the local character of bcc Mn and γFe

is considerably strong compared with that of αFe and Co.

It is beyond the scope of our calculation to estimate the ordering temperature from ΔE_{para}, but we can discuss some trend of the ordering temperature from it. We find from Figs.23 and 24 that ΔE_{para} of bcc Mn and γFe is considerably small compared with that of αFe and Co. The ordering temperature of γFe is therefore expected to be low compared with that of αFe and Co, which is consistent with experiments. The ordering temperature of bcc Mn, if it exists, is also expected to be low. Strong local character and low ordering temperature of γFe and also bcc Mn can be ascribed to the helical SDW ground state with $\cos Q_0 = 0 \sim -0.5$, since a helical SDW state with $\cos Q_0 = 0 \sim -0.5$ and a paramagnetic state are similar to each other with respect to the short-range order of spins. We suppose that the magnetism of αMn may be related to the above-mentioned situation, though the crystal structure of αMn obviously plays an important role.

As for the transition metal alloys, it is questionable to discuss the calculated phase diagrams in the rigid-band model, especially when the average number of d electrons falls into the region H. The energy difference between a helical SDW state and a paramagnetic state is small as above-mentioned, and moreover the energy difference between a helical SDW state and a certain state with short-range magnetic order[26] is expected to be even more small.

Therefore the long-range magnetic order of a helical SDW state will be violated by alloying effects, and the helical SDW ground state will be replaced by a certain ordered state.[34)]

§11. Concluding Remarks

In this part we have shown that our method can reproduce well the band structure calculation for the electronic structure of magnetic states, particularly for the unenhanced susceptibility. On the basis of the discussion about the unenhanced susceptibility, the existence of the states whose spatial variation is described by a general $\vec{Q}$ is predicted, and is ascertained by the successive calculation of the phase diagrams. It is found that the occurrence of a state with a general $\vec{Q}$ is governed by the effective interactions among near neighboring sites, which is in contrast to the nesting mechanism of chromium. The obtained phase diagrams explain the wide variety of the observed magnetism in 3d transition metals, not only for the ground state properties but also for properties at finite temperature, such as, the character of local moments and the ordering temperature. It should be emphasized that the difference of the magnetism among 3d metals is derived chiefly from the electronic structure and the number of d electrons and slightly from the strengths of the intra-atomic interactions.

We have mainly discussed the case of pure metals in this part. The discussion extended to the case of transition metal alloys is interesting, but is not so simple as pure metals. We can discuss the instability of a ferromagnetic state,[34,35] but it is very difficult to investigate the ground state when a ferromagnetic state is unstable.

Acknowledgements

The author would like to express his sincere thanks to Professor Junjiro Kanamori for his helpful discussions and continuous encouragements. He would like to thank Professor Kiyoyuki Terakura for his valuable comments about the recursion method at an early stage of this work. Thanks are also due to Professor Hirosi Miwa, Drs. Takeo Jo and Yoshihiro Teraoka for their fruitful discussions. Finally the efforts of Mrs. Akimi Egusa in preparing the manuscript are gratefully acknowledged.

Appendix A. Further Discussions about the Expression of $\Sigma_\sigma^\ell(\omega)$

We present here some discussions about the expression of $\Sigma_\sigma^\ell(\omega)$. First we discuss eq.(8.16) for the choices of b_σ^ℓ and $\tilde{p}_\sigma^\ell$. In the case of a ferromagnetic state M_{21}^ℓ, M_{22}^ℓ, M_{31}^ℓ, $\cdots$ are given by

$$M_{21}^\ell = M_2^\ell,\ M_{22}^\ell = 0\ ,$$

$$M_{31}^\ell = M_3^\ell\ ,\ M_{32}^\ell = M_{33}^\ell = 0\ ,$$

$$M_{41C}^\ell = M_{4C}^\ell,\ M_{42C}^\ell = M_{43C}^\ell = M_{44C}^\ell = 0, \qquad \text{(A. 1)}$$

then we obtain from eq.(8.16)

$$p^\ell = 1\ ,\ b_\sigma^\ell = b^\ell \text{ and } \tilde{p}_\sigma^\ell = 1. \qquad \text{(A. 2)}$$

Thus the expression (8.15) is reduced to the expression (8.6). In the case of an antiferromagnetic state in bcc with the nearest neighbor transfer only, we have

$$M_{21}^\ell = 0,\ M_{22}^\ell = M_2^\ell\ ,$$

$$M_{31}^\ell = M_{32}^\ell = M_{33}^\ell = M_3^\ell = 0,$$

$$M_{41C}^\ell = M_{42C}^\ell = 0,\ M_{43C}^\ell = M_{4C}^\ell,\ M_{44C}^\ell = 0, \qquad \text{(A. 3)}$$

then we obtain

$$p^{\ell} = 0,\ b_{\sigma}^{\ell} = b^{\ell} \text{ and } \tilde{p}_{\sigma}^{\ell} = 1, \qquad \text{(A. 4)}$$

the meaning of which is obvious. As was already discussed in §8, we have

$$M_{21}^{\ell} = M_{22}^{\ell} = \frac{1}{2} M_{2}^{\ell} ,$$

$$M_{31}^{\ell} = \frac{1}{2} M_{32}^{\ell} = M_{33}^{\ell} = \frac{1}{4} M_{3}^{\ell} ,$$

$$M_{41C}^{\ell} = \frac{1}{3} M_{42C}^{\ell} = \frac{1}{3} M_{43C}^{\ell} = M_{44C}^{\ell} = \frac{1}{8} M_{4C}^{\ell} , \qquad \text{(A. 5)}$$

in the case of a paramagnetic state with randomly oriented local moments. Then we obtain

$$p^{\ell} = 1/2 ,\ b_{\sigma}^{\ell} = b^{\ell} \text{ and } \tilde{p}_{\sigma}^{\ell} = 1/2. \qquad \text{(A. 6)}$$

Thus eq.(8.16) are free of the terms proportional to $(E_{\sigma} - E_{-\sigma})$ in the case of such simple magnetic states. We may add that eq.(8.16) can yield proper choices of b_{σ}^{ℓ} and $\tilde{p}_{\sigma}^{\ell}$ also in the case of an alloy analogy state where each local moments may point up or down[26];

$$p^{\ell} = p_1 ,\ b_{\sigma}^{\ell} = b^{\ell} \text{ and } \tilde{p}_{\sigma}^{\ell} = p_2, \qquad \text{(A. 7)}$$

where p_1 denotes the probability of finding a neighboring atom in the first shell with parallel moment and p_2 denotes that in the second shell.

As mentioned in the text, the expression (8.15) sometimes sufferes from a pathological negative density of states for $\vec{Q}$ being near $\vec{K}/2$ and $|E_\sigma - E_{-\sigma}|$ being large. In such a case we prefer to the expression (8.15) an expression which is free from such a fault given by

$$\Sigma_\sigma^\ell(\omega) = M_2^\ell \,/\, [\Xi_\sigma^\ell(\omega) - a^\ell - b_\sigma^\ell \,/\, \tilde{\Xi}_\sigma^\ell(\omega)] \,, \qquad \text{(A. 8)}$$

where

$$\Xi_\sigma^\ell(\omega) = \left(\frac{p^\ell}{\lambda_\sigma^\ell(\omega)} + \frac{1-p^\ell}{\lambda_{-\sigma}^\ell(\omega)}\right)^{-1} . \qquad \text{(A. 9)}$$

We determine $\tilde{\Xi}_\sigma^\ell(\omega)$ by following equation;

$$\begin{aligned}\Xi_\sigma^\ell(\omega) &= \omega - (p^\ell E_\sigma + (1-p^\ell)E_{-\sigma}) - \frac{\mu^\ell + p^\ell(1-p^\ell)(E_\sigma - E_{-\sigma})^2}{\omega} - \cdots \\ &= \omega - (p^\ell E_\sigma + (1-p^\ell)E_{-\sigma}) - \frac{\mu^\ell + p^\ell(1-p^\ell)(E_\sigma - E_{-\sigma})^2}{\tilde{\Xi}_\sigma^\ell(\omega)} \,,\end{aligned}$$

(A. 10)

where $\mu^{\ell} = M_{4B}^{\ell}/M_{2}^{\ell}$. We can easily see that the expression (A.8) with (A.10) is free from a pathological negative density of states when

$$\mu^{\ell} + p^{\ell}(1-p^{\ell})(E_{\sigma} - E_{-\sigma})^2 + b_{\sigma}^{\ell} > 0. \qquad \text{(A. 11)}$$

The condition is satisfied in a practical range of $|E_{\sigma} - E_{-\sigma}|$. Though eq.(A.10) is chosen arbitrarily, the expression (A.8) can reproduce the $1/\omega$ expansion of $\Sigma_{\sigma}^{\ell}(\omega)$ up to $1/\omega^3$, and in practice yields the almost same results as the expression (8.15). We show in Fig.25 some examples of the density of states obtained by the expression (8.15) and by the expression (A.8).

Appendix B. Details of the Calculation of χ_{ij}

We can calculate $\bar{G}^{mn}_{ij}(\omega)$ as well as $\bar{G}^{\ell\ell}_{00}(\omega)$ on the basis of the locator expansion discussed in §1 such that

$$\bar{G}^{mn}_{ij}(\omega) = g^m_i\, t^{mn}_{ij}\, g^n_j + \sum_{k,p} g^m_i\, t^{mp}_{ik}\, g^p_k\, t^{pn}_{kj}\, g^n_j + \cdots$$

$$= t^{mn}_{ij}/\omega^2 + \sum_{k,p} t^{mp}_{ik}\, t^{pn}_{kj}/\omega^3 + \cdots . \qquad \text{(B. 1)}$$

Considering the reducible paths, we rewrite eq.(B.1) as

$$\bar{G}^{mn}_{ij}(\omega) = \bar{G}^{mm}_{ii}(\omega)\,[t^{mn}_{ij}/\omega + \sum_{k,p} t^{mp}_{ik}\, t^{pn}_{kj}/\omega^2 + \cdots], \qquad \text{(B. 2)}$$

where such paths that return to the i-th site at intermediate steps are included in $\bar{G}^{mm}_{ii}(\omega)$. Alternatively we can rewrite eq.(B.1) as

$$\bar{G}^{mn}_{ij}(\omega) = [t^{mn}_{ij}/\omega + \sum_{k,p} t^{mp}_{ik}\, t^{pn}_{kj}/\omega^2 + \cdots\ ]\bar{G}^{nn}_{jj}(\omega), \qquad \text{(B. 3)}$$

where such paths that return to the j-th site at intermediate steps are included in $\bar{G}^{nn}_{jj}(\omega)$. Then we obtain

$$\sum_m \bar{G}^{\ell m}_{0i}(\omega)\ \bar{G}^{m\ell}_{i0}(\omega) = (\bar{G}^{\ell\ell}_{00}(\omega))^2$$

$$\times \sum_m [t^{\ell m}_{0i}\ t^{m\ell}_{i0}/\omega^2 + \sum_{j,n} (t^{\ell m}_{0i}\ t^{mn}_{ij}\ t^{n\ell}_{j0} + t^{\ell n}_{0j}\ t^{nm}_{ji}\ t^{m\ell}_{i0})/\omega^3 + \cdots] \ ,$$

(B. 4)

which can be approximately rewritten in terms of $\tilde{\Lambda}^{\ell}(\omega)$ as

$$\sum_m \bar{G}^{\ell m}_{0i}(\omega)\bar{G}^{m\ell}_{i0}(\omega) = (\bar{G}^{\ell\ell}_{00}(\omega))^2$$

$$\times \left[\frac{m^{\ell}_2(i)}{(\tilde{\Lambda}^{\ell}(\omega) - a^{\ell} - \frac{b^{\ell}}{\tilde{\Lambda}^{\ell}(\omega)})^2} + \frac{m^{\ell}_4(i)}{(\tilde{\Lambda}^{\ell}(\omega) - a^{\ell} - \frac{b^{\ell}}{\tilde{\Lambda}^{\ell}(\omega)})^2 (\tilde{\Lambda}^{\ell}(\omega))^2} \right] \ ,$$

(B. 5)

where

$$m^{\ell}_2(i) = \sum_m t^{\ell m}_{0i}\ t^{m\ell}_{i0}$$

$$m^{\ell}_4(i) = \sum_{j,n} \sum_m \sum_{k,p} t^{\ell n}_{0j}\ t^{nm}_{ji}\ t^{mp}_{ik}\ t^{p\ell}_{k0} - m^{\ell}_2(i) \cdot (a^{\ell})^2 .$$

(B. 6)

We can easily show that the expression (B.5) satisfies the sum rule which is given by

$$\frac{d}{d\omega}\,\overline{G}^{\ell\ell}_{00}(\omega) = -\sum_{i,m}\,\overline{G}^{\ell m}_{0i}(\omega)\overline{G}^{m\ell}_{i0}(\omega). \qquad \text{(B. 7)}$$

References

1) T. Moriya: Prog. Theor. Phys. 33 (1965) 157.

2) Y. Teraoka and J. Kanamori: Physica 91B (1977) 199.

3) F. Ducastelle and F. Cyrot-Lackmann: J. Phys. Chem. Solids 31 (1970) 1295.

4) J. P. Gaspard and F. Cyrot-Lackmann: J. Phys. C6 (1975) 3077.

5) R. Haydock, V. Heine and M. J. Kelly: J. Phys. C5 (1972) 2845.

6) R. Haydock, V. Heine and M. J. Kelly: J. Phys. C8 (1975) 2591.

7) V. Heine, R. Haydock and M. J. Kelly: Solid State Physics Vol.35 (Academic, New York, 1980).

8) N. I. Akhiezer: The Classical Moment Problem (Oliver and Boyd, London, 1965).

9) J. A. Shohat and J. D. Tamarkin: The Problem of Moment (American Mathematical Society, New York, 1970).

10) D. G. Pettifor: J. Phys. C5 (1972) 97.

11) D. G. Pettifor: J. Phys. C2 (1969) 1051.

12) R. Haydock and M. J. Kelly: Surf. Sci. 38 (1973) 139.

13) H. Shiba: Prog. Theor. Phys. 46 (1971) 77.

14) P. Soven: Phys. Rev. 156 (1967) 809.

15) B. Velicky, S. Kirkpatrick and H. Ehrenreigh: Phys. Rev. 175 (1968) 747.

16) R. J. Jacobs: J. Phys. F3 (1973) 933.

17) F. Ducastelle and F. Gautier: J. Phys. F6 (1976) 2039.

18) G. Treglia, F. Ducastelle and F. Gautier: J. Phys. F8 (1978) 1437.

19) H. Miwa: Prog. Theor. Phys. 52 (1974) 1.

20) N. Hamada and H. Miwa: Prog. Theor. Phys. 59 (1978) 1045.

21) P. W. Anderson: Phys. Rev. 124 (1961) 41.

22) J. Friedel, G. Leman and M. Olszewski: J. Appl. Phys. 32 (1961) 325S.

23) D. R. Penn: Phys. Rev. 142 (1966) 350.

24) S. Asano and J. Yamashita: Prog. Theor. Phys. 49 (1973) 373.

25) L. M. Roth: Proc. Int. Conf. Physics of Transition Metals, Toronto, 1977 (Institute of Physics, London, 1977) p.473.

26) S. H. Liu: Phys. Rev. B17 (1978) 3629.

27) P. Lederer and A. Blandin: Phil. Mag. 14 (1966) 363.

28) W. M. Lomer: Proc. Phys. Soc. 80 (1962) 489.

29) A. Kotani (Shibatani), K. Motizuki and T. Nagamiya: Phys. Rev.177 (1969) 984.

30) A. Yoshimori: J. Phys. Soc. Jpn. 14 (1959) 807.

31) J. Villain: J. Phys. Chem. Solids 11 (1959) 303.

32) T. Moriya: Prog. Theor. Phys. 34 (1965) 329.

33) M. V. You, V. Heine, A. J. Holden and D. J. Lin-Chung: Phys. Rev. Lett. 44 (1980) 1282.

34) T. Jo: J. Phys. Soc. Jpn. 40 (1976) 715.

35) T. Jo: J. Phys. Soc. Jpn. 50 (1981) 2209.

Figure Captions

Fig. 1. (a) A reducible path $P_r P_s P_t$ consists of three irreducible paths P_r, P_s and P_t. (b) A path of ν steps and θ_1, θ_2, $\cdots\theta_\nu$ are the inflection angles of the path.

Fig. 2. The fourth order paths of fcc structure and the classification of them.

Fig. 3. The fourth order paths of bcc structure.

Fig. 4. Schematic expression of Σ_B; (a) on a Bethe type lattice (b) improved one in which we include triangles.

Fig. 5. Diagrams of the first few terms in the expresseion (3.2) for Σ_B and those in the expression (3.3) or (3.18) for Σ_C.

Fig. 6. Density of states for bcc and fcc d band from the present calculation by use of the average locators given by eq.(3.15). Histograms are those from the band structure calculation.

Fig. 7. Density of states for bcc and fcc d band from the improved calculation by use of the average locators given by eq.(3.20).

Fig. 8. Partial density of states belonging to $d\varepsilon$ and $d\gamma$ symmetry from the improved calculation.

Fig. 9. Results of the simplified expressions. The solid lines indicate the results in which eq.(3.20) for

Λ^{α} and eq.(3.21) for Σ_B are used (i.e. the same figure as Fig. 7). The dashed lines indicate the results in which eq.(3.23) is used in place of eq.(3.21) and the dot-dashed lines indicate those in which eq.(3.26) and (3.23) are used.

Fig. 10. Some examples of the density of states ρ_A and ρ_B for various values of E_A-E_B obtained from the present calculation (left side) and those from the CPA calculation (right side) in the case of fcc transition metal alloys $A_{50}B_{50}$.

Fig. 11. Results similar to Fig. 10 in the case of bcc transition metal alloys $A_{50}B_{50}$.

Fig. 12. Change of the density of states ρ_A and ρ_B obtained from the present calculation with the alloy concentration in the case of fcc. We fix the value of E_A-E_B at -0.04 Ry.

Fig. 13. Results similar to Fig. 12 in the case of bcc.

Fig. 14. Change of the density of states $\rho_{\uparrow}$ and $\rho_{\downarrow}$ of helical SDW states with the value of Q in the case of bcc transition metals. We fix the value of $E_{\uparrow}-E_{\downarrow}$ at -0.04 Ry.

Fig. 15. Results similar to Fig. 14 in the case of fcc transition metals.

Fig. 16. The unenhanced susceptibilities of bcc transition metals obtained from (a) the Lindhard expression (9.1) and from (b) the expression (9.2), for the

wave vector $\vec{Q}=2/a(0,0,Q)$ where Q=0 (ferro), $Q=\pi/2$ and $Q=\pi$ (antiferro). We show the region in which $\chi(Q)$ has the maximum value at a general Q and also the region in which $\chi(Q)$ has the maximum value at $Q\sim\pi$. In the inset the dotted lines correspond to those for some other wave vectors.

Fig. 17. Results similar to Fig. 16 for fcc transition metals.

Fig. 18. The unenhanced susceptibilities of bcc transition metals for various values of Q in the vicinity of chromium; i.e. E_F=0.004, 0.008, 0.012 and 0.016 (Ry). The solid lines indicate those from the expression (9.1) and the dahsed lines indicate those from the expression (9.2).

Fig. 19. The calculated $\chi_{0\delta}$ for various neighbors including χ_{00} of bcc transition metals. We also show $\rho(E_F)$ which is responsible for the Stoner criterion, while χ_{00} is responsible for the Friedel one. We show the region where $Q_0\neq 0$ and $Q_0\neq\pi$ obtained from eq.(9.7).

Fig. 20. Results similar to Fig. 19 for fcc transition metals.

Fig. 21. The phase diagram of bcc transition metals. The dashed lines indicate the phase lines corresponding to $\cos Q_0$=0.5, 0.0 and -0.5. The dot-dashed line indicates the phase boundary above which a paramagnetic solution can be found.

Fig. 22. The phase diagram of fcc transition metals.

Fig. 23. The magnitude of local moments (solid line) and the energy difference from the paramagnetic state (dashed line) of various states in the vicinity of (a) bcc Mn (U_R=0.0272 Ry) and (b) bcc Fe (U_R=0.0336 Ry). The scales of the magnitude of local moments and the energy difference are shown on left and right vertical axes, respectively. The numbers .5, .0, etc. indicate the helical SDW states with cosQ= 0.5, 0.0, etc..

Fig. 24. The same quantities as Fig. 23 in the vicinity of (a) fcc Fe (U_R= 0.0312 Ry) and (b) Co (U_R= 0.0344 Ry).

Fig. 25. Comparison between the expression (8.15) and the expression (A.10) in the case of fcc transition metals.

Table I. Slater-Koster parameters used by Pettifor[11,12] (in Rydbergs).

structure	ddσ	ddπ	ddδ
fcc	-0.027784	0.012535	-0.001554
bcc (nearest)	-0.03248	0.01538	-0.00200
(next nearest)	-0.01341	0.00487	-0.00049

Table II . The numerical values of m_4^{ℓ} for the fourth order paths of fcc structure shown in Fig. 2.

	m_4^{ℓ} (10^{-8} Ry^4)				asymptotic relation
	dε	dγ	total		
A_1, A_2	15.721	8.684	12.906	(1.000)	1
A_3	7.521	-2.420	3.544	(0.275)	1/4
A_4, A_5	3.294	3.079	3.208	(0.249)	1/64
B_1, B_3	3.667	2.519	3.208	(0.249)	1/64
B_2	4.212	2.544	3.544	(0.275)	1/4
B_4	15.721	8.684	12.906	(1.000)	1
C_1	1.039	-1.248	0.124	(0.010)	1/4096
C_2	-0.928	0.398	-0.397	(-0.031)	1/256
C_3, C_6	0.193	-0.203	0.034	(0.003)	1/4096
C_4	2.732	0.324	1.769	(0.137)	1/16
C_5	-0.405	-0.386	-0.397	(-0.031)	1/256

Table III . The numerical values of m_4^{ℓ} for the fourth order paths of bcc structure shown in Fig. 3.

	m_4^{ℓ} (10^{-8} Ry^4)				
	$d\varepsilon$	$d\gamma$	total		asymptotic relation
A_1, A_2	38.341	3.731	24.497	(1.000)	1
A_3	9.197	2.128	6.370	(0.260)	1/9
A_4	0.645	1.432	0.960	(0.039)	0
A_5, A_6	0.038	1.617	0.669	(0.027)	$1\cdot\alpha^4$
A_7	0.019	0.407	0.174	(0.007)	$1/4\cdot\alpha^4$
B_1, B_5	0.977	0.934	0.960	(0.039)	0
B_2, B_3	7.723	4.339	6.370	(0.260)	1/9
B_4	38.341	3.731	24.497	(1.000)	1
B_6, B_7	0.645	1.432	0.960	(0.039)	0
B_8	0.019	0.407	0.174	(0.007)	$1/4\cdot\alpha^4$
B_9	0.038	1.617	0.669	(0.027)	$1\cdot\alpha^4$
C_1, C_3	-4.380	-2.449	-3.607	(-0.147)	1/81
C_2	0.537	0.422	0.491	(0.020)	1/81
C_4, C_9	-0.145	-0.010	-0.091	(-0.004)	0
C_5, C_8	0.250	0.761	0.454	(0.019)	0
C_6	-0.362	0.316	-0.091	(-0.004)	0
C_7	0.020	0.354	0.153	(0.006)	0
C_{10}	0.019	0.146	0.070	(0.003)	$1/16\cdot\alpha^4$

where $\alpha \doteqdot$ t(next nearest)/t(nearest)

Table Ⅳ . The numerical values of the first few terms in eq. (1.7) for fcc structure (in units of 10^{-1} Ry).

	s band	d band		
		total	dε	dγ
M_2^{ℓ}	12	0.26185	0.29564	0.21116
M_3^{ℓ}	-48	-0.01528	-0.02177	-0.00555
M_4^{ℓ}	540	0.12642	0.15858	0.07819
M_{4A}^{ℓ}	144	0.07028	0.08740	0.04459
M_{4B}^{ℓ}	132	0.05479	0.06418	0.04071
M_{4C}^{ℓ}	264	0.00136	0.00700	-0.00711
$M_3^{\ell}/(M_2^{\ell})^{3/2}$	-1.155	-0.114	-0.135	-0.057
$M_4^{\ell}/(M_2^{\ell})^2$	3.750	1.844	1.814	1.754
$M_{4A}^{\ell}/(M_2^{\ell})^2$	1.000	1.025	1.000	1.000
$M_{4B}^{\ell}/(M_2^{\ell})^2$	0.917	0.799	0.734	0.913
$M_{4C}^{\ell}/(M_2^{\ell})^2$	1.833	0.020	0.080	-0.159

In the calculation of the s band we set t=-1.

Table V . The numerical values of the first few terms in eq. (1.7) for bcc structure (in units of 10^{-1} Ry).

	s band	d band		
		total	dε	dγ
M_2^{ℓ}	9.5	0.27310	0.33433	0.18124
M_3^{ℓ}	-36.0	-0.01760	0.00926	-0.05789
M_4^{ℓ}	365.625	0.12970	0.16773	0.07266
M_{4A}^{ℓ}	90.25	0.08020	0.11178	0.03285
M_{4B}^{ℓ}	81.875	0.06021	0.07560	0.03712
M_{4C}^{ℓ}	193.5	-0.01071	-0.01964	0.00269
$M_3^{\ell}/(M_2^{\ell})^{3/2}$	-1.229	-0.123	0.048	-0.750
$M_4^{\ell}/(M_2^{\ell})^2$	4.051	1.739	1.501	2.212
$M_{4A}^{\ell}/(M_2^{\ell})^2$	1.000	1.075	1.000	1.000
$M_{4B}^{\ell}/(M_2^{\ell})^2$	0.907	0.807	0.676	1.130
$M_{4C}^{\ell}/(M_2^{\ell})^2$	2.144	-0.143	-0.176	0.082

In the calculation of the s band we set t(nearest)=-1 and t(next nearest)=-1/2.

Table VI. The numerical values of the parameters which we use in the calculations (in units of 10^{-1} Ry).

	fcc		bcc	
	$\ell\in d\varepsilon$	$\ell\in d\gamma$	$\ell\in d\varepsilon$	$\ell\in d\gamma$
M_2^ℓ	0.29564	0.21116	0.33432	0.18124
a^ℓ	-0.07363	-0.02627	0.02770	-0.31943
b^ℓ	-0.00349	-0.05180	-0.06060	-0.09477
$(b^\ell)^*$	-0.00218	-0.05454	-0.06929	-0.07073
$M_2^\ell(d\varepsilon)$	0.24404	0.07740	0.29853	0.05370
$M_2^\ell(d\gamma)$	0.05160	0.13375	0.03580	0.12754
$\mu_1^\ell(d\varepsilon,d\varepsilon)$	0.20672	0.19899	0.19900	0.29709
$\mu_1^\ell(d\varepsilon,d\gamma)$	0.04207	0.03870	0.03563	0.02909
$\mu_1^\ell(d\gamma,d\varepsilon)$	0.06450	0.07359	0.04699	0.04983
$\mu_1^\ell(d\gamma,d\gamma)$	0.12717	0.12074	0.11835	0.11464
	$\alpha=d\varepsilon$	$\alpha=d\gamma$	$\alpha=d\varepsilon$	$\alpha=d\gamma$
$\tilde{\mu}^{\alpha,d\varepsilon}$	0.20537	0.07026	0.20951	0.04899
$\tilde{\mu}^{\alpha,d\gamma}$	0.04149	0.12310	0.03493	0.11574
$\tilde{a}^{\alpha,d\varepsilon}$	-0.27722	0.14089	0.03997	-0.10230
$\tilde{a}^{\alpha,d\gamma}$	0.0	-0.20273	-0.05970	-0.15830
$\tilde{\mu}^\alpha$	0.24686	0.19336	0.24443	0.16473
$\tilde{a}^\alpha$	-0.23063	-0.07787	0.02573	-0.14164
$\tilde{b}^\alpha$	0.24861	0.24011	0.23426	0.18909

*) The value of b^ℓ when the expression (3.22) or (3.23) is used in place of the expression (3.21).

Table VII. The chosen positions in the phase diagrams corresponding to 3d transition metals.

		N_d	U_R(Ry)	$\cos Q_0$		M(μ_B)	local character
bcc	Cr	4.56	0.0165	-1.	(AF)	0.5	weak
	(Mn)	6.4	0.0272	-0.2	(H)	2.3	very strong
	Fe	7.4	0.0336	1.	(F)	2.5	strong
fcc	Mn	6.0	0.0272	-1.	(AF)	2.3	weak
	Fe	7.0	0.0312	-0.5	(H)	1.7	very strong
	Co	8.2	0.0344	1.	(F)	1.8	strong
	Ni	9.4	0.0388	1.	(F)	0.6	weak

(a)

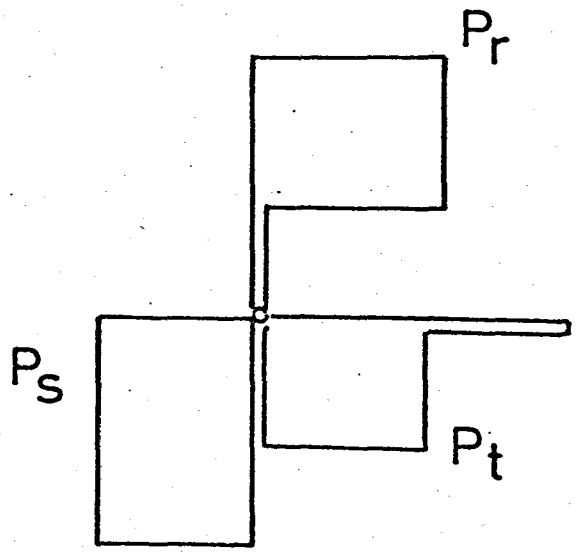
P_r
P_s
P_t

(b)

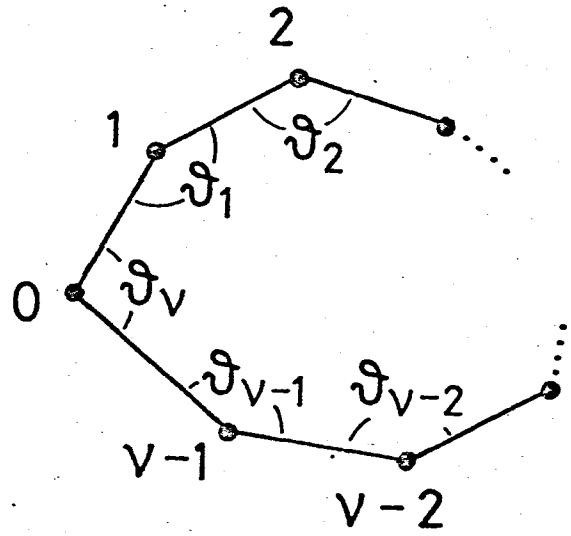
2
1
ϑ_2
ϑ_1
0
ϑ_ν
$\vartheta_{\nu-1}$
$\vartheta_{\nu-2}$
$\nu-1$
$\nu-2$

Fig. 1

fcc

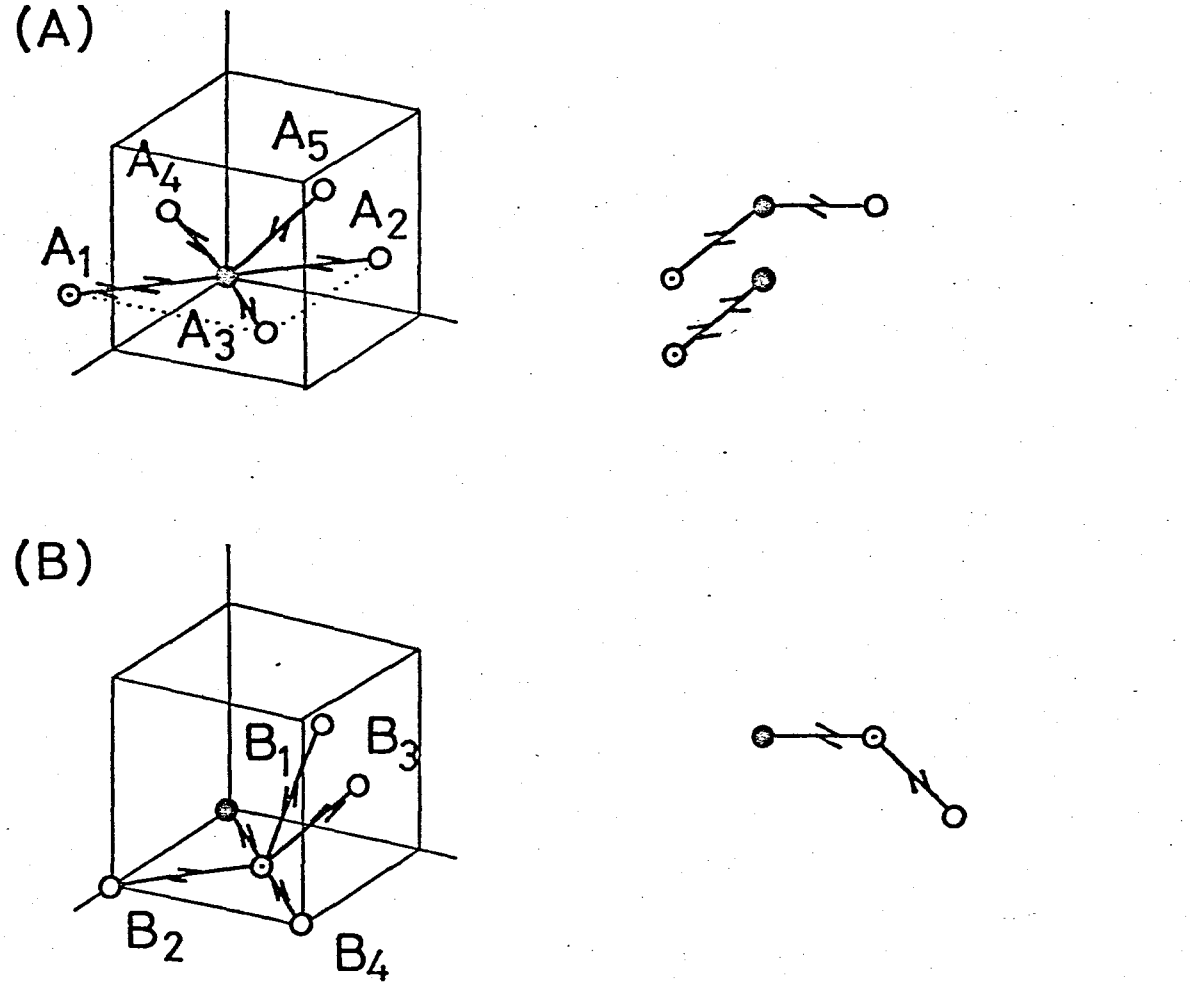

Fig. 2

bcc

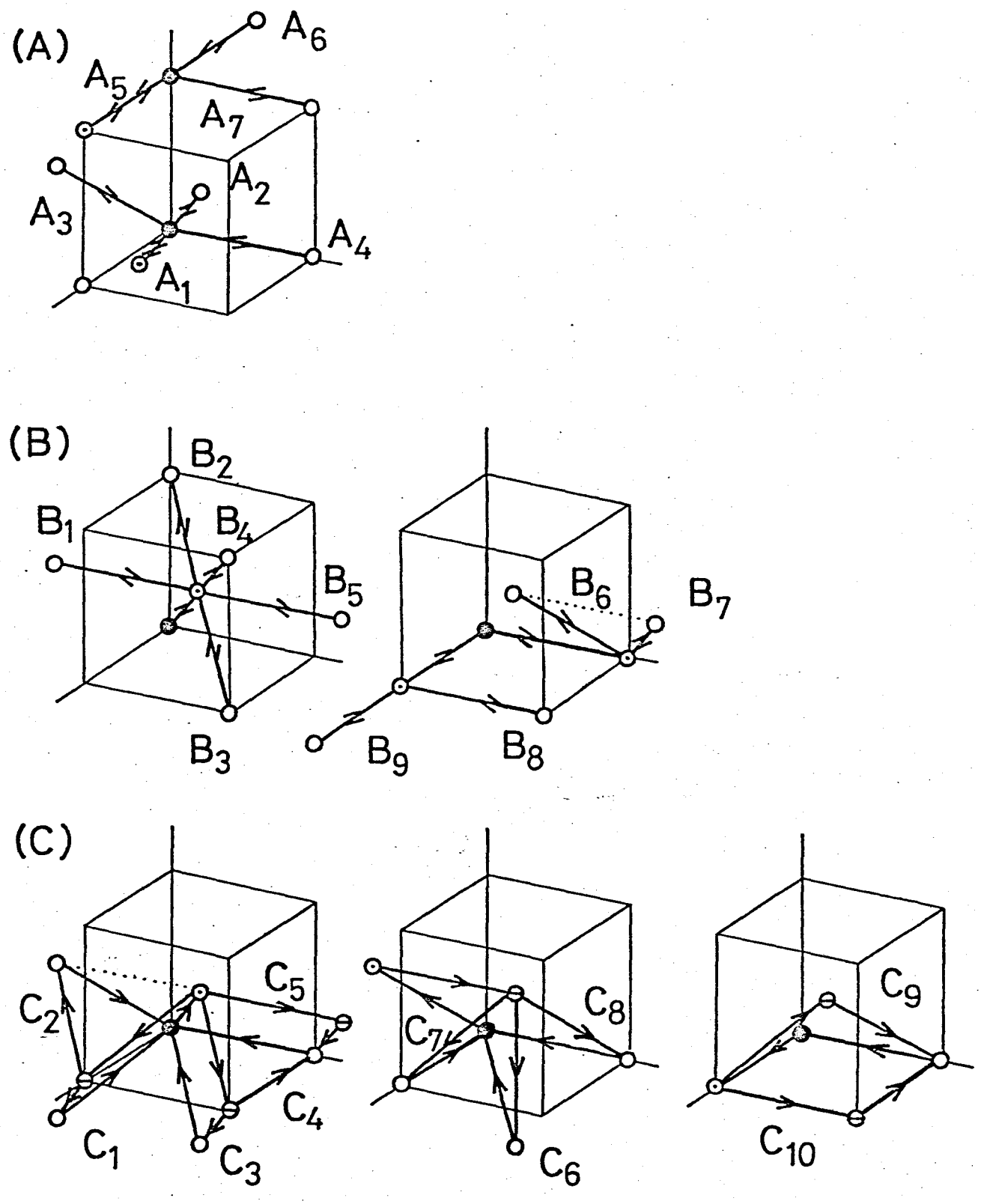
(A)
A6
A5
A7
A2
A3
A4
A1
(B)
B2
B1
B4
B5
B6
B7
B3
B9
B8
(C)
C5
C2
C8
C7
C9
C4
C1
C3
C6
C10

Fig. 3

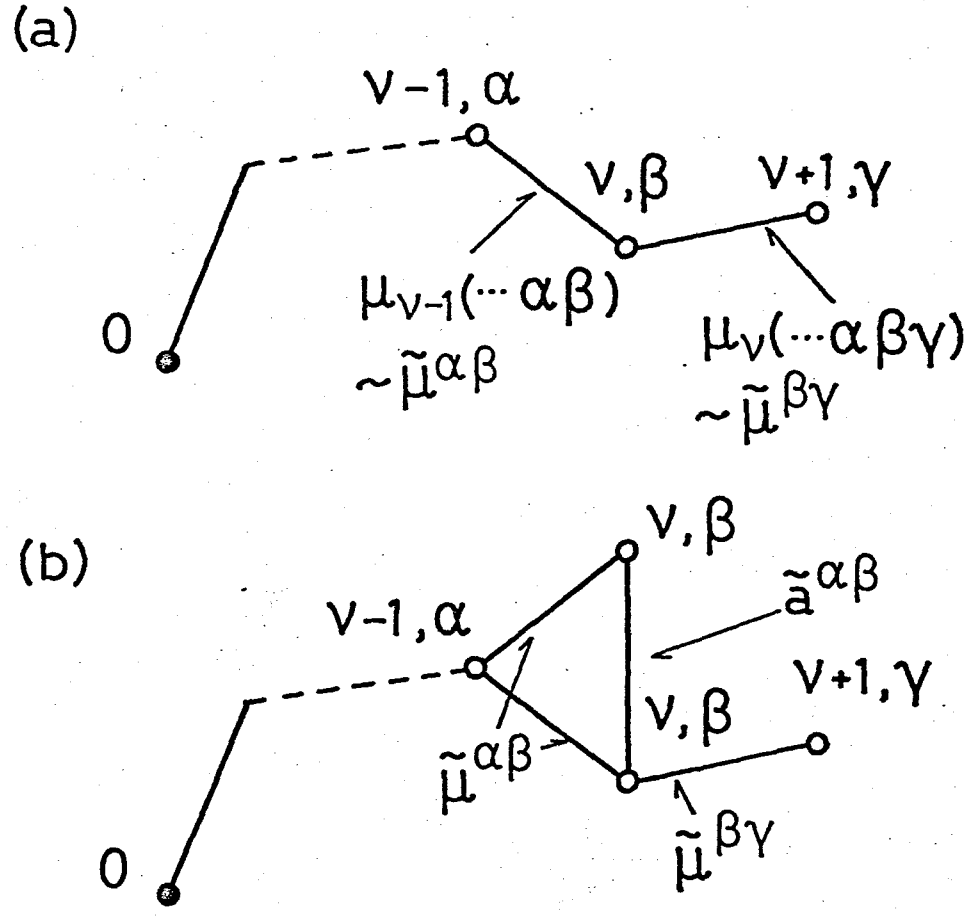

Fig. 4

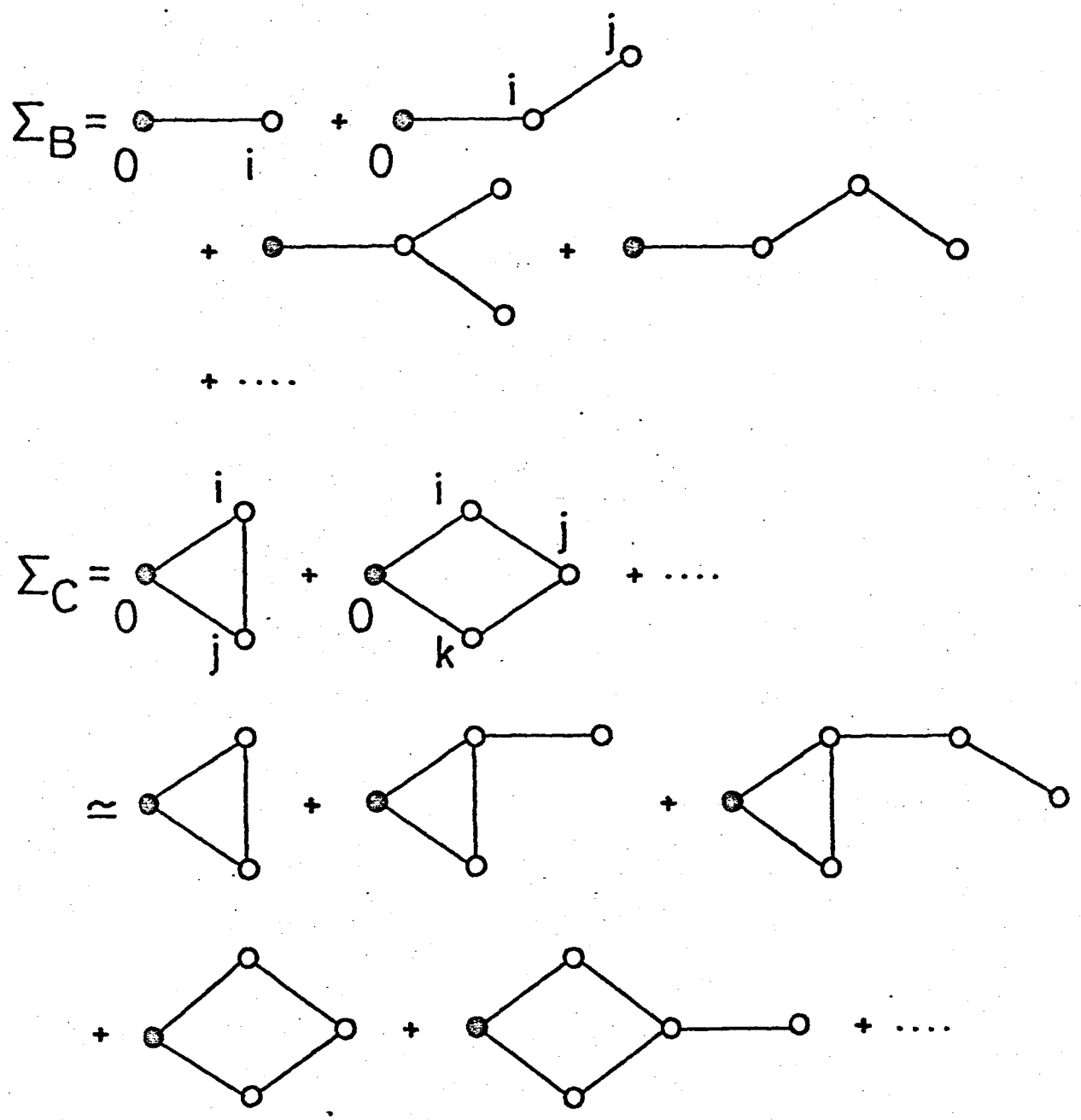

Fig. 5

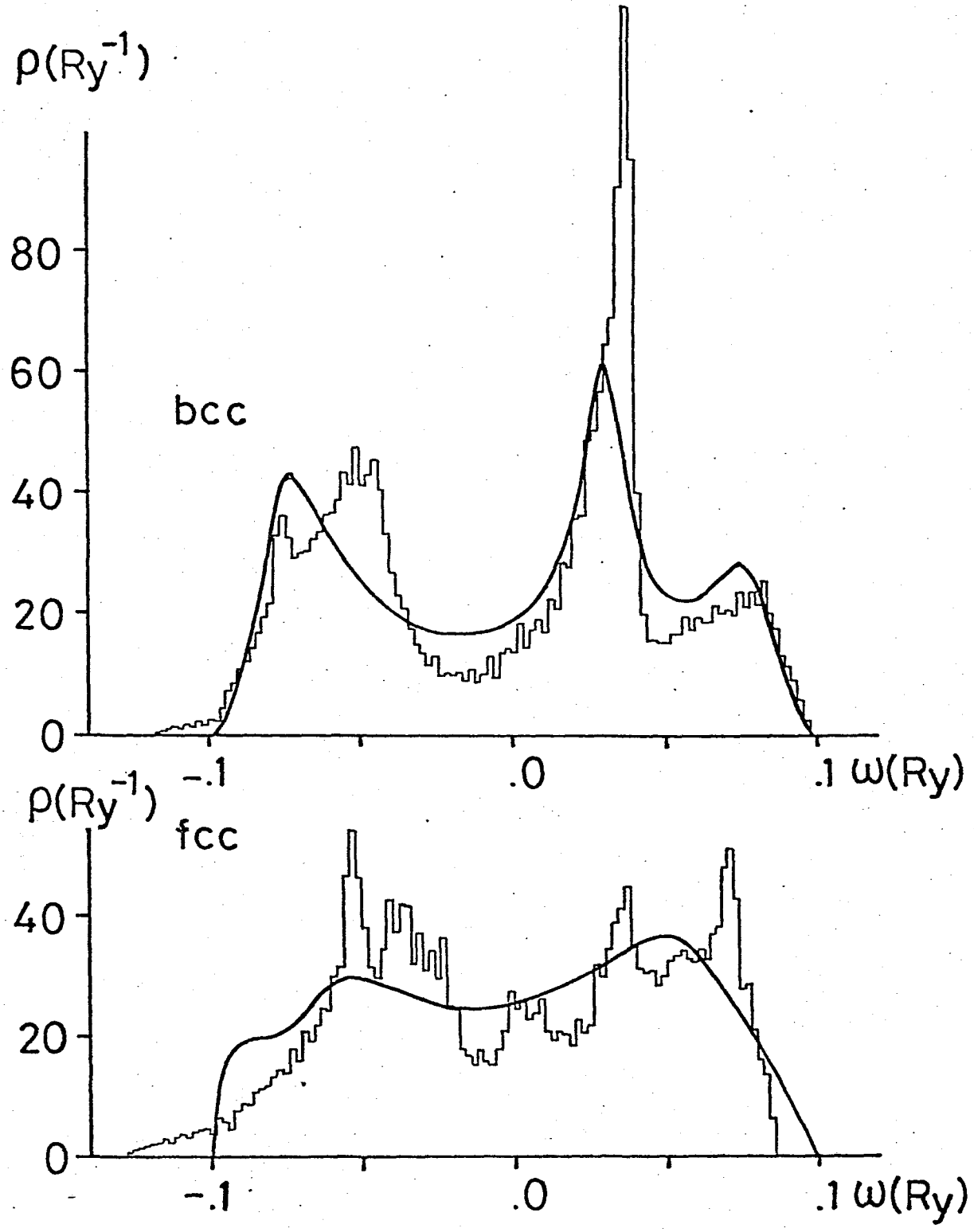

Fig. 6

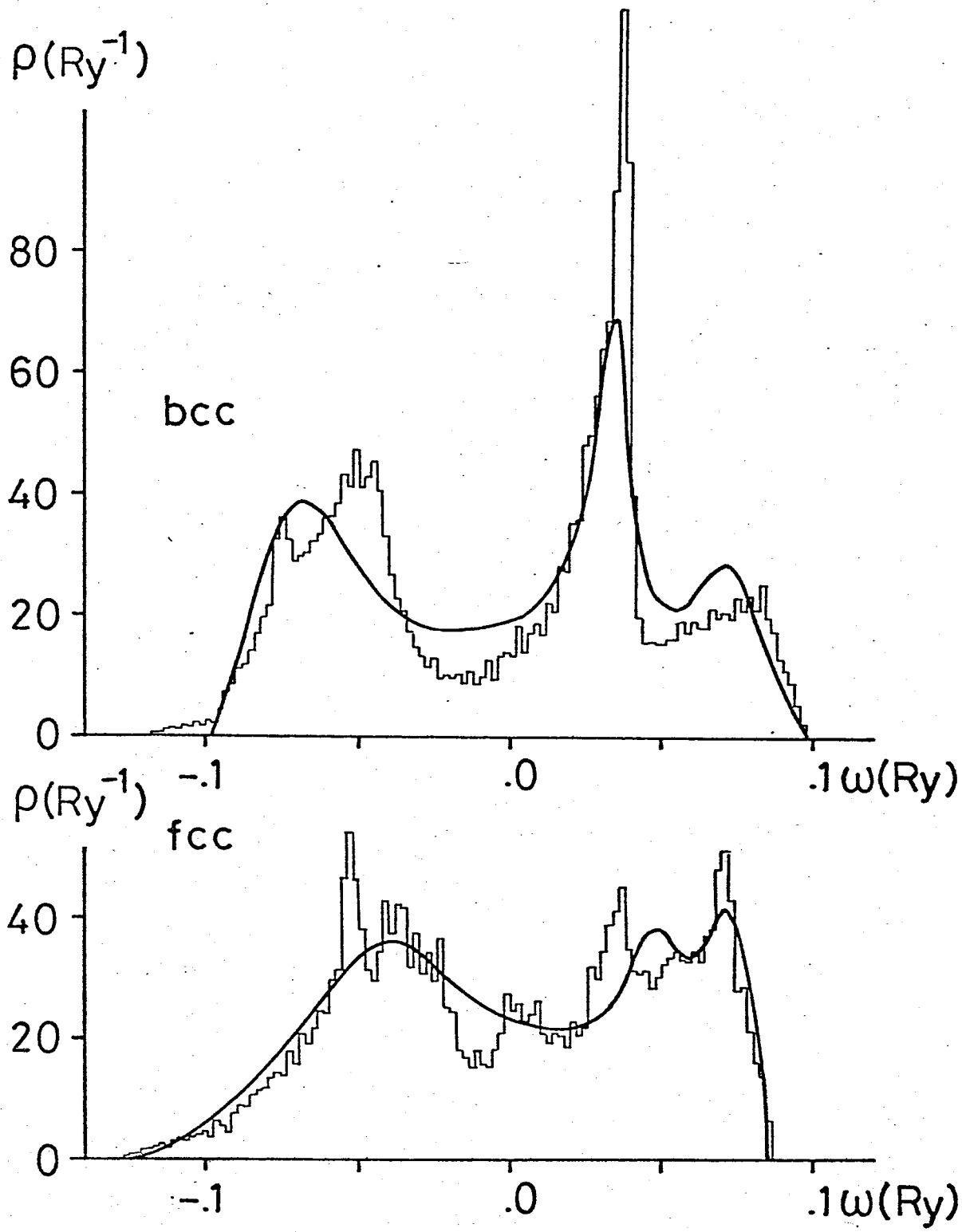

Fig. 7

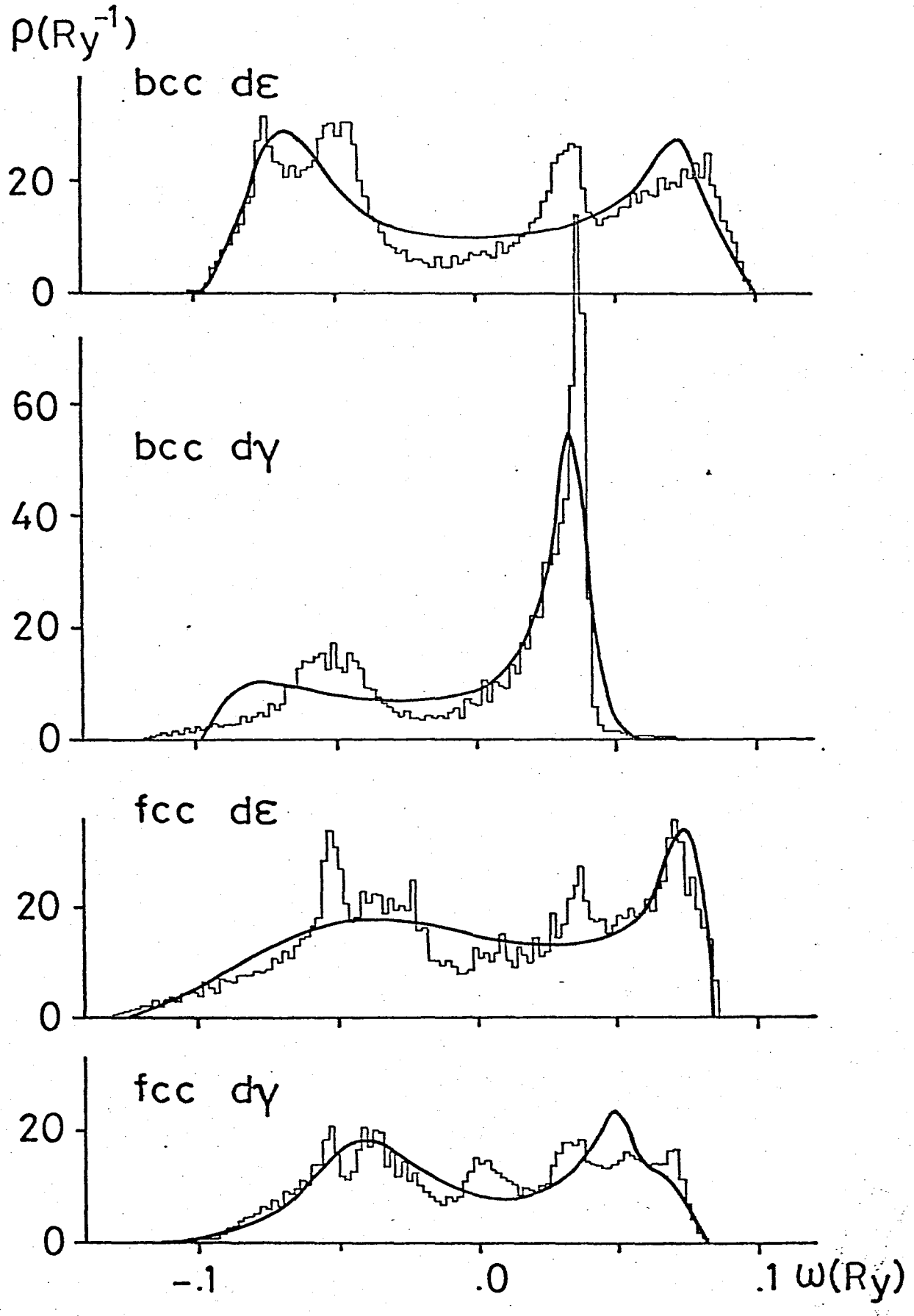

Fig. 8

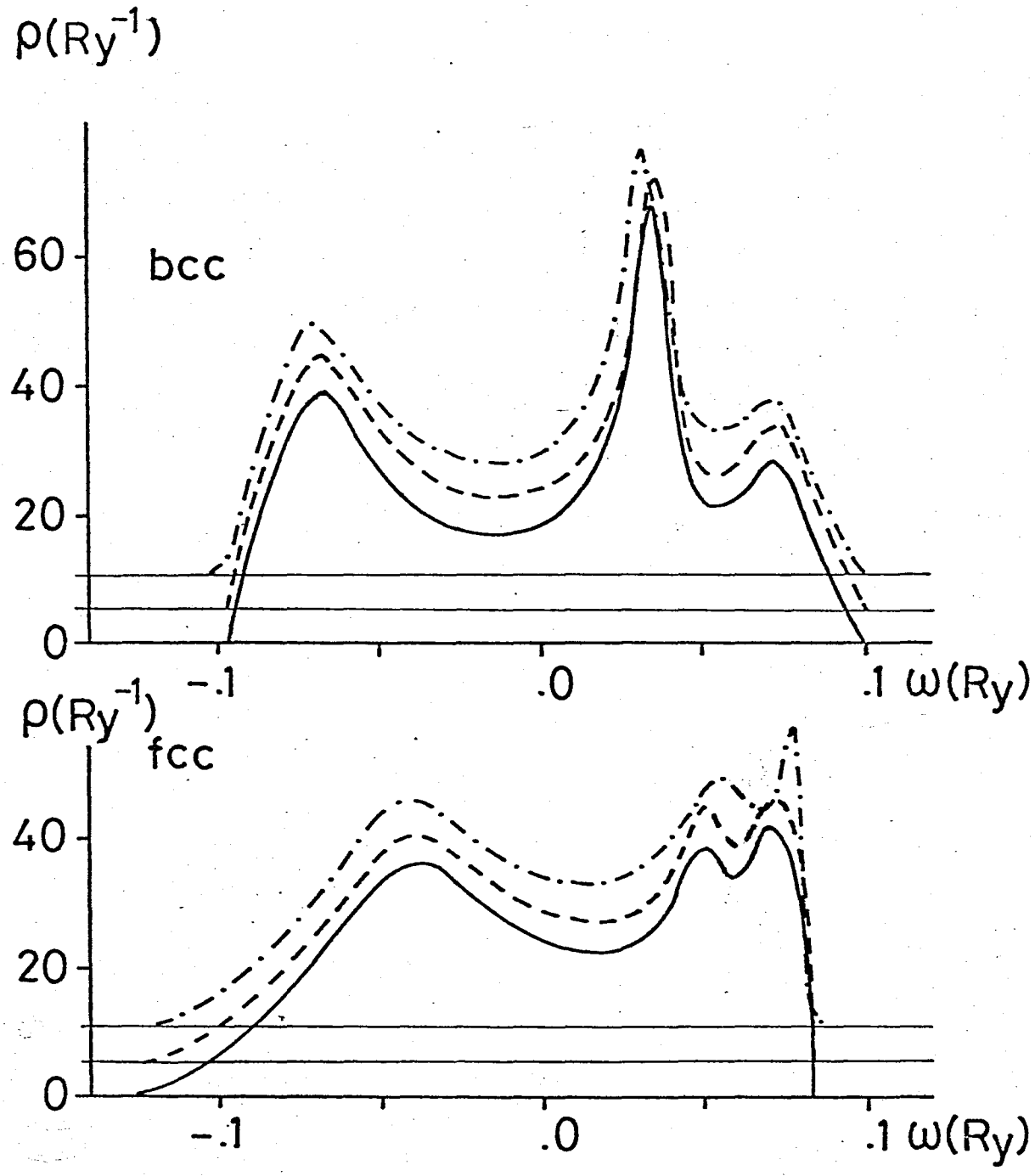

Fig. 9

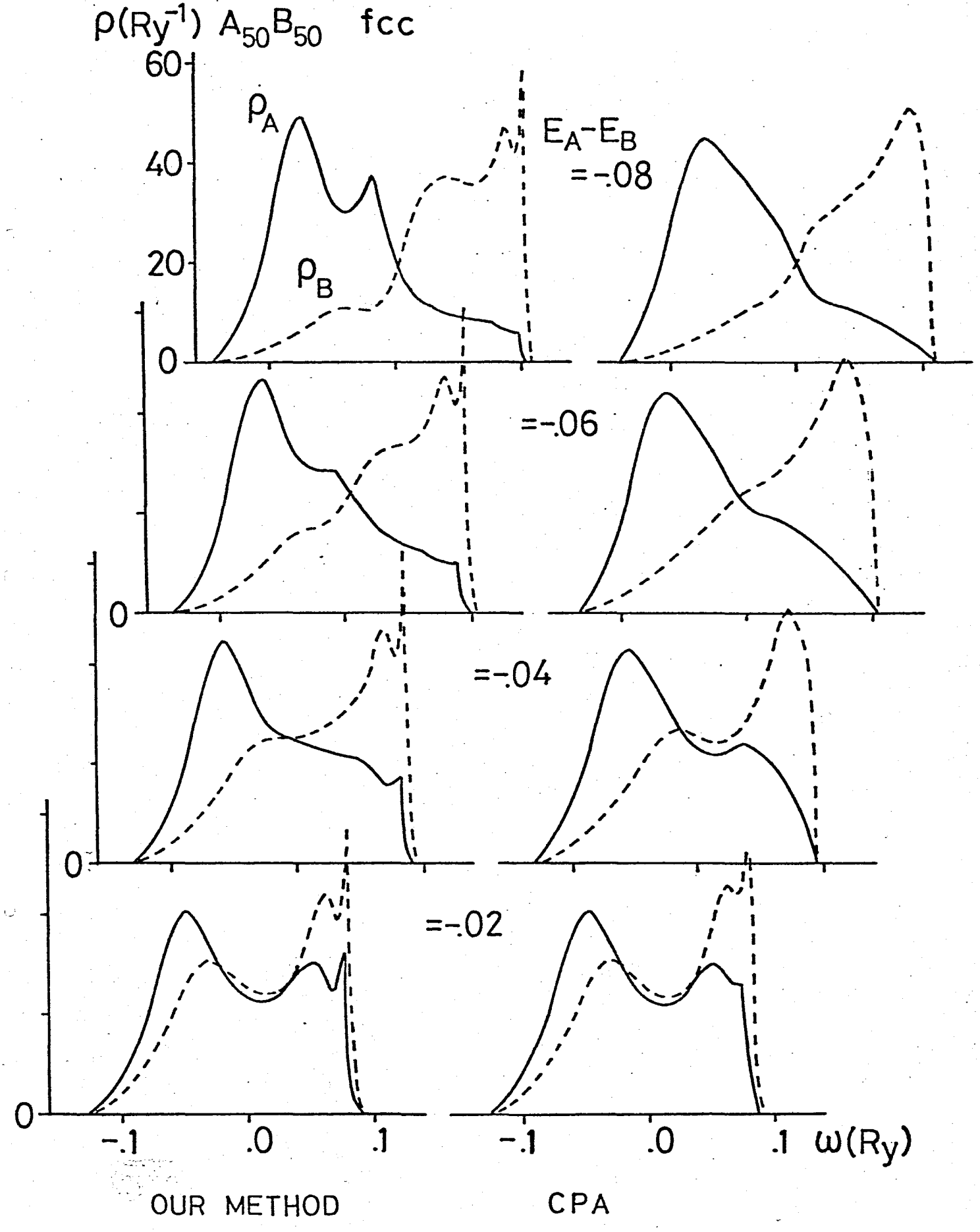
ρ(Ry⁻¹) A50B50 fcc
60
40
20
0
ρA
ρB
EA-EB
=-.08
=-.06
=-.04
=-.02
-.1
.0
.1
ω(Ry)
OUR METHOD
CPA

Fig. 10

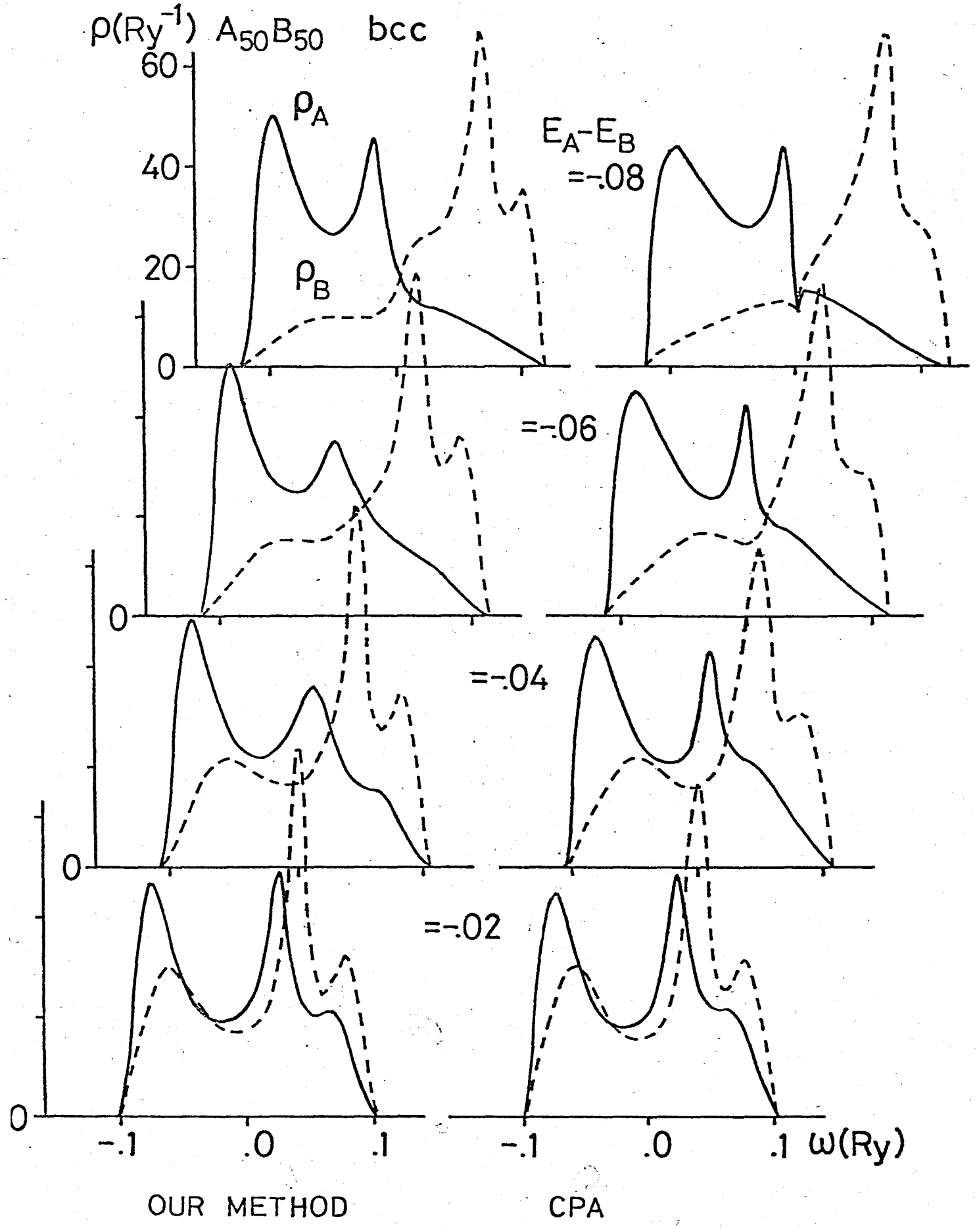
ρ(Ry⁻¹) A50B50 bcc
60
40
20
0
ρA
ρB
EA-EB
=-.08
=-.06
=-.04
=-.02
-.1
.0
.1
ω(Ry)
OUR METHOD
CPA

Fig. 11

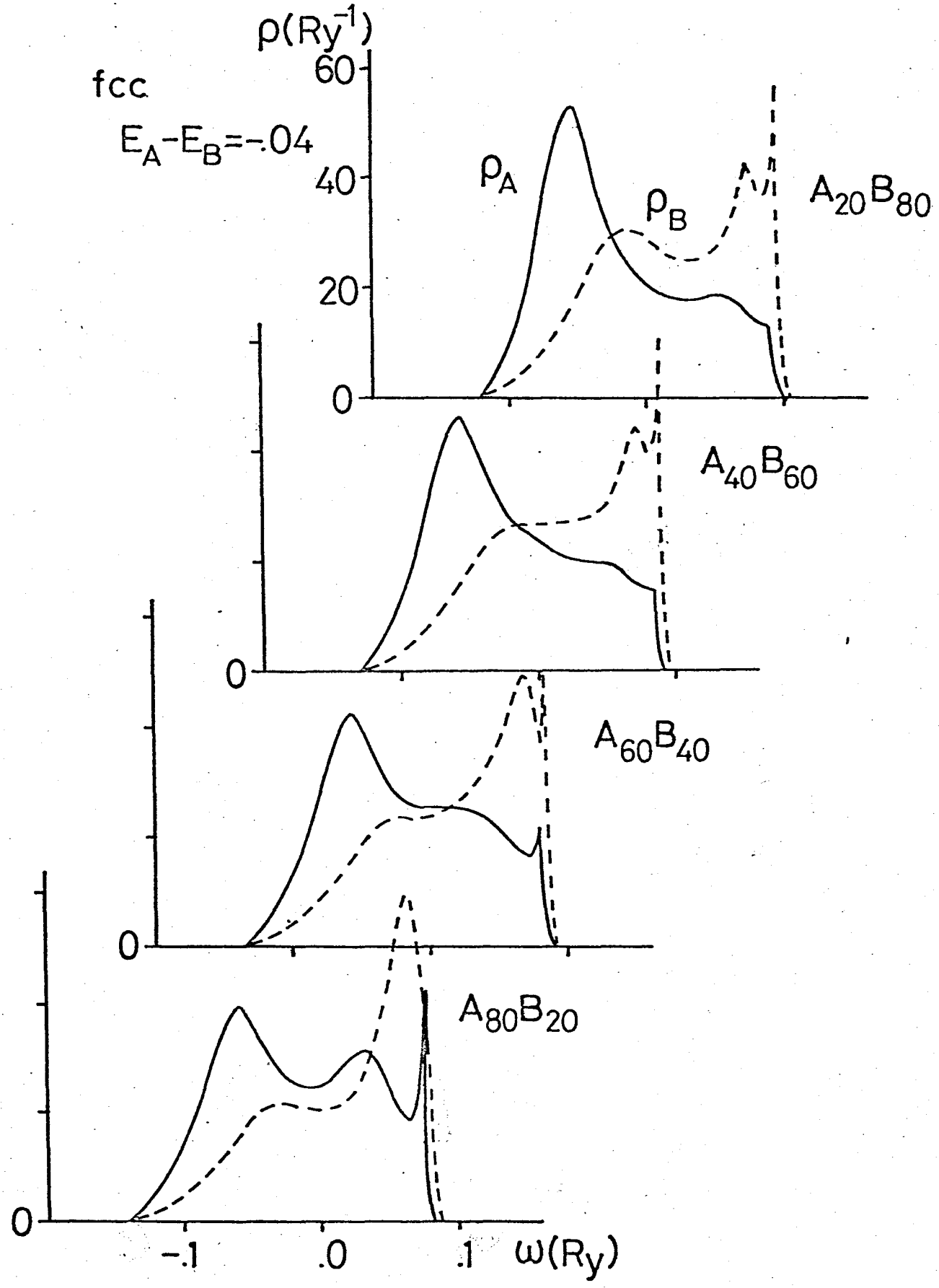
ρ(Ry⁻¹)
fcc
E_A-E_B=-.04
60
40
20
0
ρ_A
ρ_B
A20B80
A40B60
A60B40
A80B20
-.1
.0
.1
ω(Ry)

Fig. 12

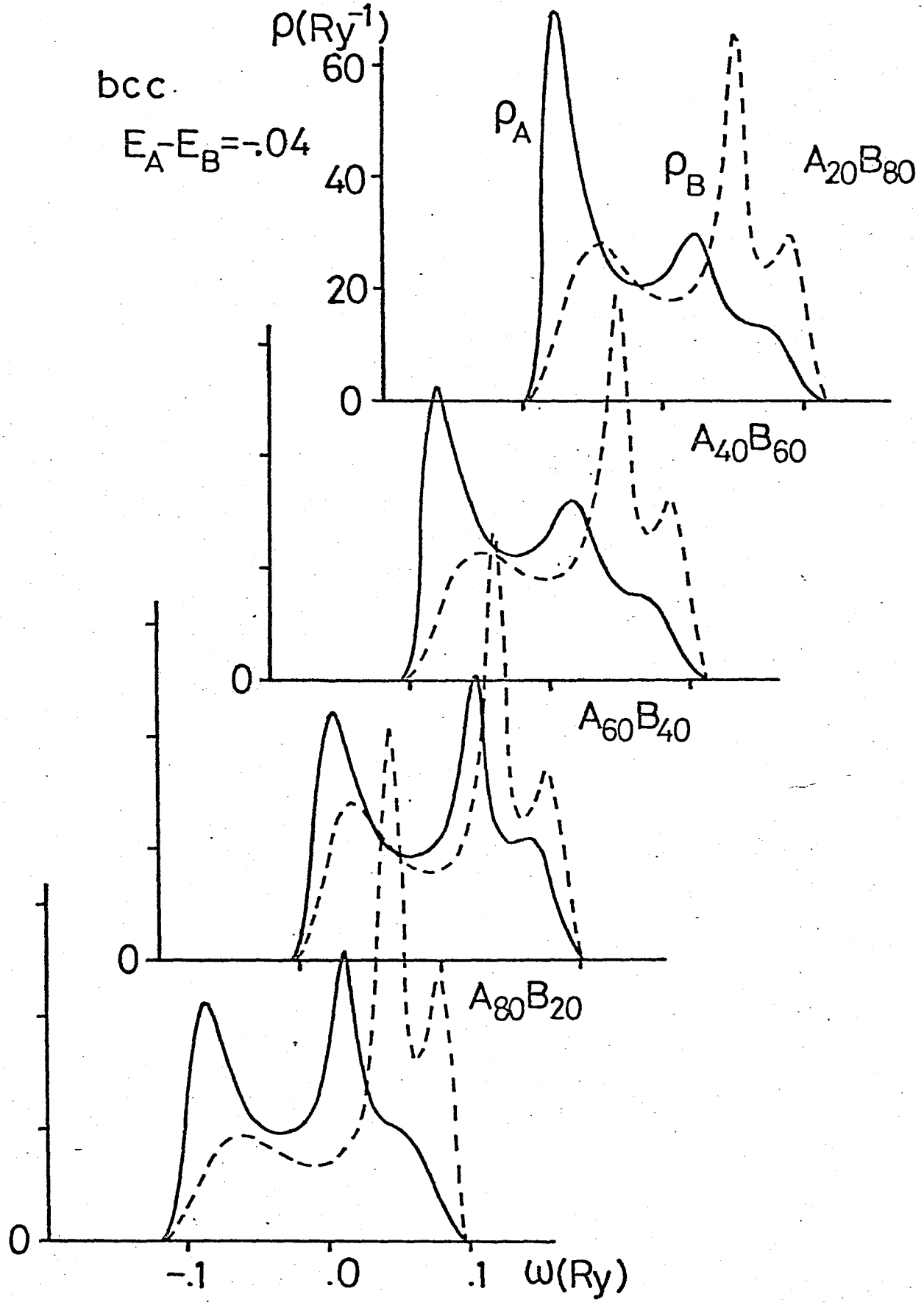
ρ(Ry⁻¹)
bcc
E_A-E_B=-.04
60
40
20
0
ρ_A
ρ_B
A20B80
A40B60
A60B40
A80B20
-.1
.0
.1
ω(Ry)

Fig. 13

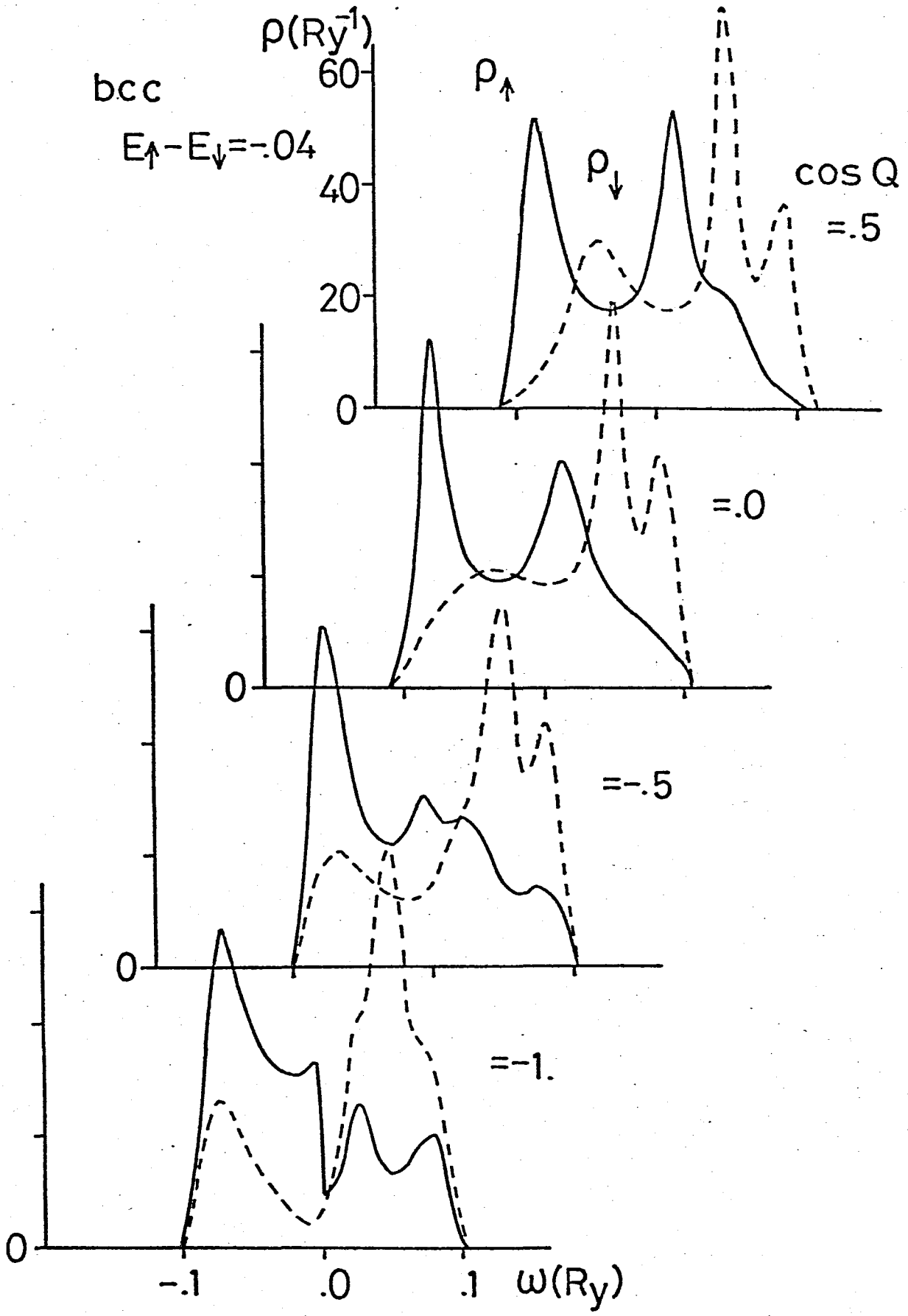

Fig. 14

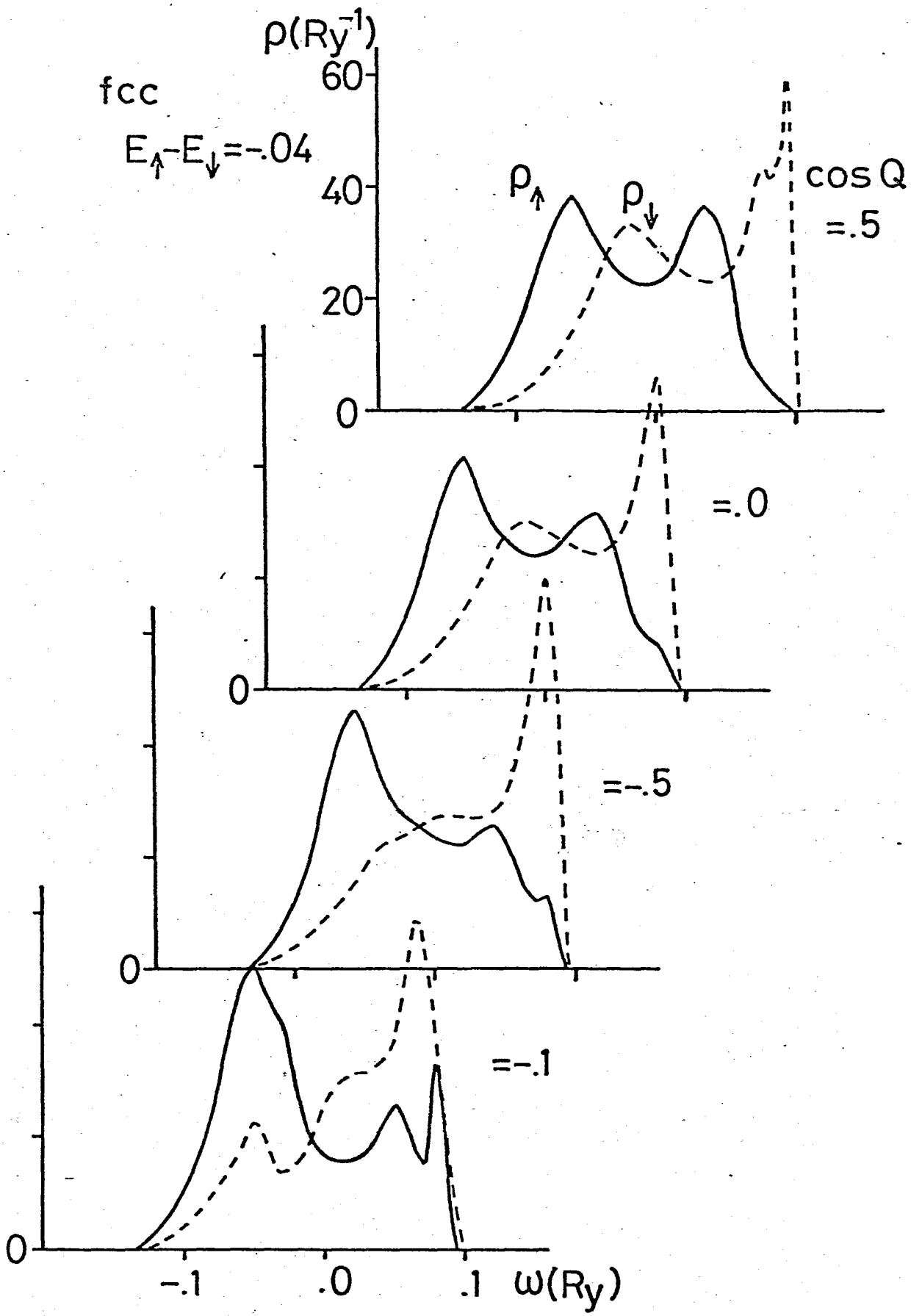

Fig. 15

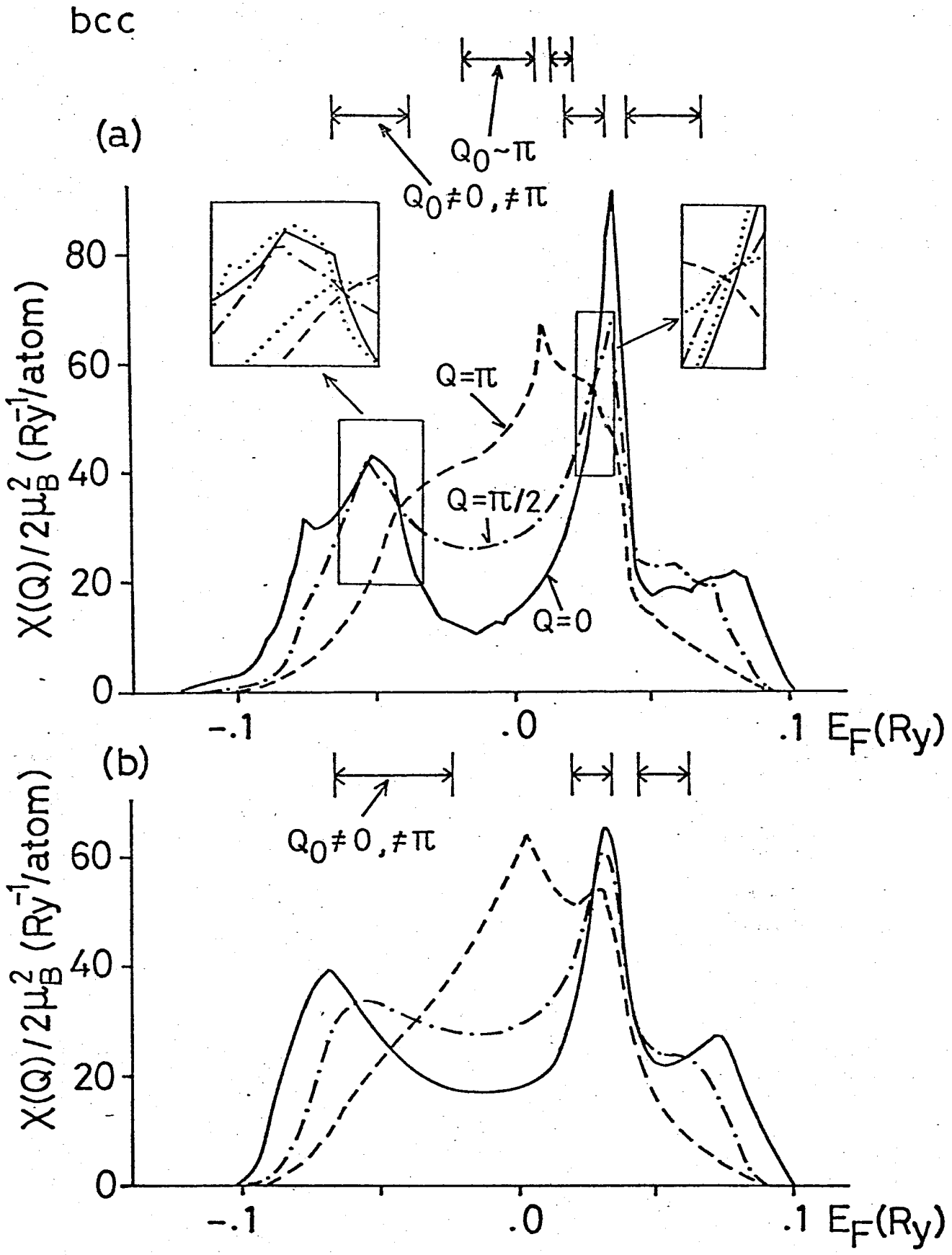
bcc
(a)
$Q_0 \neq 0, \neq \pi$
$Q_0 \sim \pi$
Q=π
Q=π/2
Q=0
80
60
40
20
0
$\chi(Q)/2\mu_B^2$ (Ry^{-1}/atom)
-.1
.0
.1
E_F(Ry)
(b)
$Q_0 \neq 0, \neq \pi$
60
40
20
0
$\chi(Q)/2\mu_B^2$ (Ry^{-1}/atom)
-.1
.0
.1
E_F(Ry)

Fig. 16

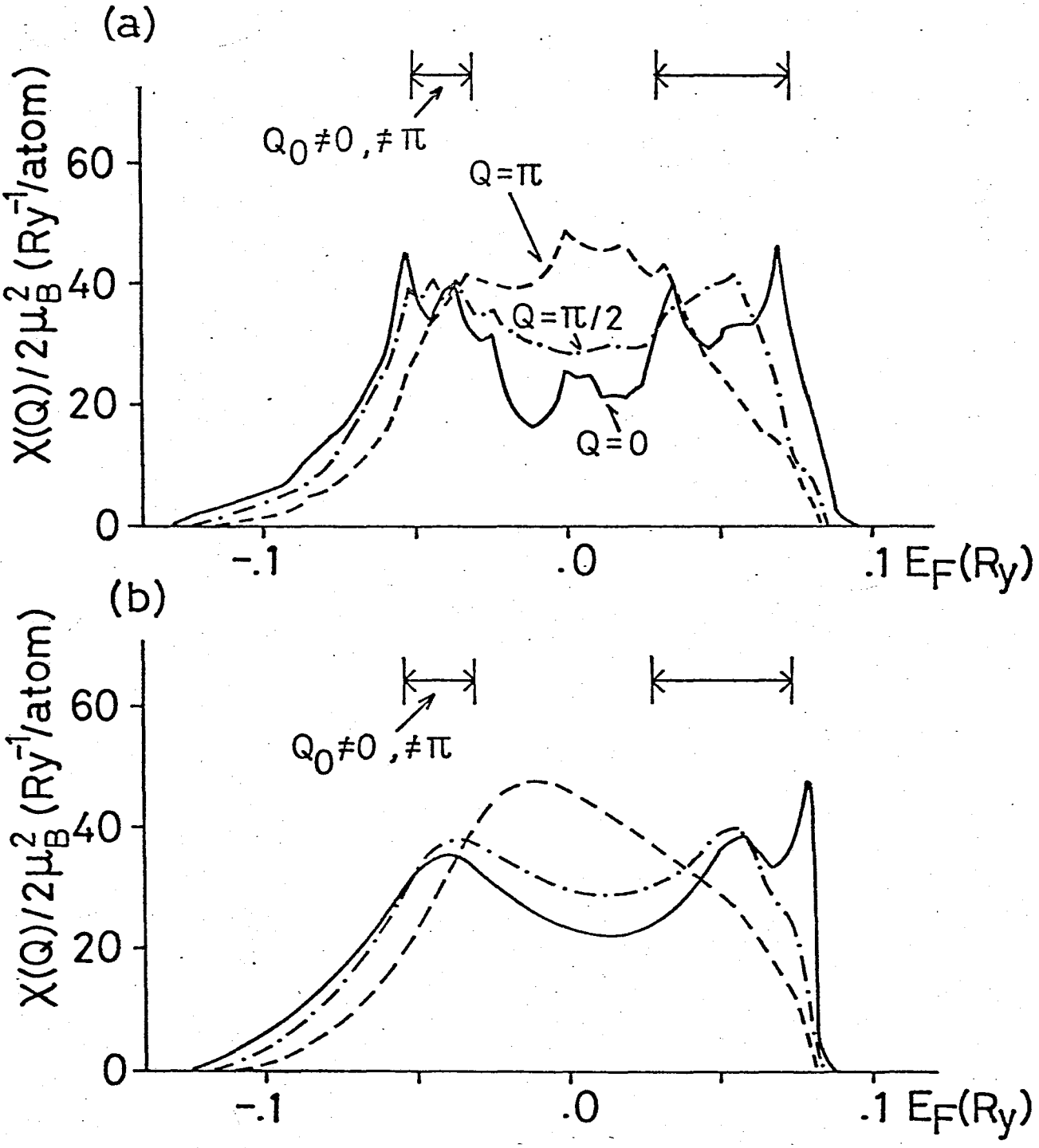
fcc
(a)
$Q_0 \neq 0, \neq \pi$
$Q=\pi$
$Q=\pi/2$
$Q=0$
$X(Q)/2\mu_B^2$ (Ry^{-1}/atom)
60
40
20
0
-.1
.0
.1 E_F(Ry)
(b)
$Q_0 \neq 0, \neq \pi$
$X(Q)/2\mu_B^2$ (Ry^{-1}/atom)
60
40
20
0
-.1
.0
.1 E_F(Ry)

Fig. 17

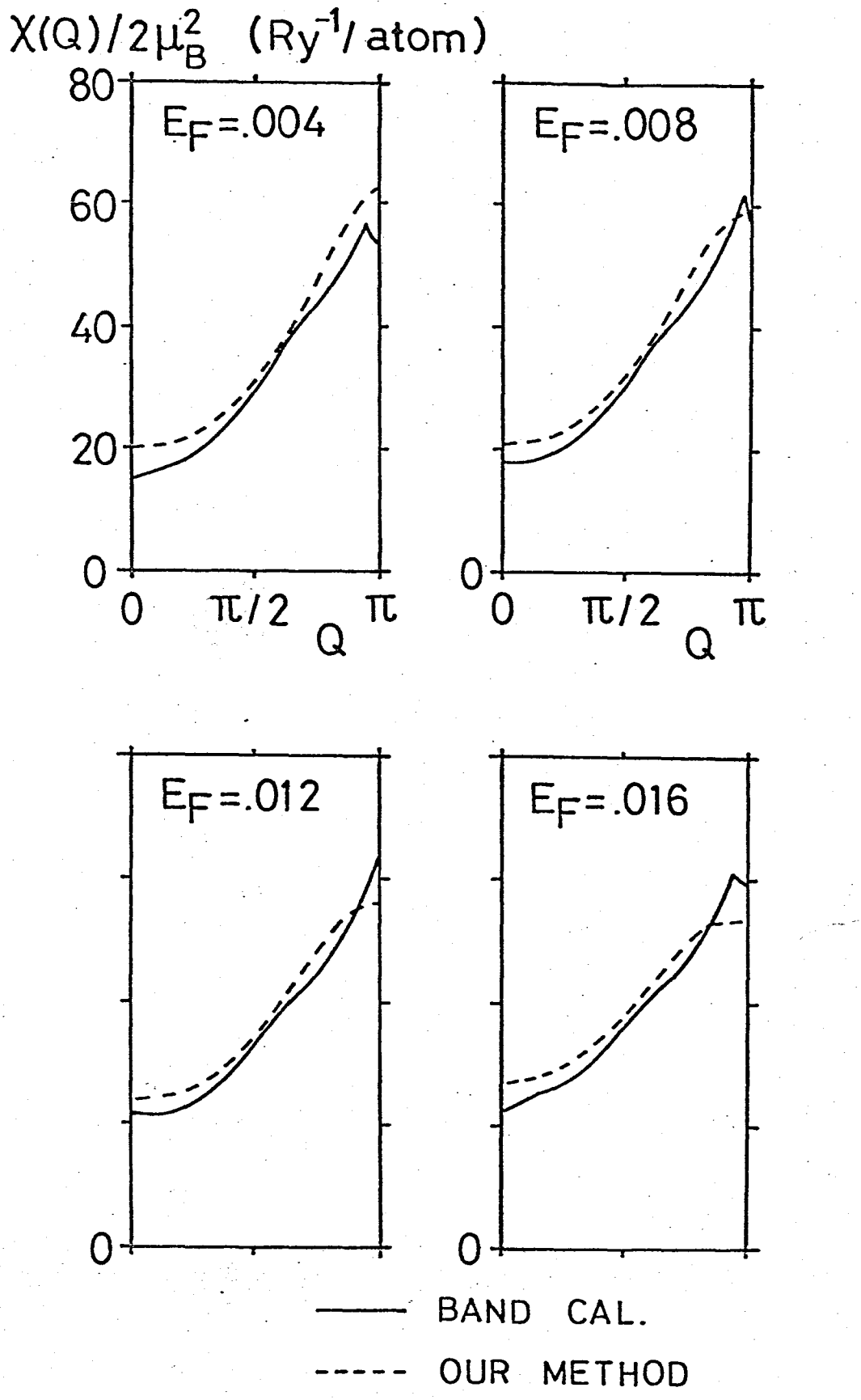
$\chi(Q)/2\mu_B^2$ (Ry^{-1}/atom)
80
60
40
20
0
E_F=.004
E_F=.008
E_F=.012
E_F=.016
0
π/2
π
Q
BAND CAL.
OUR METHOD

Fig. 18

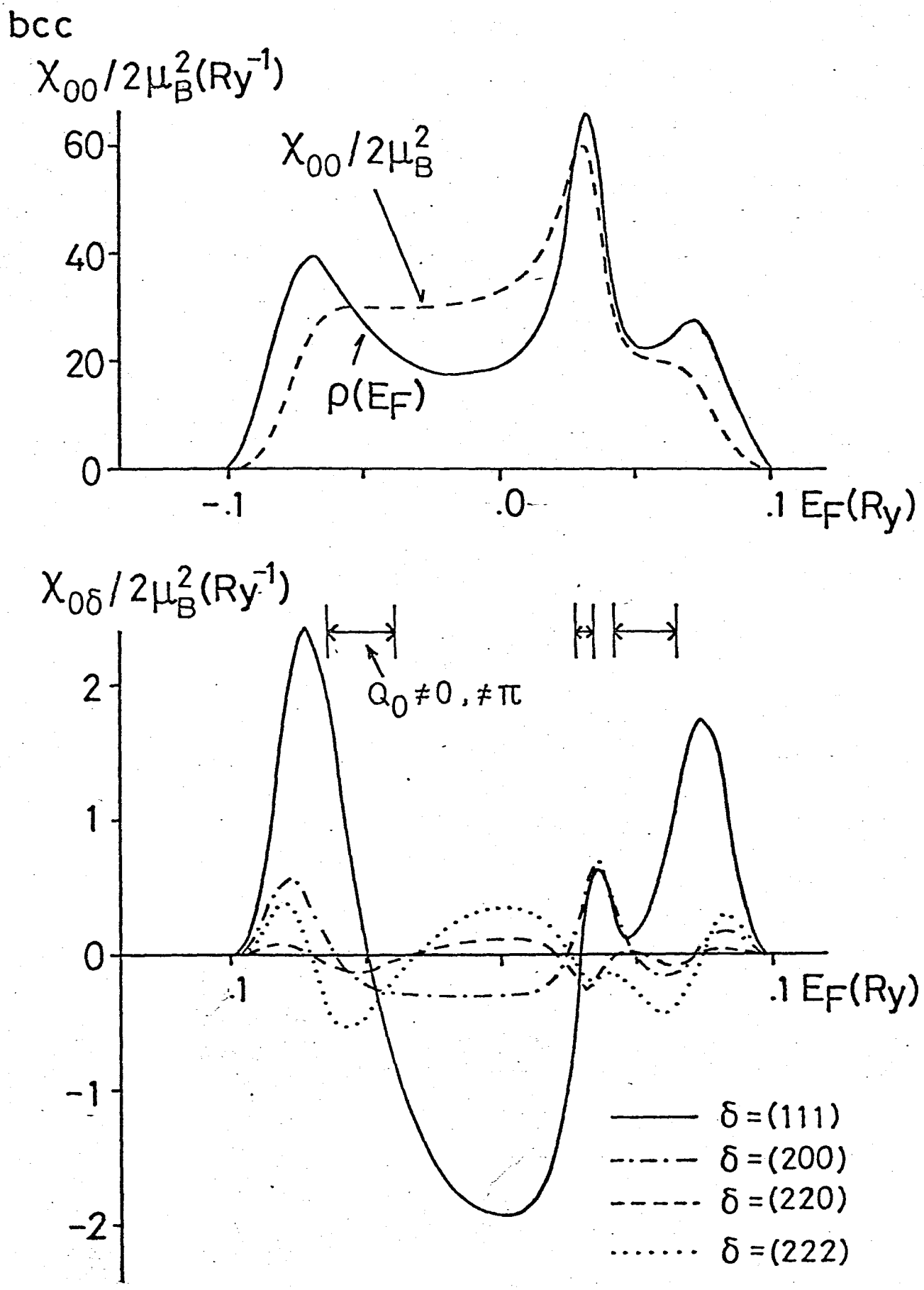
bcc
$\chi_{00}/2\mu_B^2(Ry^{-1})$
60
40
20
0
$\chi_{00}/2\mu_B^2$
$\rho(E_F)$
-.1
.0
.1 E_F(Ry)
$\chi_{0\delta}/2\mu_B^2(Ry^{-1})$
2
1
0
-1
-2
$Q_0 \neq 0, \neq \pi$
.1
.1 E_F(Ry)
δ =(111)
δ =(200)
δ =(220)
δ =(222)

Fig. 19

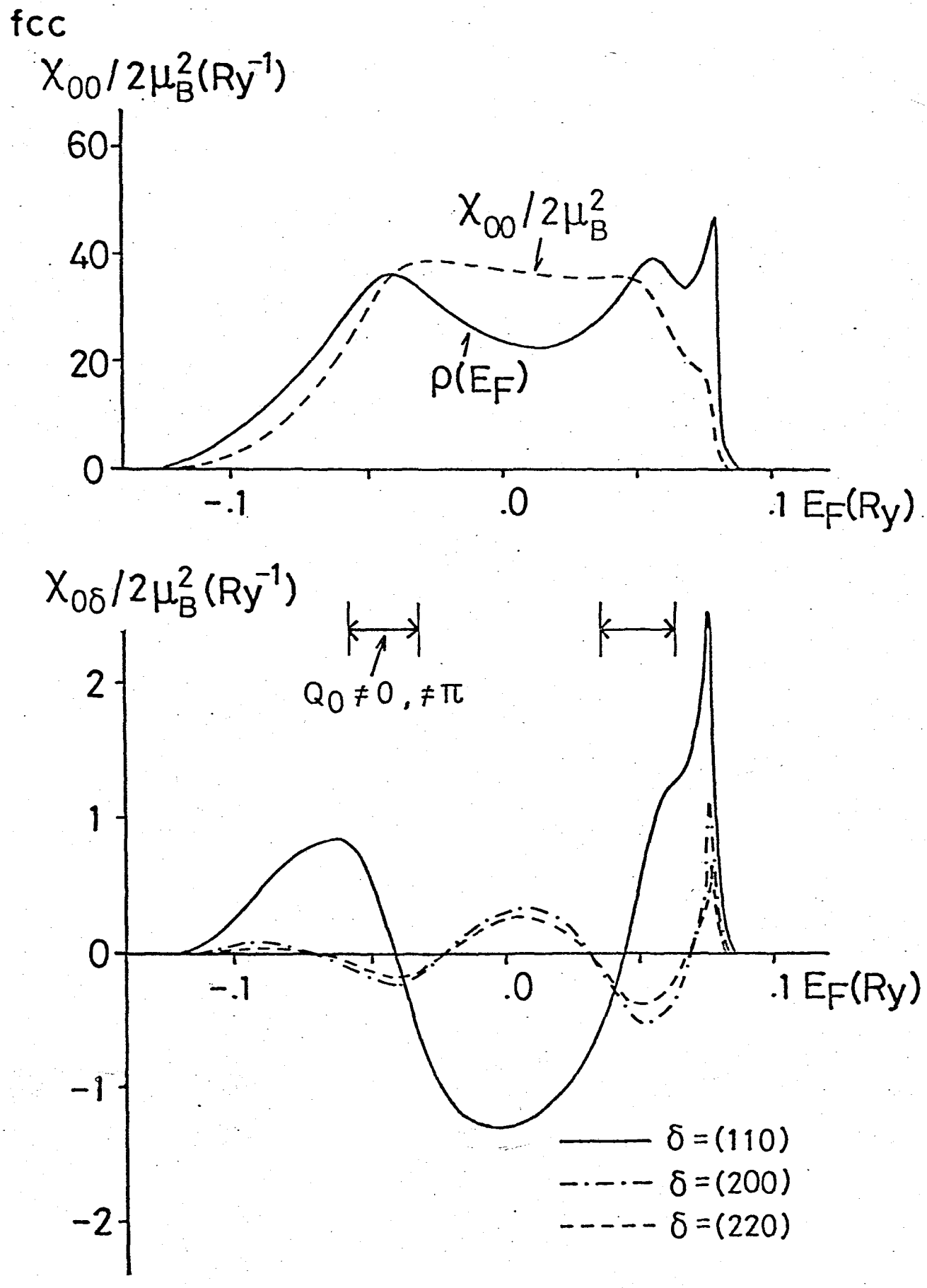
fcc
$\chi_{00}/2\mu_B^2(Ry^{-1})$
60
40
20
0
$\chi_{00}/2\mu_B^2$
$\rho(E_F)$
-.1
.0
.1 E_F(Ry)
$\chi_{0\delta}/2\mu_B^2(Ry^{-1})$
$Q_0 \neq 0, \neq \pi$
2
1
0
-1
-2
-.1
.0
.1 E_F(Ry)
δ=(110)
δ=(200)
δ=(220)

Fig. 20

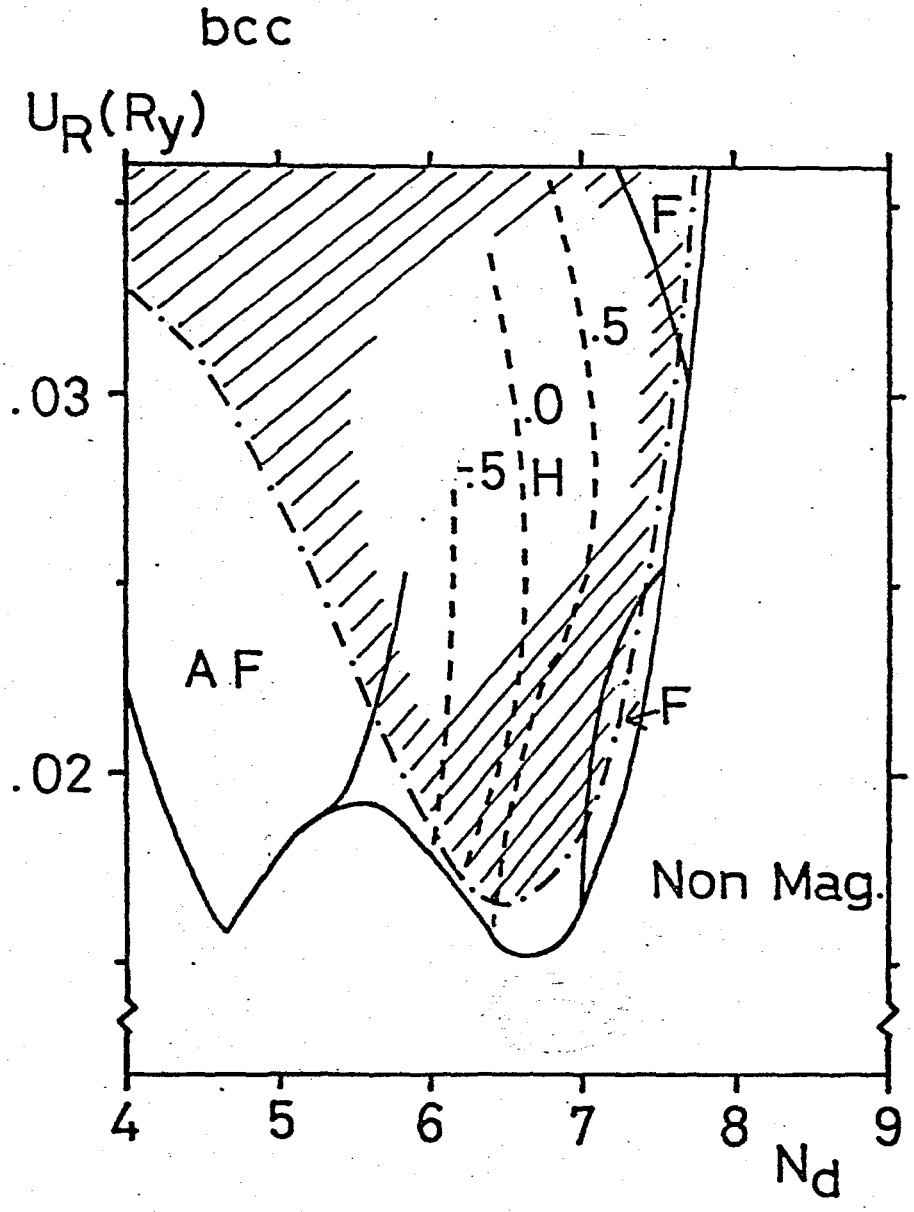

Fig. 21

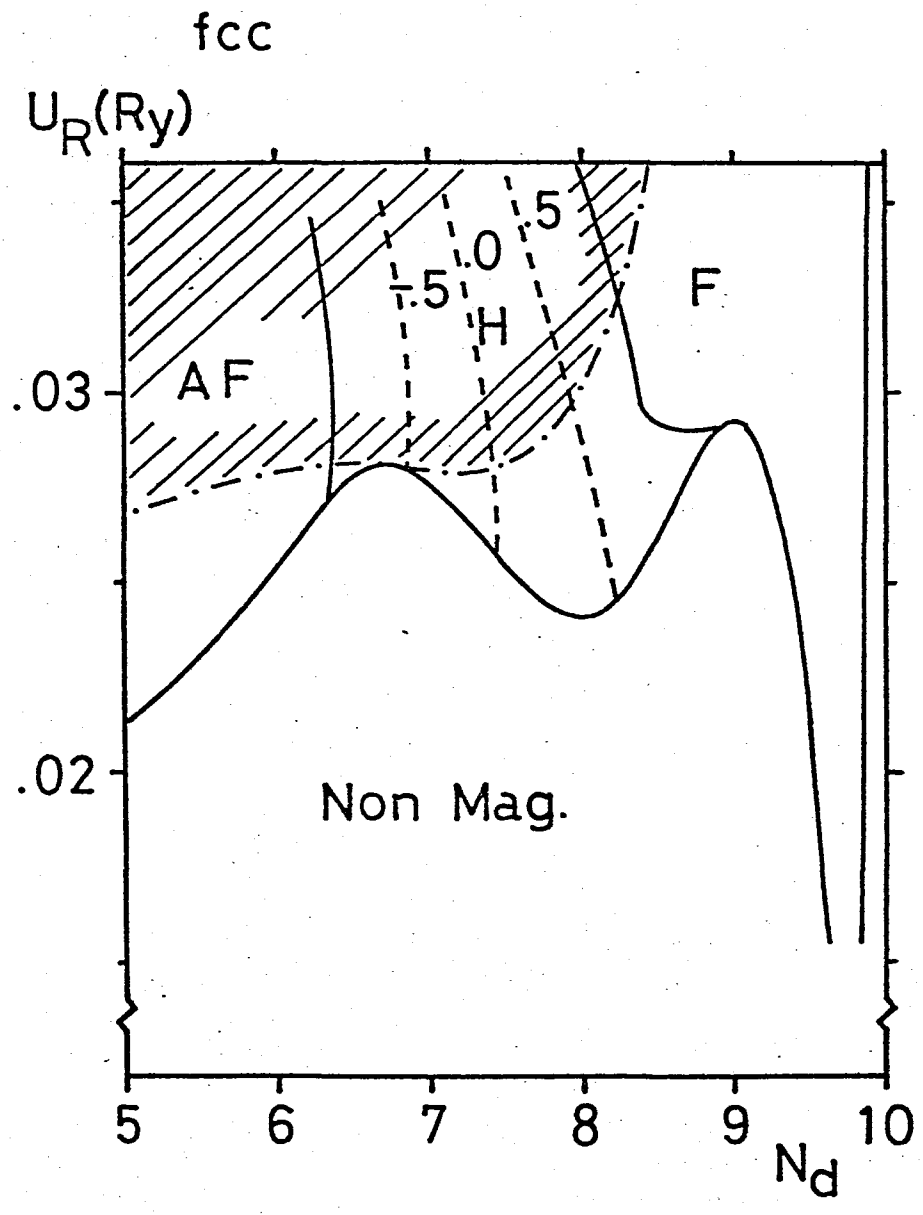

Fig. 22

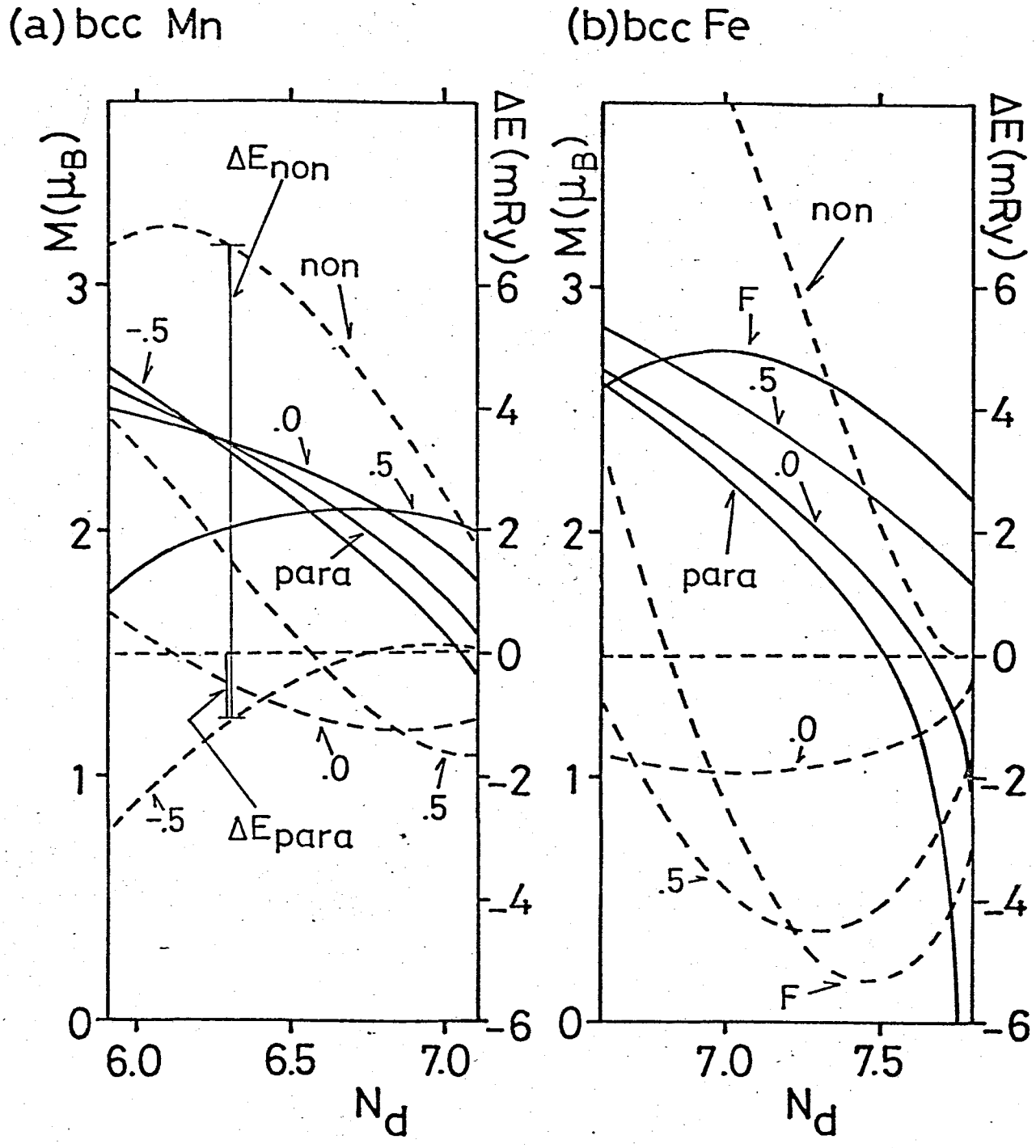
(a) bcc Mn
(b) bcc Fe
M(μB)
ΔE(mRy)
ΔEnon
ΔEpara
non
para
F
-.5
.0
.5
3
2
1
0
6
4
2
0
-2
-4
-6
6.0
6.5
7.0
7.5
Nd

Fig. 23

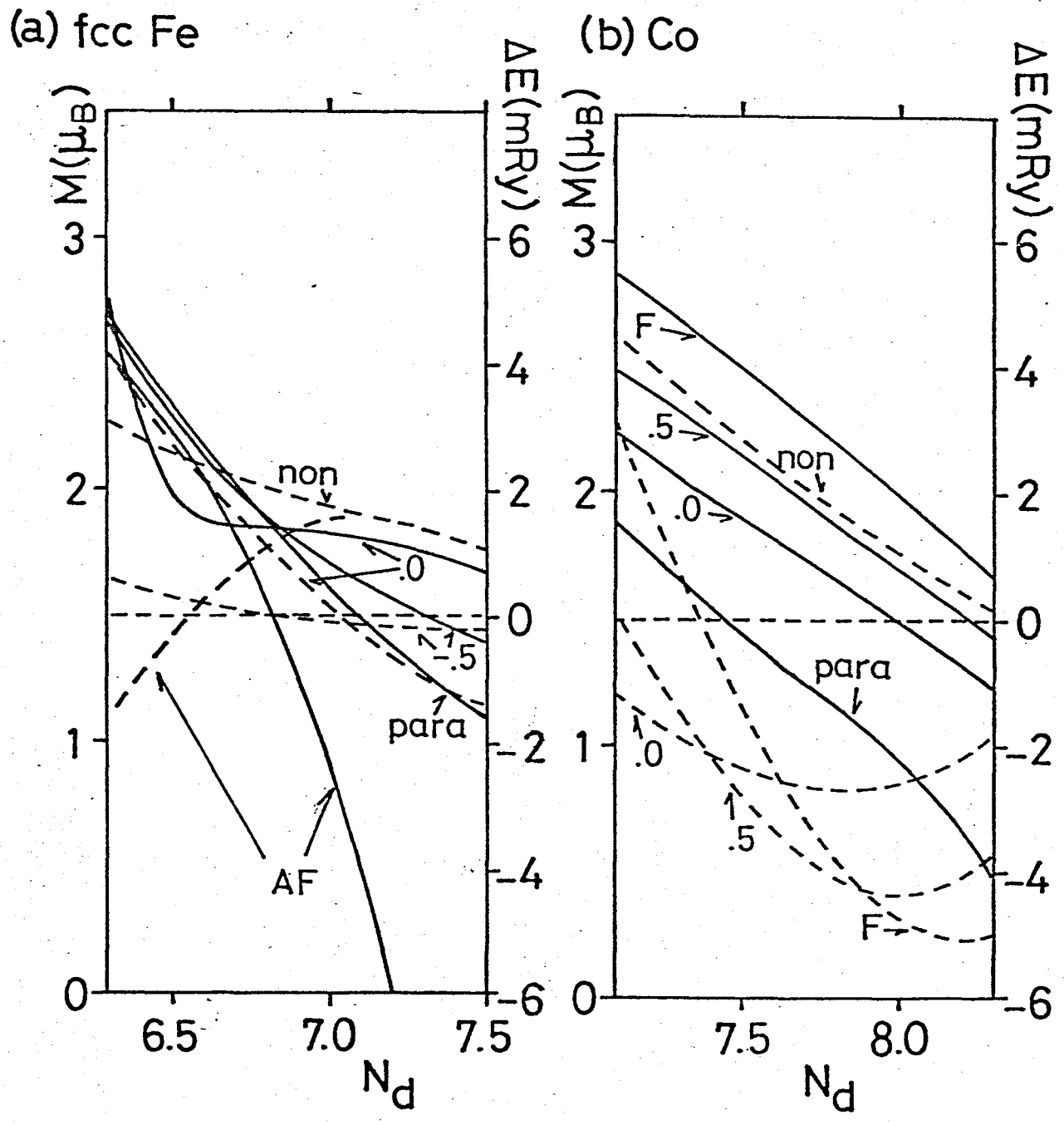

Fig. 24

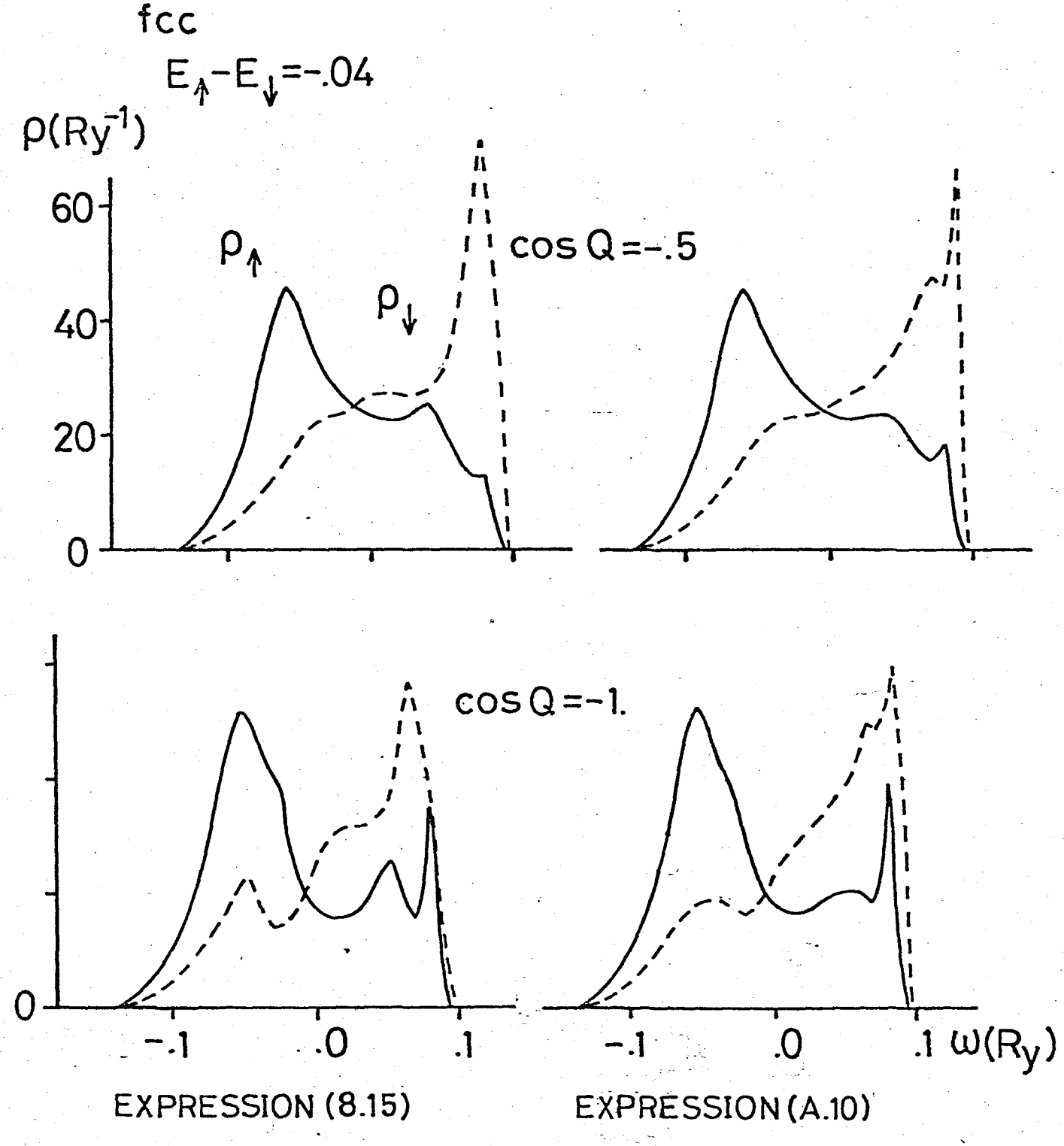
fcc
$E_\uparrow - E_\downarrow = -.04$
$\rho(Ry^{-1})$
60
40
20
0
$\rho_\uparrow$
$\rho_\downarrow$
cos Q = -.5
cos Q = -1.
0
-.1
.0
.1
-.1
.0
.1
$\omega(R_y)$
EXPRESSION (8.15)
EXPRESSION (A.10)

Fig. 25